INFN - Laboratori Nazionali di Frascati

Servizio Documentazione

LNF-87/6(R)

13 Febbraio 1987

DESIGN STUDY FOR THE TRIESTE SYNCHROTRON LIGHT SOURCE

Scientific Editor
S. TAZZARI

Technical Editor
L. INVIDIA

Printed and Published by:
Servizio Documentazione
dei Laboratori Nazionali di Frascati
P.O. Box, 13 - 00044 Frascati (Italy)

INFN - Laboratori Nazionali di Frascati

Servizio Documentazione

LNF-87/6(R)

13 Febbraio 1987

DESIGN STUDY FOR THE TRIESTE SYNCHROTRON LIGHT SOURCE

Authors

Cap. 1	**S. Tazzari**
Cap. 2	M. Biagini, C. Biscari, E. Gianfelice, S. Guiducci, L. Palumbo, P. Patteri, **M.A. Preger,**
Cap. 3	C. Biscari, E. Gianfelice, **L. Palumbo,** M. Zisman
Cap. 4	R. Coisson, B. Diviacco, **R. Rosei**
Cap. 5	**A. Cattoni,** S. Faini , C. Sanelli
Cap. 6	**R. Boni,** F. Tazzioli
Cap. 7	A. Aragona, **V. Chimenti,** S. Faini, G. Turchetti,
Cap. 8	**M. Pelliccioni**
Cap. 9	S. De Simone, **M. Serio**
Cap. 10	S. Kulinski*, B. Spataro, P. Patteri, **F. Tazzioli,** S. Tazzari, M. Vescovi
Cap. 11	**A. Cattoni,** S. Faini, C. Sanelli

Scientific Editor
S. TAZZARI

Technical Editor
L. INVIDIA

* On leave from Institute for Nuclear Studies - Swierk - Poland

INDEX

DESIGN STUDY FOR THE TRIESTE SYNCHROTRON LIGHT SOURCE

1. - GENERAL DESCRIPTION OF THE FACILITY

1.1. - Introduction

Intense, polarized photon beams, ranging in energy all the way from the infrared to the hard X-ray region are obtained from electron storage rings and are finding application in an ever increasing number of branches of science and technology.

The wealth of novel experimental results in both the fundamental and the applied sciences, has been so remarkable over a wide spectrum of disciplines (Basic condensed matter physics, Materials science and technology, Biology, Biophysics and Medicine, etc.) that the number of SR Sources, in operation or under design all over the world, has been growing fast.

The great majority of experiments requires that the largest possible number of photons in the desired energy bin reach the sample in any given time interval, so that samples containing fewer and fewer atoms (dilute solutions, very small biological samples or crystals, monoatomic surface layers, dynamic behaviours, ...) can be studied. Also, the photons reaching the sample should have the smallest possible angular divergence (diffraction is often involved). In terms of source characteristics this means high spectral brilliance.

The pulsed time structure, typical of a storage ring, also offers the possibility of time resolved studies.

The first synchrotron radiation users, back in the sixties, parasitically utilized the radiation from the bending magnets of HEP colliding beam facilities. These were the first generation synchrotron light sources.

With the rapid expansion of the field, dedicated storage rings started being built and novel radiation sources such as wiggler magnets and undulators being develope. These were the second generation.

Third generation machines covering different ranges of photon energies aim at improving the brilliance by several orders of magnitude by optimizing the storage ring magnetic lattices for low emittance and high circulating currents, and through the extensive use of insertion devices. Various third generation machines, covering a wide range of energies, are at present under design.

In Fig.1.1 the wavelength range and the brilliance of the proposed machine are given for a sample of possible insertion devices. More details on performance are given in Chapter 4.

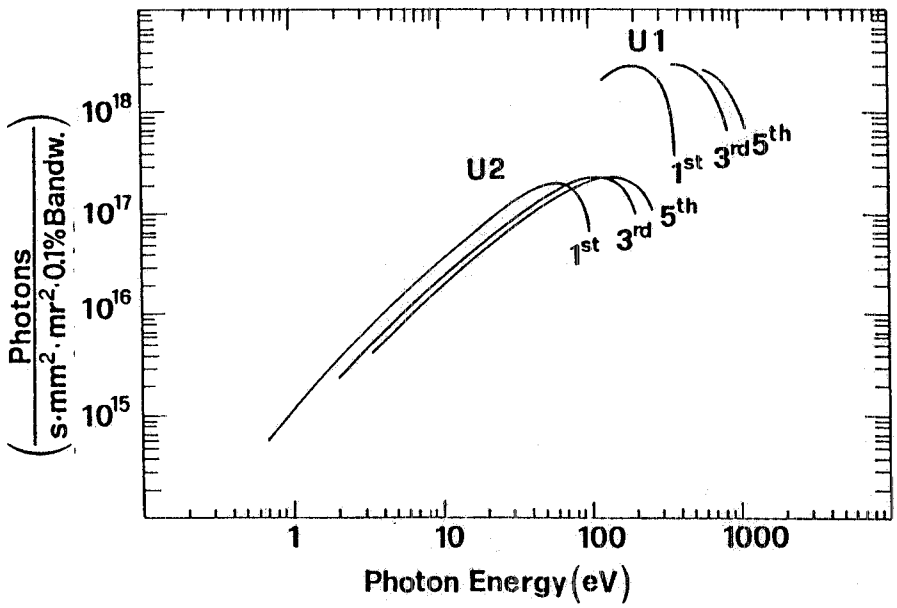

FIG. 1.1 - Average spectral brilliance as a function of photon energy for two typical undulators.

The proposed facility belongs to the third generation. It consists of an electron storage ring, the **main ring (MR)** that can reach 2 GeV and capable of accomodating up to fourteen beam lines from insertion devices and up to sixteen beam lines from bending magnets, a full energy **positron injector (INJ).**

The main ring has a large number of straight sections capable of accomodating a variety of insertion devices.

The storage ring emittance, in the range of 4 10^{-9} π·m·rad at 1.5 GeV, allows radiation beams with the highest brilliance, in the range of 10^{19} ph/s/mm^2/.1%/mrad^2, to be produced.

The radiation beam time structure consists of gaussian pulses with a standard deviation in the order of 100 ps (fwhm).

Since several experimental stations can be derived from a single bending magnet or wiggler beam line, more than 30 stations could eventually be made available. An initial complement of **6 beam lines (BL)**, corresponding to 11 experimental stations, is included in the proposed construction budget.

The injector complex consists of a **preinjector** linear accelerator (**LINAC**) followed by a **booster synchrotron (BSYN)** operating at ten Hertz.

A full set of parameters is given in the Parameter List, Appendix 1.

1.2. - Performance specifications

1.2.1. - The main specification concerns the minimum wavelength to be obtained, in the first harmonic, from an undulator magnet. This was indicated by the users to be in the range from 10 to 20 Å corresponding to an energy of $\approx 0.5 \div 1$ KeV, an energy region lower than and complementary to that for which the third generation high energy, hard X-ray machines under construction (in Europe the ESRF) are optimized.

Typical novel experimental work in the disciplines of materials science and technology, biology, biophysics, medicine, and for industrial applications can be done with high brightness beams in this wavelength range.

From the specification of the first harmonic undulator wavelength and of its tunability range, and from the state of the art in storage ring design and in the fabrication of undulator magnets follows the main ring **design energy.**

1.2.2. - The highest brilliance can only be obtained if the size of the electron beam circulating in the main ring, or else the electron beam emittance (the area occupied by the beam in phase space), is of the same order as the minimum x-ray beam size determined by diffraction. For the energy range one is concerned with, the emittance should be in the range of 10^{-8} m·rad, or slightly lower (see also Chapter 4.). This requires a special magnetic lattice with very strong focalization.

1.2.3. - The lattice should include a large number of long straight sections to accomodate a variety of insertion devices. The number and lenght of these straights was not specified in strict way. It was however felt that not less than ten long straights should be made available for the purpose, and that at least 5 m of free space in each of them should be provided. The betatron functions in the straights should be adjustable to maximize the performance of the insertion devices and minimize harmful effects possibly deriving from their installation.

1.2.4. - A long electron beam lifetime in the order of many hours, and therefore a very high vacuum inside the beam enclosure, has also to be achieved. This requires special care because of the high radiation power impinging on the vacuum chamber walls in a high current, high energy storage ring. Scattering on the residual gas and intrabeam scattering have also to be carefully considered in the energy range one is dealing with.

1.2.5. - A time structure consisting of very short intense pulses, and with variable time interval in between pulses is also desired. In particular it is important to foresee a mode of operation where a single intense bunch is present in the machine.

1.2.6. - Last, the radiation beam spot size at the location of the experiment, tens of meters away from the source point, can be of the order of of a few tens of micrometers. The machine is therefore required to provide a large number of beams each of which has to be reproducibly positioned to that accuracy, and kept stable over weeks and months of operation. This requires special care in the selection of the site, the control of ground vibrations and in the design of the lattice, the beam monitoring and control equipment, the magnet supports and the ancillary equipment.

1.3. - Design options

1.3.1 - Energy

A maximum energy of 2 GeV has been chosen for the present design study; a detailed justification is given in Chapter 4.

1.3.2. - Choice of the lattice

In the design of very low emittance magnetic lattices like the one required for the present machine one has to deal with a number of problems connected with the very strong required focussing, with very strong geometric and chromatic aberrations up to high order, with extreme sensitivity to magnetic and alignmlent imperfections, with current and lifetime requirements, etc.

Systematic work on this subject, by various groups in Europe and in the USA[1.1,1.2], has started to be performed only in the past three to four years. Since one is dealing with complicated nonlinear dynamics problems, the main tools to study a lattice performance are numerical codes. One is forced to simulate the behaviour of many particles circulating in the machine, following them over a large number of turns. The work is very time consuming and a very large number of parameters is involved so that no simple rule exists for optimizing the overall source performance.

It is therefore also of paramount importance that the lattice be flexible enough to allow for improvements, modifications and unforeseen modes of operation to come up during the machine commissioning and operation.

In the present design study it was felt important not to duplicate efforts being pursued elsewhere, but to explore the feasibility of new or not fully studied solutions. While providing a sound basis for a cost and feasibility estimate, the choice of the lattice presented in **Chapter 2.**, will also provide a further valuable term of comparison at the time when the design will have to be finalized. As it is explained under 2.1., other configurations have also been considered, although not in as much detail, and further work is needed before a final decision can be reached.

One of the main options available to the designer is the choice of the lattice periodicity. This determines the machine circumference and the maximum number of long straight sections but also affects many other relevant parameters. It therefore influences both performance and cost and may be influenced by the choice of the site.

The solution presented here, of a sixteen period main ring with twelve to fourteen long straights available for the experiments, is based on several arguments. The number of straights is fulfilling the specification with some margin. A higher periodicity is beneficial in that it allows for the design emittance to be reached with a relatively 'relaxed' lattice, to the advantage of reliabilty and flexibilityand therefore of overall performance. In comparison with similar projects it fully exploits the unique features of the proposed site - size and ground quality - at an extra cost that is minor on the scale of the whole project. Furthermore, in the long run, extra floor space at accelerator facilities has always paid off in terms of future unforeseen developments.

It is shown in Chapter 2 that a satisfactory lattice can be found under these conditions. In fact at least two equally promising solutions, of which one is presented in detail are still being considered.

1.3.3. - Injector

The basic design choices for the injector complex concern the type of stored particle (electrons or positrons) to be stored, the injection energy and the repetition rate.

The question of electrons versus positrons has considerable implications concerning the size and cost of the preinjector. The reason for considering positrons (the more costly solution) is that an electron beam can, under certain circumstances, trap ions created in the residual gas. The trapped ions, besides possibly altering the local residual gas pressure, produce strongly nonlinear fields that can drive resonances, instabilities and coupling of the vertical to the horizontal motion, thereby blowing the emittance up, lowering the lifetime and in general leading to less stable beams.

For very low emittance lattices one would predict ion trapping to be impossible or easily avoidable under most operating conditions. However the theory is in qualitative agreement only with the scarce experimental results available on existing storage rings. Furthermore, no data are available on rings with the kind of performance one is considering for third generation machines. Given also that the achievement of the design brilliance is the main justification for the construction of the source, the additional safety margin provided by a positron injector is considered to be well justified.

The injector is designed to reach the main ring maximum design energy of 2 GeV. Several reasons for this choice can be given. First, the desired beam orbit position stability and reproducibility, requiring a significant improvement over the present state of the art, do not seem to be achievable if the ring magnets have to be ramped from injection energy to full energy

at every injection cycle.

Second, the very good vacuum necessary for the source to achieve its design lifetime will only be achieved after a conditioning corresponding to about 150 A·h of circulating full energy beam. The conditioning time has to minimized when, as is the case for SR source, frequent openings of the vacuum vessel to air are foreseen. With a full energy injector it can be kept in the order of a few days of continuous operation. An inadequate injection energy, entailing too low an injection rate, could stretch this time to a point where the machine performance would be seriously jeopardized.

In addition, the allowed injection rate is inversely proportional to the main ring damping time which decreases as the third power of energy and therefore increases as the third power of energy (this is expecially important when positrons are considered). Furthermore full energy injection maximizes the effective transfer efficiencies.

In order to further enhance the overall injection efficiency the booster has also been designed to provide a rather low emittance ($\approx 5\ 10^{-7}\ \pi$ m rad).

Having taken all the above considerations into account, an injector complex consisting of a positron preinjector Linac followed by a low emittance 2 GeV booster synchrotron is proposed. A detailed description is given in Chapter 10. The Linac is designed for optimum cost effectiveness and uses an advanced RF-pulse compression scheme. The positron energy is 200 MeV, allowing for easy injection into the booster. The booster repetition rate is chosen to be 10 Hz, a value that guarantees high injection rates and ease of operation while still avoiding the special technical solutions that would be required for much higher repetition rates. The design positron injection rate is such that the main ring can be filled to its maximum design current of .4 A in less than 10 minutes.

REFERENCES

(1.1) ESRF, Report of the ESRP, presented by B.Buras and S.Tazzari, CERN, October '84
BESSY II, Eine optimierte U/W-Speicherring Lichtquelle, Berlin , Ed. by A.Gaupp et al., Nov. '86.
ESRF, Foundation Phase Report , The machine, Ed. by J.L.Laclare et al., Grénoble, To be published.

(1.2) SSRL 6 GeV SR Source, H.Wiedemann, Proc SRI-85 Conference, IEEE Trans NS 1-2
GeV SR source, Conceptual design report, Ed. by M. Cornacchia et al., Berkeley, June '86, LBL Pub-5172.
6 GeV Synchrotron X-ray source, Conceptual design report, Ed. by Y. Cho et al., Argonne, Feb.'86, ANL-86-8.
Preliminary design of a dedicated SR storage ring, G.Vignola, NSLS, BNL-35678.

2. - STORAGE RING LATTICE

2.1. - Introduction

The general characteristics of the proposed synchrotron radiation facility have been described in Section 1. We recall here their main specifications concerning the magnetic structure of the ring:

- Nominal energy	1.5	Gev
- Maximum energy	2.0	Gev
- Number of long straight sections for insertion devices	14	
- Free straight section length	6	m
- Natural emittance at maximum energy	$<10^{-8}$	m.rad
- Vanishing dispersion in the insertion straights		
- Tunability of the ß functions in the insertion straights		
- High positional and angular stability of the extracted radiation beams.		

In the past few years the increasing interest in high brilliance synchrotron radiation sources has stimulated the development of low emittance lattices for electron (or positron) storage rings, and a sound theoretical basis on this subject is now available in the literature (Refs. 2.1-2.7). The main problems connected with the realization of low emittance lattices are related to the strong focusing that is required and that implies strong chromatic and geometric aberrations, and high sensitivity to magnetic and alignment imperfections.

Several types of low emittance lattices have been proposed for synchrotron radiation dedicated storage rings. They are mainly constrained by the condition of vanishing dispersion in the straight sections where the insertion devices are to be installed. The insertion straights must therefore be connected to each other through curved sections having vanishing dispersion and vanishing first derivative of the dispersion at both ends. Such curved sections are called "achromats", and a low emittance lattice can be imagined as a periodic structure in which a period consists of an achromat terminated on each side by one matched half insertion straight.

The different proposed low emittance lattices are characterized by the structure of the achromat. We briefly recall here the most common ones that have all been explored in the preliminary phase of the design study (Refs. 2.8-2.23):

- The "Chasman-Green" double bend achromat (CG) in its simplest configuration consists of two bending magnets separated by a straight section with one horizontally focusing quadrupole in its center. If a vertically focusing quadrupole is added at each end of the straight section between the bending magnet and the central quadrupole, the possibility of

changing the dispersion and the betatron functions within the achromat is greatly enhanced thus improving the overall lattice tunability.

- The FODO achromat consists of a sequence of FODO-like cells, matched to the insertion straigths by dispersion suppressors. It was originally intended to follow the typical simple scheme of high energy electron-positron storage colliders or synchrotrons. However the scheme has to be adapted to a small ring with a large number of dispersion free long straights; in the process its simplicity is largely lost.
- The "Expanded Chasman-Green" (ECG) achromat is an attempt at combining the best features of the CG and the FODO schemes. It consists of two bending magnets separated by an arbitrary odd number of quadrupoles of alternating polarity in a typical FODO arrangement: it is therefore also called "Empty FODO", since the central FODO part has been 'emptied' of its bends.
- The "Triple Bend Achromat" (TBA) uses three bending magnets per achromat. Horizontal focusing is provided by two quadrupoles symmetrically placed with respect to the central magnet, while vertical focusing is supplied by adding a fixed quadrupole field, obtained through a field index, in the bending magnets. The condition of vanishing dispersion outside the achromat defines the strength of the focusing quadrupoles and the dispersion in the central bending magnet. An additional degree of freedom can be introduced if two more quadrupoles are added symmetrically with respect to the central bending magnet.

The optical properties of these achromats have been carefully studied and comparisons have been made regarding their applicability to various proposed synchrotron radiation facilities (Refs. 2.24-2.27).

In general since the chromatic behaviour of low emittance lattices cannot be completely described in an analytic way, one is forced to use tracking programs to evaluate the vital properties of each individual one such as: the stable region for betatron oscillations (somewhat improperly called "dynamic aperture"), the dependence of betatron tunes on the energy and the oscillation amplitude of the particles, and the sensitivity of the lattice parameters to alignment and field errors.

It follows that simple general criteria for optimizing a lattice do not as a rule exist but one has to go through a time consuming iterative procedure to determine the basic properties of any given structure. Notwithstanding, some general properties of the described achromats can be evidenced:

- In the achromats having two bending magnets only , the CG and the ECG, the horizontal phase advance through the achromat itself is very close to an odd multiple of π (it is exactly a multiple of π if the magnets are treated as localized angular pertubations): this limits the possibility of changing the values of the ß functions in the insertions without changing the working point in the tune diagram and results in a limited amount of flexibility.

The CG achromat has the lowest natural emittance for any given periodicity and requires

the minimum number of magnetic elements, an obvious advantages when the ring circumference is limited by site or other constraints.

- The ECG and the FODO are characterized by rather small values of the ß functions within the achromat which is a good feature. However, the horizontal and vertical ß functions are in general not too well separated and the dispersion function is small ewerywhere in the lattice so that the sextupole strengths required to correct the chromaticity are in general larger than those required for the CG and the TBA.
- In the TBA the total bend angle per achromat is divided over three rather than two bending magnets and a field index in the bends is also provided. As a consequence of the smaller bend angle per magnet a smaller emittance than that of a CG can be achieved for the same periodicity (see Eq. 2.2.1). Moreover, the focusing in the bending magnets leads to a smoother behaviour of the ß functions throughout the lattice. It does also further decrease the horizontal emittance through a more favourable damping partition.

On the negative side, the field index gives some additional problems concerning high order components in the magnetic field and positioning sensitivity and makes the spectrum of radiation from the bending magnets position dependent which may be disturbing for some of the experimenters.

- The FODO achromat always exhibits a high density of magnetic elements leading to layout and engineering problems. Because for the same emittance the number of bending magnets is large compared to that of other lattices the extraction of synchrotron radiation beam lines from the structure is also more difficult.

All lattices described above have been studied, to different levels of optimization, as possible candidates for the Trieste machine, and have shown comparable performance in terms of non linear behaviour and lattice sensitivity to magnetic and alignment imperfections (Refs. 2.8 - 2.23).

An ECG structure that has been studied in the most detail is used in the present design study for several reasons: it provides a sound basis for a cost estimate, it has an overall performance in some respect superior to that of other solutions (with a somewhat more complicated sextupole arrangement) and finally it provides, at design study level, a much needed comparison with other lattices notably the LBL (Berkeley) synchrotron radiation source (Ref. 2.28).

In the absence of site restrictions we were led to explore the advantages to be obtained from a rather large machine circumference and a larger than usual number of achromats. The choice of sixteen periods was thus determined by the opportunity of providing, at a limited expense, at the same time a larger complement of experimental beam lines and a more flexible, reliable machine.

Along the same lines a second lattice has also been studied in some detail (Ref.2.29) that exhibits a performance comparable to that of the proposed ECG with a smaller number of

magnetic elements (it needs only 80 to 112 quadrupoles instead of the 176 needed for the ECG structure, and 112 sextupoles instead of 192). The basic structure is a CG achromat modified by the addition of a vertically focusing quadrupole field in the bending magnet corresponding to a field index n=20. The lattice is also shorter than the ECG (233 m instead of 300 m) for the same number and length of insertion straights. It is not being proposed as a first choice in the present study because not all the various time consuming computations have been completed. It is however the object of further work and we believe it could turn out to be a further important candidate for an optimized facility.

2.2. - Linear optics

The lattice discussed here is the so called "Expanded Chasman-Green" (Ref. 2.23). Its basic achromat consists of two dipoles separated by a straight section containing an odd number of quadrupoles arranged in a FODO sequence.

The minimum natural emittance of the ECG lattice is dependent on the total number of dipoles in the machine according to the well known relationship

$$\varepsilon_{min} = (1/(4\sqrt{15}))\, C_q \gamma^2 \theta^3 \qquad (2.2.1)$$

where $C_q = 3.84\ 10^{-13}$m, θ is the bending angle of each magnet, and γ is the energy of the particles in units of the rest energy.

The minimum emittance is obtained when the horizontal betatron function has a minimum ($\beta_{xmin} = \sqrt{15}\ L/40$, where L is the length of one dipole) at a point located at 3/8 of the bending magnet length. The condition can easily be met from the linear optics point of view but quadrupole gradients and maximum β functions tend, as the required emittance decreases, to become large leading to strong chromatic and geometric aberrations.

Various considerations (see § 1.3) led us to the choice of a 16 fold periodicity for the lattice. The corresponding minimum emittance would be $\varepsilon_{min} = 1.6\ 10^{-9}$ m.rad (at 1.5 GeV), but the design value, $\varepsilon_x = 4.7\ 10^{-9}$m.rad, is three times higher to obtain a smoother behaviour of the betatron functions with a minimum of β_x inside the magnet that is not too deep and maxima that are consequently less pronounced.

The achromat includes five quadrupoles in between the dipoles. Furthermore, two triplets are added in each insertion to allow the betatron function to be adjusted over a rather large range of values in the 6 meter long dispersion-free section. This will allow the beam dimensions and divergences in the insertion straights to be individually adjusted to provide the best possible performance for each individual insertion device.

A list of parameters of the linear lattice is given in Tab. 2.1, while Tab. 2.2 gives the lengths and strengths of the magnetic elements. Fig. 2.1 shows the behaviour of the optical functions over one period. The one standard deviation maximum sizes of the gaussian beam are

shown in Fig. 2.2: the horizontal beam sizes correspond to no coupling while the vertical ones correspond to full coupling. Actual beam sizes will be smaller, depending on the achieved coupling coefficient.

TABLE 2.1 - Parameters of the linear lattice

Energy (Gev)	1.5		2.0
Natural emittance (m.rad)	4.7×10^{-9}		8.4×10^{-9}
Natural energy spread	5.7×10^{-4}		7.6×10^{-4}
Momentum compaction		6.8×10^{-4}	
Horizontal betatron tune		19.830	
Vertical betatron tune		11.643	
Natural horizontal chromaticity		-32.43	
Natural vertical chromaticity		-22.92	
Circumference (m)		300.22	
Horizontal betatron damping time (ms)	33.8		14.2
Vertical betatron damping time (ms)	33.5		14.1
Synchrotron damping time (ms)	16.7		7.0
Number of periods		16	
Number of bending magnets		32	
Bending radius (m)		5.0	
Field index		0	
Shape		Rectangular	
Bending field (T)	1.0		1.333
Number of quadrupoles		176	
Number of independent quadrupole families		6	
Maximum gradient (T/m)	12.8		17.0

TABLE 2.2 - Magnetic structure of half superperiod (2 Gev).

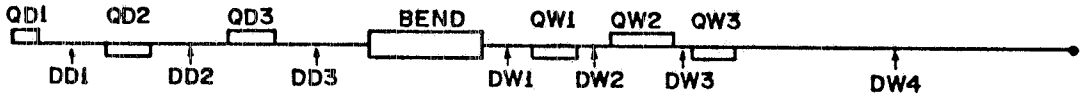

Name	Type	Length (m)	Gradient (T/m)	Field (T)
QD1*	H-Quadrupole	0.2	11.6625	
DD1	Drift	0.7		
QD2	V-Quadrupole	0.4	12.8178	
DD2	Drift	0.7		
QD3	H-Quadrupole	0.4	15.7034	
DD3	Drift	0.8		
Bend	Bending magnet	0.98175		1.3333
DW1	Drift	0.4		
QW1	V-Quadrupole	0.4	15.7061	
DW2	Drift	0.3		
QW2	H-Quadrupole	0.55	17.0318	
DW3	Drift	0.15		
QW3	V-Quadrupole	0.4	8.3111	
DW4	Drift	3.0		

* The second half period is obtained by reflection with respect to the center of QD1, which is therefore only half of a single 0.4 m quadrupole. Gradients are calculated for 2 Gev.
H denotes a horizontally focusing quadrupole, while V is for vertically focusing quadrupole.

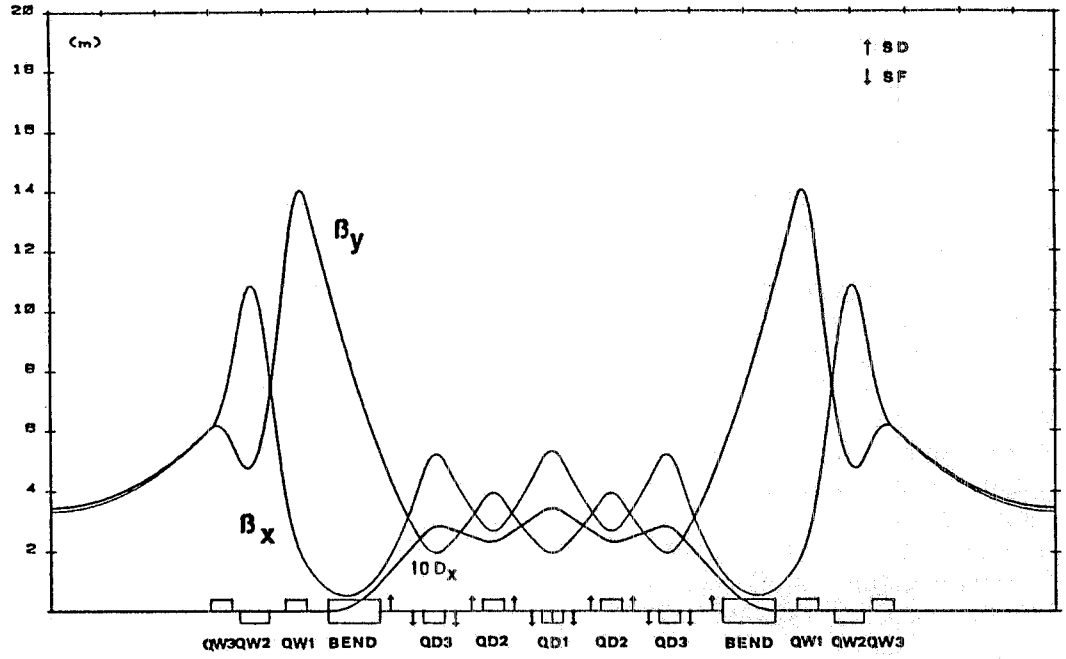

FIG. 2.1 - β functions and dispersion in one period of the ECG structure.

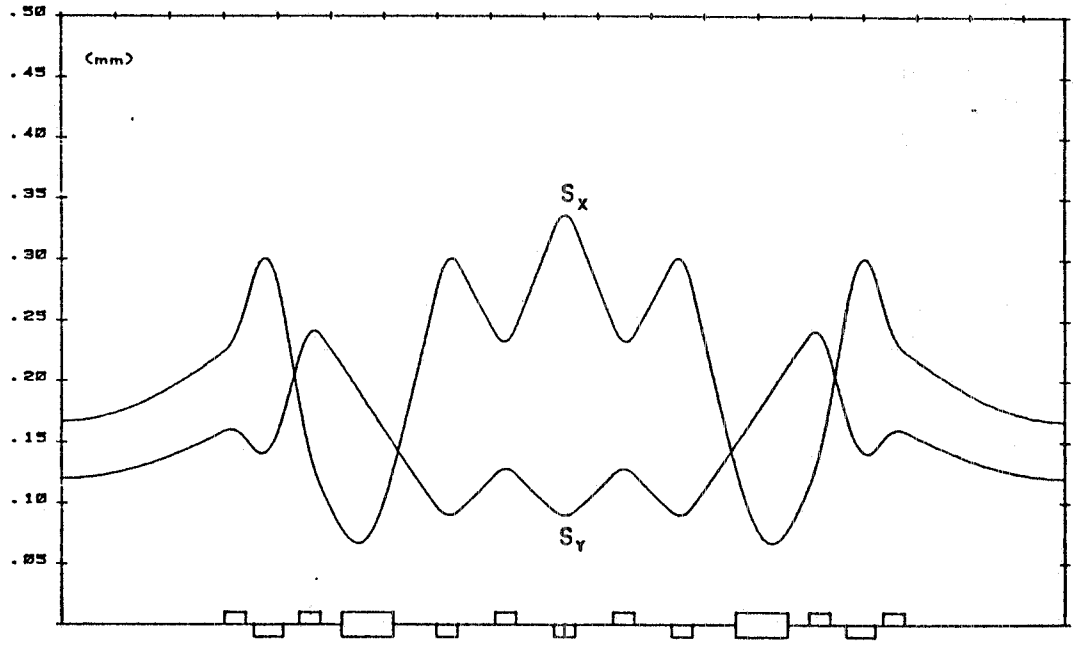

FIG. 2.2 - R.m.s. beam size in one period of the machine at maximum energy (2 Gev). The horizontal beam size is calculated without coupling, while the vertical is in full coupling.

2.3. - Chromaticity correction and aperture

2.3.1. - Perfect machine

The chromaticities ($\xi = \Delta Q / (\Delta p/p)$) of low emittance lattices for synchrotron light sources are normally rather large in both planes and have to be corrected. The correction, as computed by the program PATRICIA (Ref.2.30), requires two independent sextupole families, SF and SD. Their distribution is shown in Fig. 2.1. The sextupole gradients needed for zero

chromaticity at 2 Gev, with 0.2 m long sextupoles are:

$$(\delta^2 B/\delta x^2)_{SD} = 615 \quad T/m^2 \qquad (\delta^2 B/\delta x^2)_{SF} = 522 \quad T/m^2 \qquad (2.3.1)$$

These values are higher than required by other lattices of the same kind, because of the small value of the dispersion ($D_x \sim 0.3$ m) and of the small separation of the ß functions in the achromat. The total number of sextupole magnets is 192. The sextupoles must also minimize other unwanted non-linear effects such as the dependence on momentum of the tune, the β functions and the dispersion D_x.

For good Touschek lifetime, as computed with the program ZAP (Ref. 2.31), a good behaviour of these functions in the range $-3\% \leq \Delta p/p \leq 3\%$ is required.

Figures 2.3 and 2.4 show the behaviour of the functions β and D_x at the insertion point versus energy deviation. Fig. 2.5 shows the behaviour of the tunes.

The overall lattice behaviour versus particle oscillation amplitude, deduced from tracking and shown in Fig. 2.6, is good up to amplitudes corresponding to ≈100 beam dimension standard deviations for on-energy particles. No additional sextupole families are needed to correct the tune-shift on amplitude. The tune behaviour as a function of particle amplitude for off-energy particles (± 3%) is also plotted in Fig. 2.6.

The aperture has been computed using the program DIMAD (Ref. 2.32) that allows many particles to be tracked simultaneously.

Particles at three fixed momentum deviations, $\Delta p/p = 0, -3\%, +3\%$, have been tracked over 400 turns . Note that one full synchrotron oscillation corresponds to about 160 turns. The results are shown in Fig. 2.7.

The dynamic aperture for on-energy particles is good. We want to stress that in calculating dynamic apertures a particular care has been put into ensuring, by suitably smoothing the contours, that no unstable islands exist within the indicated stable area. Fig. 2.8 shows some examples of space-phase trajectories for on-energy particles with different horizontal initial conditions and vanishing vertical initial amplitudes and angles. Under some condition the dynamic aperture for off-energy particles is reduced, but is still sufficient to achieve the required Touschek lifetime (Ref. 2.31).

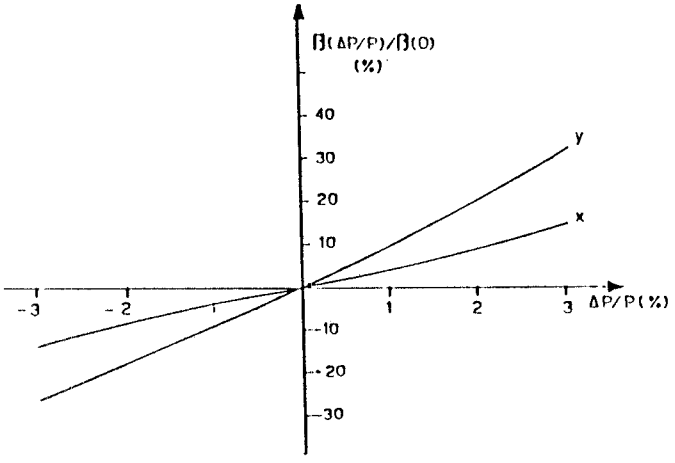

FIG. 2.3 - Dependence of β functions in the center of the undulator straight section on momentum deviation.

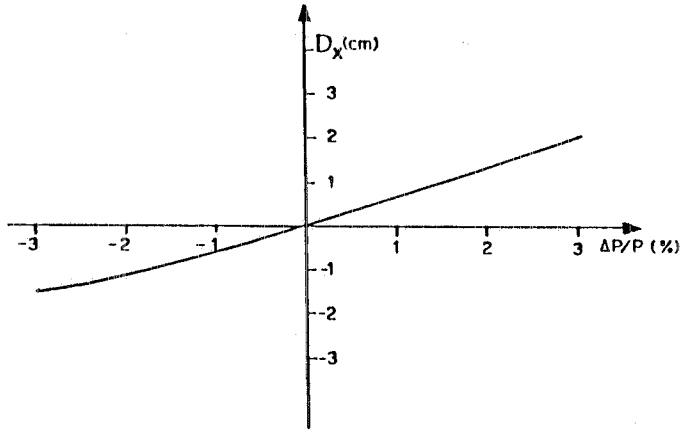

FIG. 2.4 - Dependence of the horizontal dispersion in the center of the undulator straight section on momentum deviation.

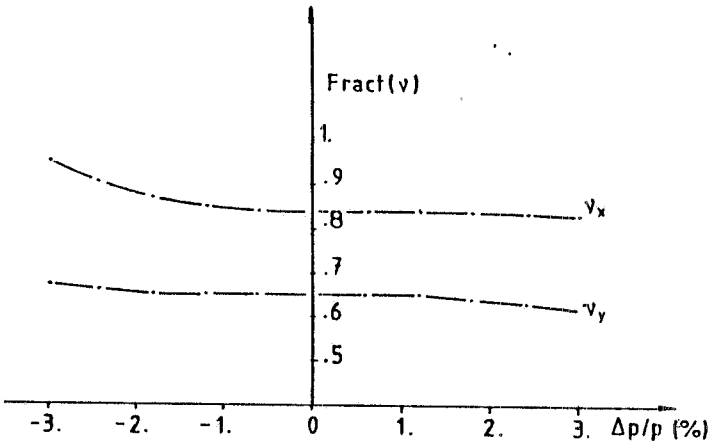

FIG. 2.5 - Dependence of betatron tunes on momentum deviation.

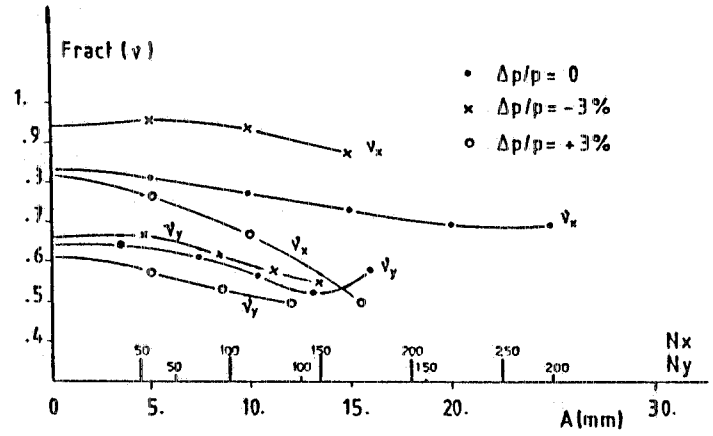

FIG. 2.6 - Dependence of tunes on betatron oscillation amplitude for on energy and off energy particles.

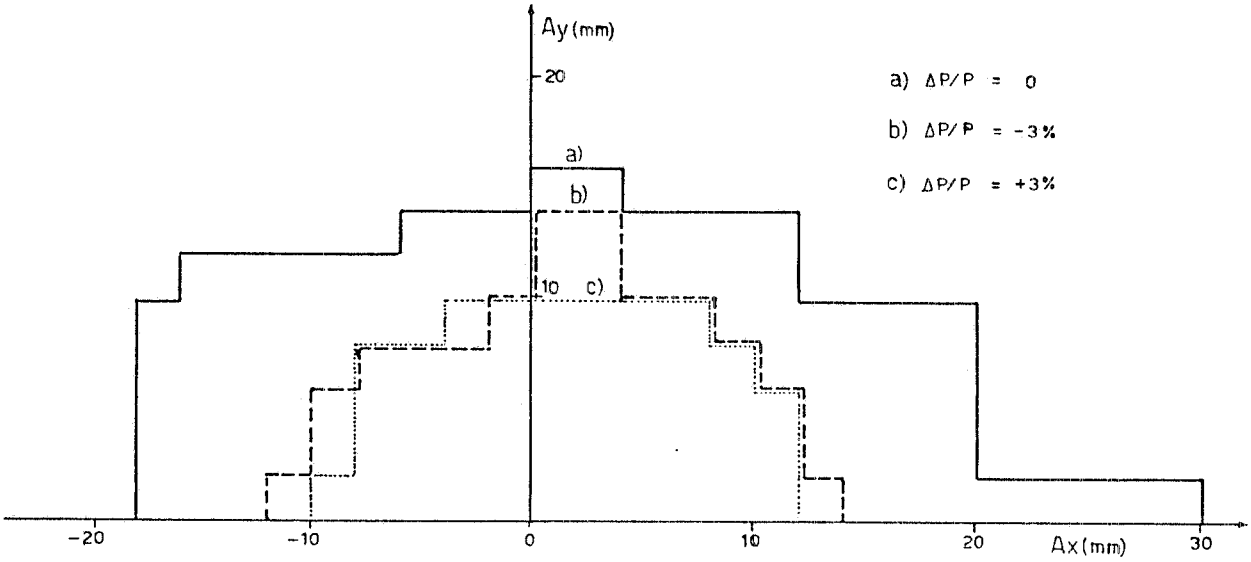

FIG. 2.7 - Dynamic aperture for on energy particles and for energy deviations of +3% and -3%.

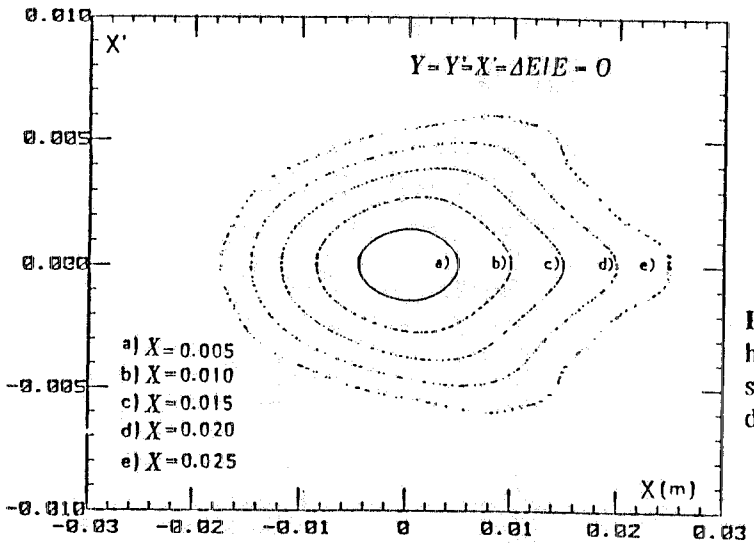

FIG. 2.8 - Phase space trajectories in the horizontal plane at the center of the undulator straight section for betatron oscillations with different initial conditions.

2.3.2. - Effect of field errors on the aperture

The effect of field errors on particle stability and the related aperture limitations have been investigated using DIMAD (Ref. 2.34). The error magnetic field is expanded in terms of multipole components, defined in the program by the relation :

$$B(x) = B\rho \, \Sigma_n \, K_n \, (x^n/n!) \qquad (2.3.2)$$

where n = 0 corresponds to the dipole term, n = 1 to the quadrupole term, etc., and the sum is carried over all relevant multipoles.

A set of "systematic" errors , as calculated by the program MAGNET (Ref. 2.33), has been used (see Table 2.3). The error field values are computed at a distance x = 0.01 m from the axis. The "random" components coming from construction tolerances are of course different for each magnet and are present in principle at all orders.

To test the lattice sensitivity a complete study has been carried out (Ref. 2.34) using three different sets of possible values for the theoretically most dangerous multipoles.

Table 2.4 lists the multipole components and their rms strengths, as obtained from the estimated construction tolerances, for the set (SET 1) which is considered the the most likely to actually occur.

TABLE 2.3 - Systematic field errors.

	DIPOLES		QUADRUPOLES	
n	B_n/B_o	K_nL (m^{-n})	G_n/G_o	K_nL (m^{-n})
1	6.4×10^{-6}	1.3×10^{-4}	0.	0.
2	1.7×10^{-5}	6.8×10^{-2}	0.	0.
5	0.	0.	1.3×10^{-4}	$6. \times 10^{5}$

N.B.: The '0.' means the component is not dangerous, and has therefore been neglected.

TABLE 2.4 - Random errors - Set 1.

	DIPOLES		QUADRUPOLES	
n	B_n/B_o	K_nL (m^{-n})	G_n/G_o	K_nL (m^{-n})
1	10^{-5}	2.0×10^{-4}	10^{-5}	4.0×10^{-6}
2	10^{-4}	4.0×10^{-1}	10^{-5}	8.0×10^{-4}
3	10^{-5}	12.0	10^{-5}	0.24
4	10^{-5}	4.8×10^{3}	10^{-5}	96.0
5	0.	0.	10^{-5}	4.8×10^{4}
9	0.	0.	10^{-7}	1.5×10^{14}

Fig. 2.9 shows the effect of systematic components in the bending magnets and in the quadrupoles. The unperturbed dynamic aperture is also shown.

Fig. 2.10 shows the aperture in the presence of both systematic and random multipoles, the latter corresponding to the values of SET 1, computed for four different arrangements of random errors. The aperture reduction is small.

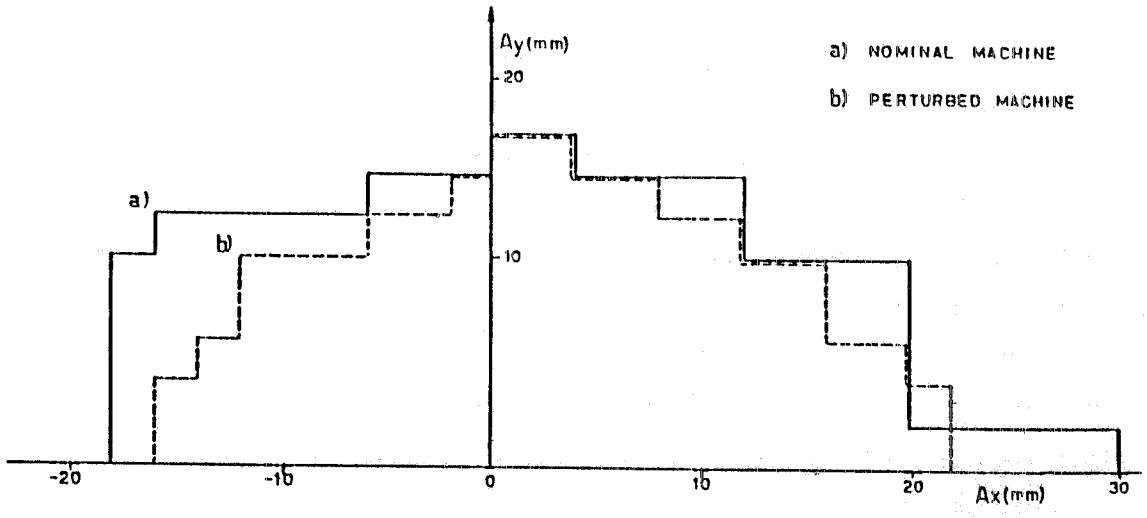

FIG. 2.9 - Reduction of dynamic aperture due to systematic high order field components in dipoles and quadrupoles (Table 2.3).

The shapes of the aperture when SETS 2 or 3 are used instead of SET 1, are not too different from those shown in Fig. 2.10 (see Fig. 10 in Ref. 2.34). We can therefore conclude that the reduction of the dynamic aperture caused by any one of the the three possible sets of random errors is well tolerable.

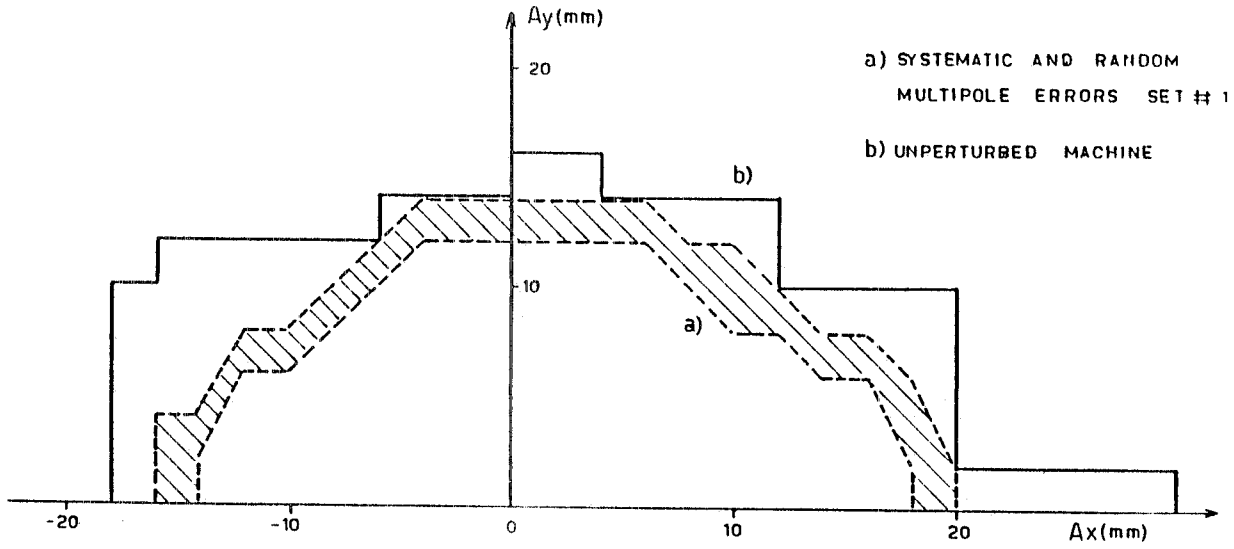

FIG. 2.10 - Reduction of dynamic aperture due to both systematic and random high order field components in dipoles and quadrupoles (Tables 2.3 and 2.4). The band in the figure includes 4 different simulations of random errors.

2.4. - Sensitivity to alignment and field errors. Orbit correction

2.4.1. - Sensitivity to alignment and field errors

The sensitivity of the machine to alignment and field errors has been investigated, using the program PETROS (Ref. 2. 35).

The simulation of 10 machines has been carried out under the assumption of Gaussian distributions of errors with the following rms values:

- horizontal displacement	Δx	=	0.1	mm
- vertical displacement	Δy	=	0.1	mm
- tilt	$\Delta\alpha$	=	0.01°	
field strength	$\Delta B/B$	=	5×10^{-4}	

All machines were stable.

Quadrupole displacements are shown to be responsible for the largest contributions to closed orbit distorsions. To check misalignment tolerances, the same 10 machines have been simulated with quadrupole displacements increased by factors from 2 to 5. The percentage of stable machines for each case is given in Table 2.5.

TABLE 2.5 - Results of PETROS simulations.

Errors	ε	2ε	3ε	4ε	5ε
Stable machines over 10 simulations	10	10	6	3	1
ε = nominal error sets					

Some characteristic parameters averaged over the machines that were simulated using the nominal set of errors are given in Table 2.6 together with the corresponding unperturbed values. Note that some of the latter differ slightly from those shown in Table 2.1; this is due to the fact that in the PETROS simulation runs the quadrupoles were split in order to provide room for the orbit correctors designed to be implemented by auxiliary coils on the quadrupoles themselves (Ref. 2.35).

TABLE 2.6 - Parameters of the ring before and after correction.

Parameters		Unperturbed machine	Perturbed machine	Corrected machine
Q_x		19.828	19.783 ± 0.033	19.836 ± 0.008
Q_y		11.673	11.624 ± 0.024	11.679 ± 0.008
$J_x/2$		0.500	0.5260 ± 0.018	0.4980 ± 0.001
$J_y/2$		0.500	0.5010 ± 0.003	0.5000 ± 0.000
$J_s/2$		1.000	0.9720 ± 0.018	1.0020 ± 0.002
$\langle x^2 \rangle^{1/2}$	(mm)	0.0	4.0 ± 1.7	0.2 ± 0.2
x_M	(mm)	0.0	8.4 ± 3.2	0.6 ± 0.4
$\langle y^2 \rangle^{1/2}$	(mm)	0.0	2.0 ± 0.5	0.1 ± 0.0
y_M	(mm)	0.0	6.3 ± 1.4	0.4 ± 0.2
$\langle D_x^2 \rangle^{1/2}$	(m)	0.149	0.152 ± 0.002	0.150 0.000
D_{xM}	(m)	0.342	0.384 ± 0.015	0.368 ± 0.007
$\langle D_y^2 \rangle^{1/2}$	(m)	0.000	0.015 ± 0.004	0.008 ± 0.002
D_{yM}	(m)	0.000	0.058 ± 0.012	0.028 ± 0.007
$\varepsilon_x 10^9$	(m.rad)	4.41	4.25 ± 0.22	4.45 ± 0.13
$\varepsilon_y 10^9$	(m.rad)	0.00	0.21 ± 0.02	0.03 ± 0.02
$(\varepsilon_y/\varepsilon_x)10^2$		0.00	5.10 ± 3.50	0.70 ± 0.40
$\alpha_c 10^4$		6.64	6.68 ± 0.06	6.62 ± 0.05
θ_{xm}	(mrad)	–	–	0.26 ± 0.04
θ_{ym}	(mrad)	–	–	0.27 ± 0.04

The computed amplitude of the average closed orbit is in good agreement with that estimated using the standard formula for a random distribution of quadrupole displacements with an r.m.s. value Δz:

$$< z_{co} > = ((\sqrt{\beta}\ \Delta z\ )/(\sqrt{8}\ \sin \pi\ Q\ )\ (\ \Sigma_i\ K_i^2\ L_i^2\ \beta_i)^{1/2} \qquad (2.4.1)$$

where K_i, L_i, β_i are the strength, the length and the average β at the i-th quadrupole. The amplification factors computed from Eq. (2.4.1) are:

$$<x_{co}>/\Delta x = 41 \qquad <y_{co}>/\Delta z = 28 \qquad (2.4.2)$$

Beam parameters are not very sensitive to alignment and field errors; the uncorrected closed orbit does not require additional injection aperture.

2.4.2 Closed orbit correction

The position and distribution of monitors and correctors over 1/16 of the ring is shown in Figure 2.11. A total of 80 horizontal correctors, 48 vertical correctors and 128 monitors is foreseen. The correctors are implemented using auxiliary dipole windings in the quadrupoles, capable of delivering on axis up to 10% of the maximum pole tip field; the monitors are adjacent to the quadrupoles.

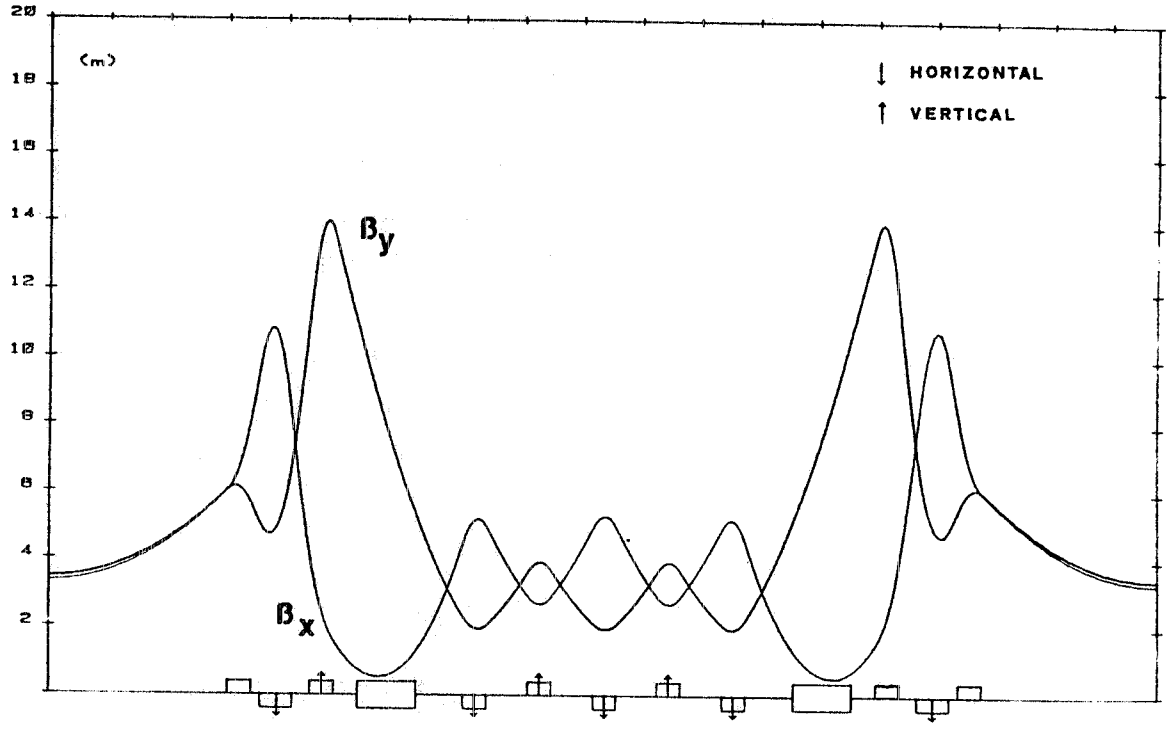

FIG. 2.11 - The position of monitors and correctors in 1/16 of the ring for the PETROS simulation of orbit correction. Upward arrows indicate the position of vertical dipole correctors, while the downward are for the horizontal ones. Position detectors are superimposed to the correctors.

In the simulation with PETROS correctors and monitors have both been placed at the midpoint of the corresponding quadrupoles. Although each of the 128 monitors could in

principle be used to measure the beam position in both planes, only 80 monitors in the horizontal plane and 48 in the vertical one (see Fig. 2.11) have actually been used for the simulation.

The best corrector method (Ref. 2.36) has been used. It proved to be effective in the vertical plane. In the horizontal plane 2 to 3 iterations have sometimes been necessary to achieve closed orbit r.m.s. amplitude smaller than 0.5 mm.

Table 2.6 gives the results , averaged over the simulated machines. The maximum required corrector strength ($\theta_{x,ym}$ in Table 2.6) is a factor of 10 below the maximum allowed one.

Monitor displacement errors of the order of the quadrupole displacements do not affect the end result but increase the required corrector strengths by $\approx 10\%$.

In conclusion, the overall correction method gives good results in both planes by letting the r.m.s. closed orbit to be reduced by a factor ≈ 20 with corrector strengths that are easily obtained by means of additional dipole windings on the quadrupoles.

2.5. - Injection scheme

The proposed lattice has very long insertion straight sections and a crowded dispersive region. A solution where all injection magnets are placed in a single long straigth section has therefore been studied.

Such a solution requires strong kickers, but has the advantage of being independent from the values of ß at the injection point. Consequently, injection into a machine configuration with a rather low β in all insertion straigths, as required for optimum brilliance, does not put any additional constraint on the lattice design or on apertures.

Injection is designed to take place in the horizontal plane: four fast kickers are used to produce a localized orbit bump at the injection point and two septum magnets, a thin one and a thicker one, are used to impart the final deflection to the incoming beam. Table 2.7 lists the characteristics of these magnetic elements.

TABLE 2.7 - Injection elements

	L(m)	α(mrad)	B(T)	Δs (mm)	τ(µs)
Kicker	0.80	12.5	0.1	-	2
Thin septum	0.60	36.0	0.4	1	30
Thick septum	1.00	146	1.0	6	100

TABLE 2.8 - Injection parametres.

Energy	Gev	2.0
Horizontal ring emittance	m.rad	$2 \times 8.3\ 10^{-9}$
Horizontal injector emittance	m.rad	$9 \times 5.9\ 10^{-7}$
β_x at injection point	m	3.3
β_x maximum	m	11.0
β_i at end of transport channel	m	1.7
Effective septum thickness	mm	5
Orbit displacement at septum	mm	13
Septum position	mm	14
Free aperture radius at injection	mm	12
Maximum horizontal aperture	mm	22
Maximum vertical aperture	mm	7

2.6. - Vacuum chamber aperture

The following requirements have to be taken into account in the choice of the vacuum chamber aperture:

- good quantum lifetime;
- space for injection in the horizontal plane;
- good Touschek lifetime;
- good gas scattering lifetime.

Table 2.9 shows the free diameter of the vacuum chamber needed to satisfy each of these requirements. The Table also lists the value of the dynamic aperture scaled to the maximum β point, so that the required physical aperture and the dynamic aperture can be directly compared.

TABLE 2.9 - Aperture requirements.

	A_x (mm)	A_y (mm)
Quantum lifetime	8.5	7.5
Injection	48	18
Gas scattering	50	29
Touschek effect	45	4
Dynamic aperture	61	63

The injection parameters, computed at 2 GeV are shown in Table 2.8: for safety a stored beam emittance a factor of two larger than the design value has been assumed. Also, to account for the injector beam not being completely damped, and to correctly estimate the injection

acceptance, the booster horizontal beam size has been taken at the 3σ point and for a vanishing coupling coefficient. A 5 mm effective septum thickness has been used to take into account power supply jitters and misalignments.

The horizontal half-aperture needed to accomodate injection is 22 mm.

In the vertical plane the required aperture has been computed using a 10% vertical to horizontal emittance ratio for the booster beam and allowing for a 2 mm position error at the septum.

A 4 mm closed orbit has been added in both planes to obtain the final required vacuum chamber aperture.

A beam stay clear region of at least 2x10 σ's is required to achieve a good quantum lifetime.

Touschek lifetime calculations are described in detail in Ref. 2.31, where it is shown that a $\pm 3\%$ momentum acceptance is needed for good lifetime. Consequently, the requirements on the chamber full aperture, A, are :

$$A \geq A_T = 2 \max \{(D_x (s) + D_x^* (\beta(s)/\beta^*)^{1/2}) (\Delta p/p)_m\} \qquad (2.6.1)$$

where $(\Delta p/p)_m = 3\%$ and D_x^*, β^* are computed at the azimuth where D_x/β is maximum.

At a nitrogen equivalent residual pressure, P, of $2.66\ 10^{-7}$ Pascal (2 nTorr) and with a $\pm 3\%$ energy acceptance the lifetime for inelastic scattering is $\tau_b = 36$ hours. To achieve a 20 hours total elastic plus inelastic gas scattering lifetime at 1.5 GeV, the elastic scattering lifetime, τ_e, must reach 45 hours. This specifies the minimum required physical (or dynamic) minimum normalized apertures. A value of 50 mm has therefore been specified.

A 50x30 mm^2 vacuum chamber cross section, that still fits within the dynamic aperture, satisfies injection and scattering lifetime requirements in both planes.

In the undulator straights a reduction of the vertical aperture to 15 mm would be tolerable because of the low value of the local β_z.

However, further considerations concerning mainly the microwave instability threshold impose a larger value for the vertical aperture in the insertion straight sections. Detailed calculations on lifetimes, instabilities, and on the effect of the chamber size and impedance are given in Chapter 3. It is concluded there that it is advisable to specify a vacuum chamber minimum vertical diameter at 50 mm everywhere except in the bending magnet where 38 mm is tolerable and in the undulators where the chamber can be reduced to 20 mm.

2.7. - Effects of Insertion Devices on the Beam

2.7.1. - Linear effect of the undulators

Beam emittance, beam size and beam energy spread have been calculated as a function of total undulator length and field (Ref. 2.37). An undulator with a period , λ_u of 2.95 cm (Ref.2.38) which, with a peak field, B_u, of 0.28 T gives 1 KeV in the first harmonic at 2 GeV, has been used. Fiver meter long modules have been considered .

Fig. 2.12 shows the behaviours of $\varepsilon/\varepsilon_0$ and of σ_p/σ_{po} as functions of the undulator field in two cases: a machine containing 6 undulator modules and one with 12 modules.

Fig. 2.13 shows the behaviour of σ_x/σ_{xo} for the same two cases. All quantities have been computed at 2 GeV.

The same calculations have been performed as a function of the number of undulator modules at a fixed peak field of .28 T. Figg. 2.14 shows the results: the effect is negligible even when all straights are occupied.

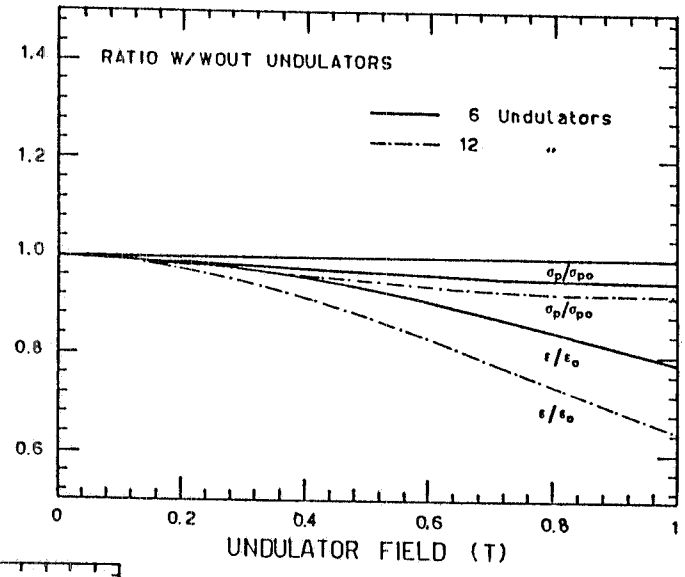

FIG. 2.12 - Beam energy spread and emittance as a function of undulator field with 6 and 12 5m long undulators, referred to their values for the machine without undulators.

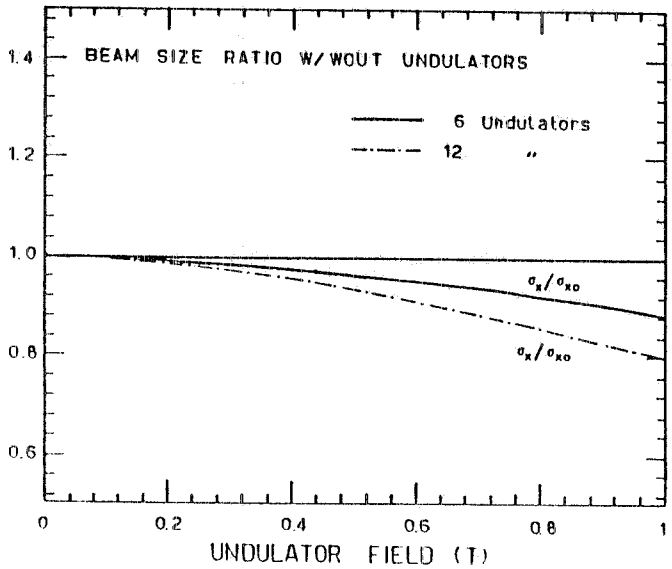

FIG. 2.13 - Horizontal r.m.s. beam size at the center of the undulator straight section as a function of undulator field with six and twelve 5m long undulators, referred to its value in the machine without undulators.

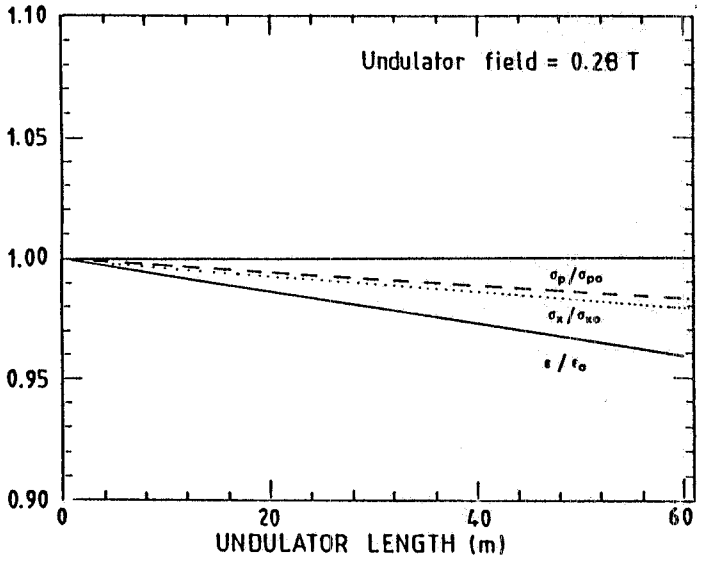

FIG. 2.14 - Energy spread, emittance and horizontal beam size at the center of the undulator straight section as a function of total undulator length (each undulator is 5m long), referred to their values for the machine without undulators.

2.7.2 - Linear effect of the wigglers

A 5 m long wiggler module with 10 poles and a period λ_w of 0.5 m has been used. Figs. 2.15 and 2.16 show the behaviours of $\varepsilon/\varepsilon_o$, σ_p/σ_{po} and σ_x/σ_{xo} as functions of the wiggler field, for a machine with 1 and 2 wigglers respectively.

The behaviour of beam emittance, size and energy spread as functions of the total wiggler length, for several peak fields, is shown in Figs. 2.17 to 2.19. The effect of one 5 Tesla wiggler module on ε and σ_x is negligible but there is a strong effect on the energy spread.

When the number of wiggler modules is increased, it is seen from the figures that the energy spread can increase by factors of the order of 1.7, thereby decreasing the relative momentum acceptance down to $\approx 23\ \sigma_p$ at 2 Gev. This figure is however still acceptable for the point of view of quantum lifetime considerations.

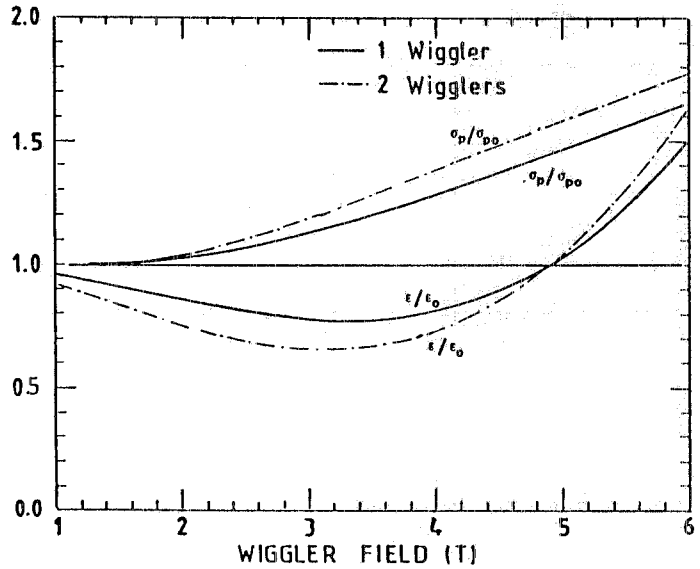

FIG. 2.15 - Beam energy spread and emittance versus maximum field of one and two 10 pole wigglers (λ_w = 0.5 m), referred to their values for the machine without wigglers.

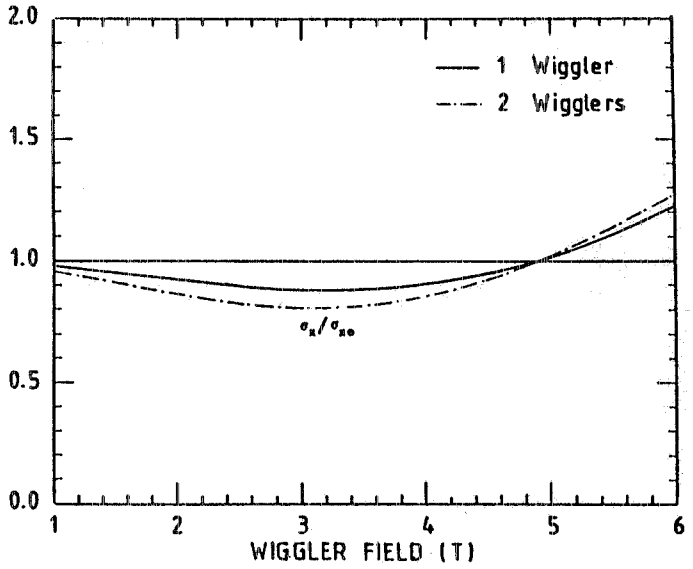

FIG. 2.16 - Horizontal r.m.s. beam size at the center of the wiggler straight section versus maximum field of one and two 10 pole wigglers (λ_w = 0.5 m), referred to its value in the machine without wigglers.

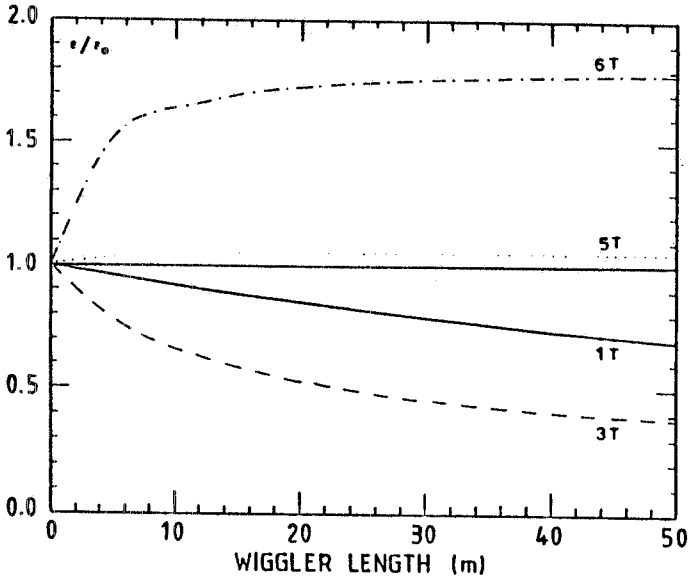

FIG. 2.17 - Beam emittance as a function of total wiggler length for different peak wiggler fields, referred to its value in the machine without wigglers.

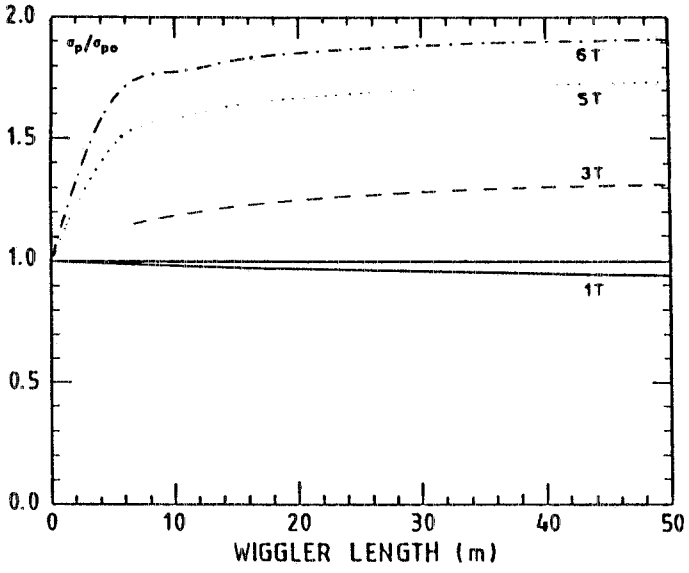

FIG. 2.18 - Beam energy spread as a function of total wiggler length for different peak wiggler fields, referred to its value in the machine without wigglers.

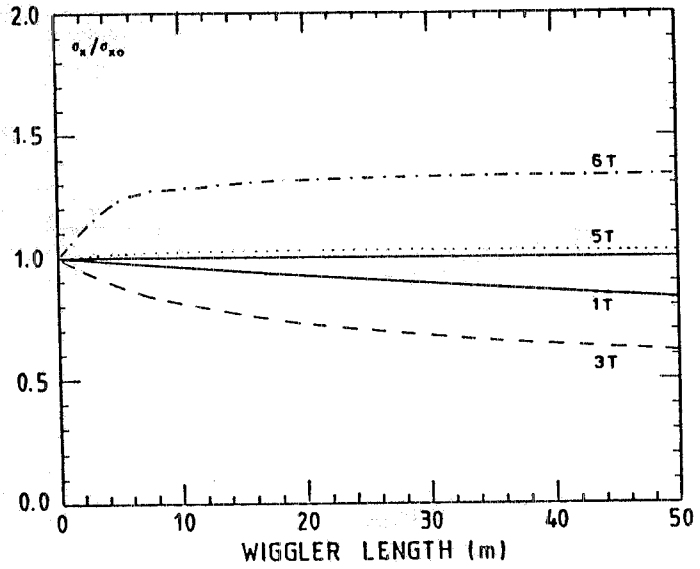

FIG. 2.19 - Horizontal r.m.s. beam size at the center of the wiggler straight section as a function of total wiggler length for different peak wiggler fields, referred to its value in the machine without wigglers.

2.7.3 - Nonlinear effect of the undulators

The effect on the dynamic aperture of the insertion of undulators in the lattice has been investigated using the program RACETRACK (Ref. 2.39). A total number of 8 undulators (0.28 T peak field) has been considered, so that the machine periodicity is reduced from 16 to 8.

The betatron functions have been matched using two of the three quadrupoles in the insertion triplets. The resulting dynamic aperture at the undulator straight section center is shown in Fig. 2.20, compared to the corresponding one of the perfect machine: the reduction is not negligible, but the stable region in the vertical plane is still larger than the undulator gap (15-20 mm).

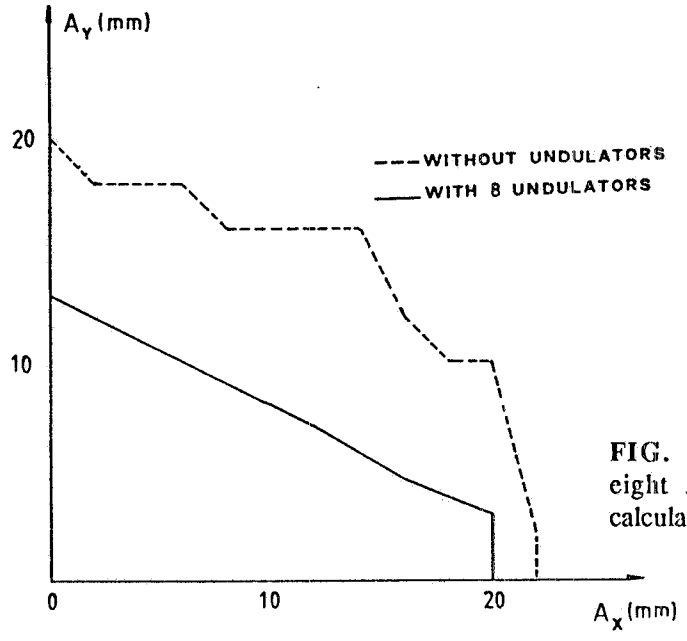

FIG. 2.20 - Dynamic aperture reduction with eight 5m long undulators (0.28 T peak field) calculated with the program RACETRACK.

2.8. - Beam parameters at the sources

The sources of synchrotron radiation are located within the straight sections where insertion devices are installed and in the neighbourhood of the leading edge of the second bending magnet in the achromat.

For the purpose of estimating the contribution of the beam parameters to the overall phase space distribution of the outcoming radiation, it is assumed that the source is point-like. Beam sizes and divergences have therefore been calculated at the center of the insertion straight section for wiggler and undulator ports, and at the leading edge of the bending magnet for magnet ports. A 10% coupling coefficient, the nominal radial emittance and the nominal energy spread have been used.

The relevant general parameters are consequently the following:

Energy	(Gev)	2.0	
Natural emittance	(m.rad)	8.4	10^{-9}
Horizontal emittance	(m.rad)	7.6	10^{-9}
Vertical emittance	(m.rad)	7.6	10^{-10}
Energy spread	(r.m.s.)	7.6	10^{-4}

and the beam size data at the source points are:

		W/U	Bend
β_H (m)		3.33	1.31
β_V(m)		3.46	5.27
$((1+\alpha^2)/\beta)_H$		0.30	1.85
$((1+\alpha^2)/\beta)_V$		0.29	1.17
D_H(m)		0.00	0.096
D'_V		0.00	0.195
σ_H	(mm)	160	124
σ'_H	(mrad)	48	191
σ_V	(mm)	51	64
σ'_V	(mrad)	15	30

where α and β are the usual lattice functions, D the dispersion and D' its space derivative, σ the beam dimension standard deviation, σ' the beam divergence standard deviation, and the subscripts H and V indicate the horizontal and vertical plane respectively.

REFERENCES

(2.1) M. Sommer "Optimisation de l'emittance d'une machine pour rayonnement synchrotron" - LAL Internal Report DCI/NI/20-81 and SUPERACO/LAL/81/05.

(2.2) D. Potaux "Quelques expressions simples concernant l'optimisation de l'invariant betatron dans un anneau pour le rayonnement synchrotron" - LAL Internal Report DCI/NI/30-81 and SUPERACO/LAL/81-06.

(2.3) H. Wiedemann "Linear theory of the ESRP lattice" - ESRP Internal Report ESRP-IRM-9/83

(2.4) D. Potaux "A lattice parametrization for emittance optimization" - ESRP Int. Rep. ESRP-IRM-87/84.

(2.5) R.H. Helm and H. Wiedemann "Emittance in a FODO cell lattice" - PEP Note 303 (1979), SLAC.

(2.6) L. Teng "Minimum emittance lattice for synchrotron radiation storage rings" - Fermilab Internal Report LS-17 (1985).

(2.7) A. Wrulich "Study of FODO structures for a synchrotron light source" - LBL Preprint LBL-21215 (1986) (Submitted to Particle Accelerators).

(2.8) M. Biagini, C. Biscari, E. Gianfelice, M. Preger "Scaling della struttura di ESRP ad un anello per luce di sincrotrone da 2 Gev" - Adone Int. Memo G-57, (1985).

(2.9) M. Preger "Struttura ottica detunata per Afrodite (AF2)" - Adone Int.Memo G-58 (1985).

(2.1) P. Patteri, M. Preger "Struttura ottica AF3 di Afrodite con 6 wigglers e 6 ondulatori" - Adone Int. Memo G-61 (1985).

(2.11) M. Preger "Struttura AF5 per Afrodite" - Adone Int. Memo G-63, (1985).

(2.12) S. Guiducci, M. Preger "Struttura AF6 per Afrodite" -Adone Int. Memo G-64 (1985).

(2.13) P. Patteri, M. Preger "Struttura AF7 per Afrodite" - Adone Int. Memo G-65 (1985).

(2.14) C. Biscari - "Struttura AF8 per Afrodite" - Adone Int. Memo G-67 (1985).

(2.15) S. Guiducci "Struttura AF9 per Afrodite" - Adone Int. Memo G-68 (1985).

(2.16) E. Gianfelice - "Struttura AF10 per Afrodite" - Adone Int. Memo G-70 (1985).

(2.17) E. Gianfelice "Struttura AF10b" - Adone Int. Memo G-74 (1986).

(2.18) C. Biscari, L. Palumbo "Struttura AF11a (Expanded Empty FODO) per Afrodite" - Adone Int. Memo G-76 (1986).

(2.19) C. Biscari, L. Palumbo "Struttura AF11b per Afrodite" - Adone Int. Memo G-77 (1986).

(2.20) M. Biagini, S. Guiducci "Ottimizzazione del punto di lavoro per Afrodite Empty-FODO a 16 periodi (AF11c)" - Adone Internal Memorandum AF-4 (1986).

(2.21) M. Biagini, S. Guiducci "TBA a 16 periodi" - Adone Int. Memo AF-8 (1986).

(2.22) C. Biscari "Struttura AF11d per Afrodite" - Adone Int. Memo AF-10 (1986).

(2.23) M. Biagini, C. Biscari "Struttura ECG16" - Adone Int. Memo AF-14 (1986).

(2.24) A. Jackson "A comparison of the Chasman Green and Triple Bend Achromat lattices" LBL Preprint LBL-21279 (1986) (Submitted to Particle Accelerators).

(2.25) M. Zisman "Parameter studies of candidate lattices for the 1-2 Gev Synchrotron Radiation Light Source" - LBL Internal Report LBL-21760.

(2.26) M. Cornacchia et al. "Comparison of lattice options for a 1-2 Gev Synchrotron Light Source" - LBL Report (to be published).

(2.27) A Ropert "A few comments on the dynamic aperture of the ESRP-27" - ESRF Int. Rep. ESRF-SR/LAT-86-01.

(2.28) "1-2 Gev Synchrotron Radiation Source" Conceptual Design Report PUB-5172 Rev LBL (1986).

(2.29) C. Biscari, S. Guiducci "Struttura CG16" - Adone Int. Memo AF-18 (1986).

(2.30) H.Wiedemann "Chromaticity correction in large storage rings" - PEP-220, 1976.

(2.31) E.Gianfelice, L. Palumbo, M. Zisman - Adone Int. Memorandum, to be published.

(2.32) R.V.Servranck, K.L. Brown, L. Schachinger, D. Douglas " User Guide to the program DIMAD" - SLAC REPORT 285 UC-28.

(2.33) A. Cattoni, C. Sanelli, private communication.

(2.34) M. Biagini "Expanded Chasman Green 16 periods dynamic aperture" - Adone Int Memo AF-22 (1986).

(2.35) C. Biscari, E. Gianfelice "Sensitivity of the ECG16b to position and field errors and closed orbit correction" - Adone Int. Memo AF-25 (1987).
(2.36) G. Guignard, Y. Marti "PETROC Users Guide" - CERN/ISR-BOM-TH/81-32.
(2.37) M. Biagini "ECG16 - Effect of undulators on beam parameters" - Adone Int. Memo AF-26 (1987).
(2.38) S. Bartalucci, R. Coisson "Un ondulatore per Afrodite: studio preliminare" - Adone Int. Memo G-69 (1985).
(2.39) A. Wrulich "RACETRACK - A computer code for the simulation of Nonlinear Particle Motion in Accelerators" - ISSN 0418-9833 DESY 84-026 (1984).

3. - BEAM STABILITY AND LIFETIMES

3.1. - Introduction

For the best performances of the synchrotron radiation source stringent requirements are placed on the beam quality. Very low emittances, high currents in the single bunch and in the multibunch mode of operation, short bunch lengths, long lifetimes and the stablest possible beams are all required at the same time, thereby putting severe constraints on the design of the overall system.

The parameters are very much interconnected: single-Touschek lifetime is important at the energies we are concerned with and is determined by the bunch density and the momentum acceptance.

In turn the bunch volume, and therefore for a given current the bunch density, is determined by longitudinal (and possibly transverse) instabilities and by intrabeam (multiple Touschek) scattering, the momentum acceptance, the RF parameters and the lattice. Lifetimes and the currents are determined by the lattice, the chamber geometry and the RF cavity properties.

A self consistent computation has therefore to be carried out and an optimum, not easily definable in terms of simple rules, seeked.

In the following we present a short discussion of the main phenomena:

- single bunch instabilities:
- turbulent bunch lengthening;
- coupled bunch instabilities;
- emittance growth and;
- lifetimes.

Self consistent beam parameters are found using the code ZAP[3.1].

3.2. - Impedances

Instabilities can occur in both the longitudinal and the transverse space. They are caused by electromagnetic fields, excited in the interaction of the beam with its surroundings, acting back on the beam itself. The effect of the surroundings on the beam is schematized by means of "impedances" that can either appear at precise given frequencies (narrow band impedances) or be distributed over a wide frequency band (broad band impedances). Impedances determine instability thresholds and rise times.

Narrow band impedances have their origin either in the main RF cavities or in various cavity like structure that may be part of the vacuum chamber. They are characterized by a resonant angular frequency ω_r, a quality factor Q_S, and a shunt impedance R_S. The longitudinal impedance of a resonator is given by:

$$Z_{//}(\omega) = \frac{R_S}{[1 + iQ\,(\frac{\omega_r}{\omega} - \frac{\omega}{\omega_r})]} \tag{3.1}$$

while the transverse impedance is :

$$Z_{\perp}(\omega) = (\frac{\omega_r}{\omega}) \cdot \frac{R_{\perp}}{[1 + iQ\,(\frac{\omega_r}{\omega} - \frac{\omega}{\omega_r})]} \tag{3.2}$$

A real cavity exhibits many such sharp resonances corresponding to the various possible resonant modes of the structure that can interact with the beam. The fundamental accelerating mode supplies energy to the beam; all the others resonances are called "parasitic ".

When a bunch traverses the cavity it gains energy from the accelerating voltage (fundamental mode) but will also lose energy to the various parasitic resonances. The electromagnetic energy thus stored in the cavity can affect the longitudinal and transverse motion of the following bunches. Individual longitudinal and transverse (deflecting) parasitic modes are in fact the main causes of multibunch instabilities.

Cavities also contribute to single bunch effects. In its passage through the cavity a bunch cannot resolve all the narrow band parasitic resonances but experiences an average effect that can be approximated by a broadband resonator with $\omega_r = c/b$ (where b is the effective beam pipe radius) and $Q_S = 1$. The low frequency broad band impedance divided by the mode number $n = \omega_r / \omega_o$ (ω_o is the revolution angular frequency) is estimated using the computed (or measured) parameters of the cavity higher order modes from :

$$(Z_{//}/n)^{RF}_{BB} = \sum_{2}^{N} \frac{R_S^{\,i}\ \omega_o}{Q_i\ \omega^i_r} \tag{3.3}$$

The vacuum chamber impedance includes the contribution from all the elements (bellows, discontinuities etc.) installed along the vacuum chamber. It is usually approximated by a broad band resonator with the same ω_r and Q_S values of the RF broad band resonator.

Therefore the (low frequency) effective broad band impedance is given by the sum of (3.3) and the contribution from the vacuum chamber

$$(Z/n)_{BB} = (Z/n)^{vc}_{BB} + N_{cells} \cdot (Z/n)^{RF}_{BB} \qquad (3.4)$$

The transverse effective broad band impedance (entering the analysis of single bunch transverse thresholds) is related to the longitudinal one by:

$$| Z_{\perp} | = (2R/b^2) \; | Z/n |_{BB} \qquad (3.5)$$

where R is the storage ring average radius.

3.3. - Single Bunch Instabilities and Bunch Length

3.3.1. - Longitudinal instabilities are not necessarily destructive and those due to narrow band impedances are taken care of by mode damping by proper control of the RF system or by feedback devices. The broad band impedance produces instabilities which can not easily be suppressed. Above a certain current experimental observations in many storage rings show that the bunch lenthens with an increase of the energy spread (called turbulence), i.e. bunch widening.

To the contrary, high frequency transverse instabilities are instead most often destructive. In particular the threshold for the so called "transverse turbulence" determines the single bunch maximum current.

3.3.2. - Broad band impedances and bunch length are affected by the choice of the RF parameters. The overall beam performance have been investigated for two different frequencies: 200 and 500 MHz[3.2].

The final choice in favour of a 500 MHz RF system is mainly dictated by the experimental requirement of short bunches in the single bunch mode of operation . To estimate the value of (Z/n) the resonance parameters listed in Table 3.1, taken from the KEK 500 MHz cavity, have been used, yielding an equivalent broad band impedance of .157 Ohms/cell. The cavity impedance contribution depends on the number of RF cells required to produce the specified voltage and therefore also on the maximum voltage that can be achieved in a single RF cell. It has been assumed that the chosen RF structure yields 500 KV/cell.

In the absence of an actual impedance inventory (or, preferably, actual measurements of the vacuum chamber broad band impedance) a vacuum chamber broad band impedance of 2 Ω is assumed as design aim. This seems a reasonable value not too far from the measured impedances of existing machines.

3.3.3. - The threshold for turbulent bunch lengthening is given by:

$$I_{//} = \frac{\sqrt{2\pi}\,\eta^2\,\sigma_p{}^3\,(E/e)}{(Z/n)_{BB}\;\nu_s\;R} \qquad (3.7)$$

where $\eta \sim \alpha_c$, σ_p is the rms momentum spread, and ν_s the synchrotron tune. Above the threshold value, $I_{//}$, calculated with the natural momentum spread the turbulence increases the momentum spread and the bunch lengthens.

The transverse threshold is given by :

$$I_{\perp} = \frac{4\,\eta^2\,\sigma_p{}^2\,(E/e)}{|Z_{\perp}|\,<\beta>\,b\;\nu_s\;R} \qquad (3.7)$$

where, assuming a circular cross section pipe, $<\beta>$ is the largest between the horizontal and vertical average beta functions around the machine.

Both thresholds increase with the momentum spread but the bunch lengthening one increases faster. The maximum allowed σ_p is that making the two thresholds the same. It is given by:

$$\sigma_p = \sqrt{2/\pi}\;(b/<\beta>) \qquad (3.8)$$

and is used in the calculations to determine the maximum allowed bunch current from Eq.3.7. The calculation could be pessimistic because experimental observations of bunch lengthening at SPEAR show that for bunches short in comparison with the beam pipe radius the effective longitudinal broad band impedance seen by the bunch decreases rapidly with bunch length, according to the so called "SPEAR scaling" law. The thresholds are correspondingly higher than those computed from equation (3.6).

In Fig. 3.1 the turbulent longitudinal and transverse peak current thresholds, and the average maximum bunch current, are shown as functions of the applied RF voltage for both the normal and the SPEAR scaling regimes. The nominal RF voltage is accordingly chosen to be 1.5 MV, as a compromise between performance and cost.

The nominal voltage can be obtained by using only three basic RF cells; it gives a bucket corresponding to a 3% momentum acceptance.

Fig. 3.2 shows the expected bunch lengthening versus the average bunch current at 1.5 MV.

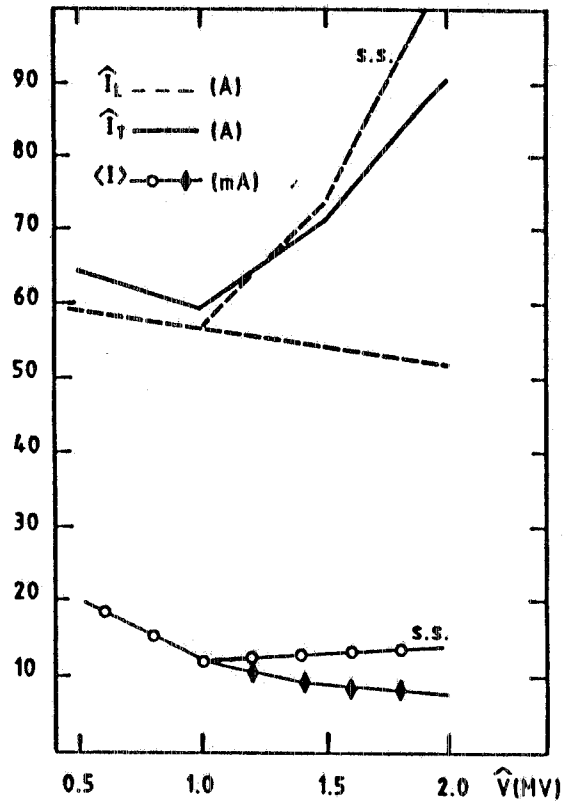

FIG. 3.1

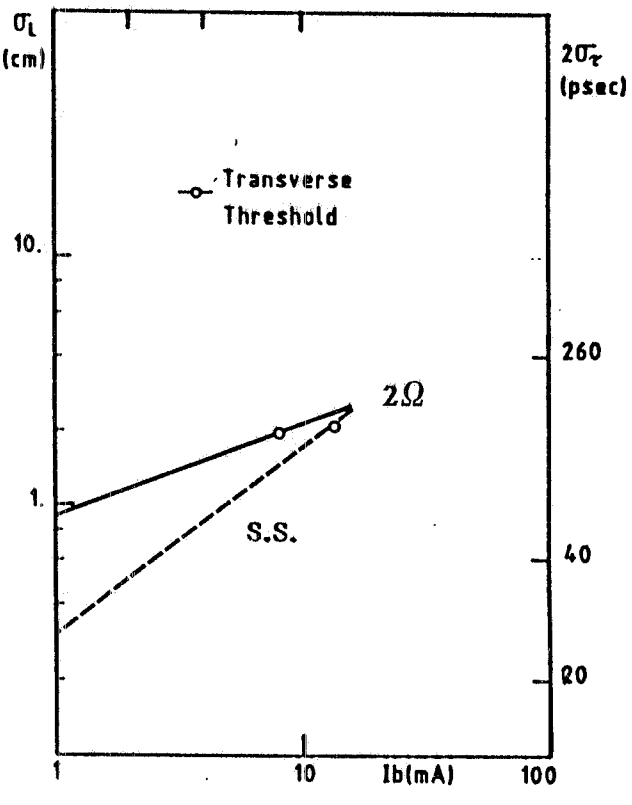

FIG. 3.2

3.4. - Coupled bunch instabilities

The motion of a set of M identical bunches can be considered as the superposition of the oscillation modes within a single bunch (dipole, quadrupole etc.) and the relative oscillation modes of M rigid bunches.

The relative oscillation modes are M and are characterized in phase space by a phase shift between two contiguous bunches.

$$\Delta\Phi = 2\pi n/M \; ; \quad n = 0,1, \ldots \; (M-1) \tag{3.9}$$

The spectrum consists of lines (sidebands) at the frequencies:

$$\omega_p = \omega_o \, (pM + n + a\, \nu_s) \tag{3.10}$$

where ω_o is the revolution frequency, 'a' and 'n' are the bunch and relative index mode respectively, and 'p' is an integer $-\infty < p < +\infty$. The result of the interaction between a mode of bunch oscillation and the surroundings is a shift $\Delta\omega$ in the indisturbed frequency of oscillation. The real part of $\Delta\omega$ measures the sideband real frequency shift, while the imaginary part leads (depending on the sign) to exponentially growing or damped oscillations.

Calculations have been performed using the Pellegrini-Wang[3.4] formalism and the experimentally measured data on single cell cavities similar to the ones designed for this machine listed in Table 3.1. Results for the first five fastest-growing relative dipole modes are summarized in Table 3.2a for the longitudinal case and in Table 3.2b for the transverse case.

The growth times correspond to a stored current of 400 mA with the full complement of 500 bunches; Landau damping is ineffective because of the small incoherent tune spread, while the synchrotron radiation damping is insufficient to neutralize the growth of some modes. The maximum current that can be stored without any feedback system is given in the last column. Quadrupole growth rates turn out to be much higher and compensated by the radiation damping. Full coupling of a side band with a parasitic mode would yield a threshold of few mA's therefore sufficient damping of the dangerous lines and feed-back systems will have to be provided.

TABLE - 3. 1

Cavity - Longitudinal parameters			Cavity - Transverse parameters		
ω_r	R_S (MΩ)	Q	ω_r	R_T(MΩ/m)	Q
3142	9.860	44000	4329.1	0.990	45000
4764	2.910	37000	5210.6	11.590	45000
6585	0.100	34000	6728.0	26.640	40000
8181	1.340	112000	7149.6	0.270	45000
8344	0.418	34000	7822.6	3.230	95000
10420	0.328	34000	8461.6	1.000	40000
10730	0.828	34000	9911.7	1.000	40000
11690	0.100	34000	10798.3	1.000	40000
12330	0.106	34000	12256.6	1.000	40000
13330	0.587	34000	12551.3	1.000	40000
13620	0.100	34000	12704.6	1.000	40000
			13396.4	1.000	40000

TABLE 3.2a - Longitudinal relative dipole modes.

n	$\Delta\nu_S$	$\tau(\text{sec})_{400\text{mA}}$	I_{th}(mA)
299	-6.9×10^{-4}	2.2×10^{-3}	64
158	-2.0×10^{-5}	2.6×10^{-3}	73
168	-3.4×10^{-4}	3.1×10^{-3}	86
255	1.3×10^{-4}	4.0×10^{-3}	115
207	-4.4×10^{-4}	9.5×10^{-3}	270

TABLE 3.2b - Transverse relative dipole modes.

n	$\Delta\nu_s^{\perp}$	$\tau(\text{sec})_{400mA}$	$I_{th}(mA)$
472	-8.5×10^{-5}	3.5×10^{-3}	200
401	1.6×10^{-4}	3.7×10^{-3}	214
147	7.2×10^{-5}	5.7×10^{-3}	327
473	-5.3×10^{-5}	7.8×10^{-3}	>400
471	-5.0×10^{-5}	9.3×10^{-3}	>400

3.5. - Emittance Growth

The emittance growth of the beam due to intrabeam scattering (IBS) has been computed using the results from § 3.3. For the storage ring considered having a very small natural emittance, short bunch length, and high beam current, the beam density is very high and the effects of IBS are not necessarily negligible, even at 2 GeV. Fig. 3.3 shows the equilibrium emittance versus energy, in the range 1.5 GeV - 2.0 GeV.

We have used the lowest value of vacuum chamber impedance under the SPEAR regime because, giving the shortest bunch length, it is a worst case in terms of emittance growth. For the multibunch case, we assume a total current of 400 mA corresponding to approximately .8 mA per bunch; a value of 10.mA/bunch, corresponding to the transverse threshold at 1.5 GeV, is instead used for the single-bunch operation mode. The zero current emittance is also shown for comparison.

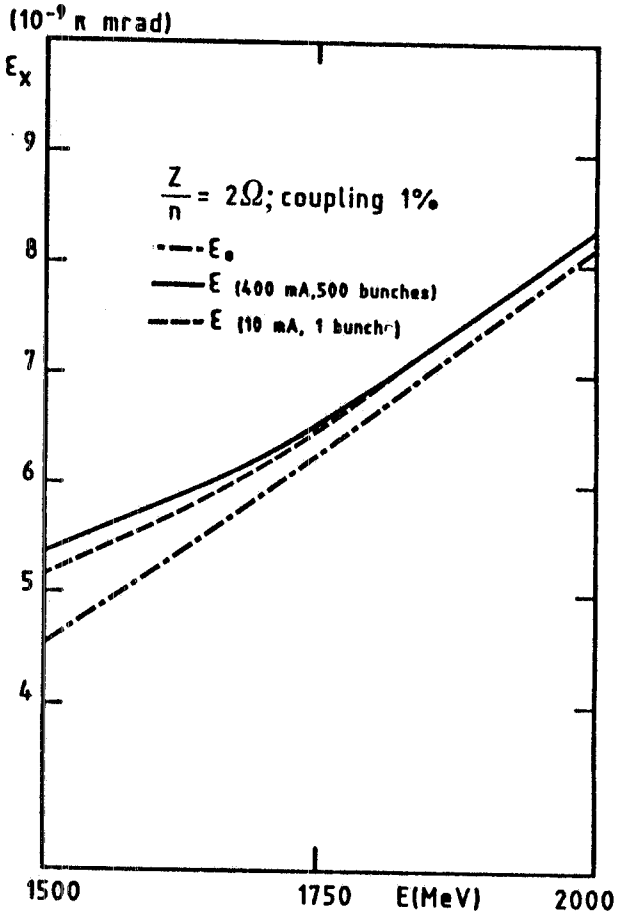

FIG. 3.3

It is clearly seen that the emittance growth due to IBS will not be a significant concern in terms of storage ring performance, even at the low value of coupling of 1% assumed in the calculations.

3.6. - Beam Lifetime

The overall lifetime of the circulating electron beam depends on the combined effects of two processes: Touschek effect and gas scattering. Losses are caused by single, large-angle intrabeam Coulomb scattering of the electrons in the case of the Touschek effect ; in the case of gas scattering the losses are due to elastic and inelastic (Bremsstrahlung) scattering of the beam electrons on molecules of the residual gas in the vacuum chamber.

Because Touschek scattering results from intrabeam collisions, the Touschek lifetime depends on the beam density. In addition, the particle loss rate depends strongly on the momentum acceptance of the lattice.

The momentum acceptance can be limited either longitudinally (by the RF or the dynamic acceptance) or transversely (by the physical or the dynamic acceptance). In performing its lifetime calculations ZAP takes all these limitations into account.

For our lattice, the limit on momentum set by a beam pipe having an horizontal half aperture of 2.5 cm is about 3.5% . On the other hand the dynamic momentum acceptance is of the order of 3%. Thus, there is no real benefit in having an RF voltage higher than that necessary to achieve a 3% bucket.

The Touschek half-lifes for our lattice with a 500 MHz RF sistem are presented in Fig. 3.4 for both the single-bunch (I_b = 10 mA) and the multibunch (I_b = .8mA) cases. Note again that the most unfavourable emittance coupling (1%) and bunch length (SPEAR regime) have been assumed.

Gas scattering calculations, assuming a 1 cm full vertical gap at the undulators and 1 nTorr Nitrogen pressure yield a beam life time of 108 hrs.

The total beam life time versus the gas pressure in nTorr is shown in Fig. 3.5. It is mainly limited by the Touschek effect and, in spite of the very conservative assumptions on the beam density, in the nominal multibunch mode of operation 10 hrs lifetimes at the pressure of 5 nTorr are achieved.

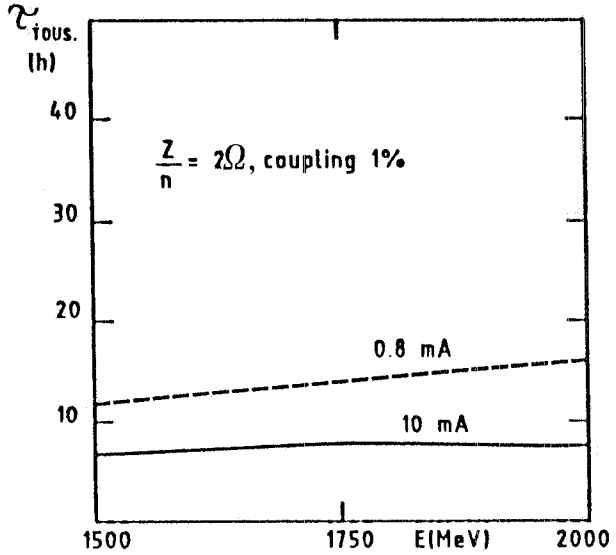

FIG. 3.4

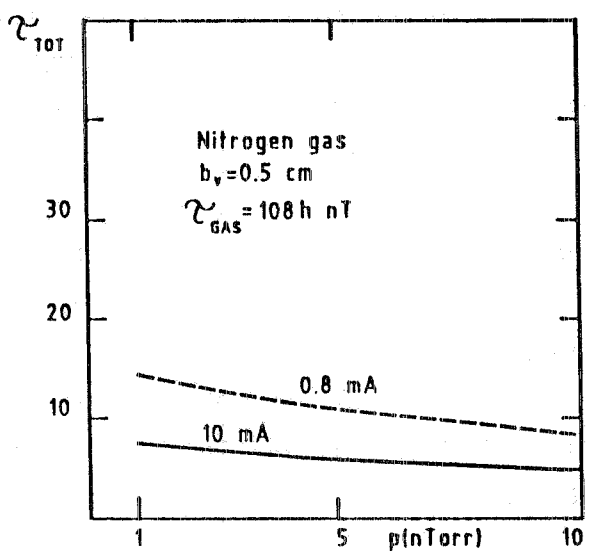

FIG.3.5

REFERENCES

[3.1] M. S. Zisman, S. Chattopadhy, J. Bisognano, LBL Report 21270, (1986).
[3.2] E. Gianfelice, L. Palumbo, M.S. Zisman, Study of collective effects for Afrodite lattices. LNF Int. Memo AF-30 (1987).
[3.3] Y. Yamazaki, K. Takata, S. Tokumoto, IEEE Trans. Nucl. Sci. NS-28, (1981).
[3.4] J.M. Wang, BNL Report 51302, (1980).

4. - UNDULATORS, WIGGLERS AND BEAM LINES

4.1. - An overview over the kind of performance and the brilliance one can expect from typical sources on the present ring is given in Fig. 1.1. A more detailed discussion of the properties of the radiation from the insertion devices is given in the following paragraphs.

4.2. - Undulators

Two different undulators have been considered in detail and their main parameters are given in Table 4.1.

TABLE - 4.1

-	Parameters of theU1 undulator		
	Period	5.5	cm
	Number of period	100	
	Minimum gap	2	cm
	Magnetic material	Sm – Co	
-	Parameters of the U2 undulator		
	Period	20	cm
	Number of periods	27	
	Minimum gap	2	cm
	Magnetic material	Sm – Co	

The undulator U1 has a period λ_u = 5.5 cm and spans the photon energy range from 100 eV to 2000 eV very nicely (considering the emission useful up to fifth harmonic); it is therefore a good candidate for most of the soft X-ray beam lines. For this reason its theoretical emission characteristics have been studied in detail. Fig. 4.1 shows he tunability range of the undulator U1 for the first, the third and the fifth harmonic with the machine energy set at 1.5 GeV. Fig. 4.2 shows the tunability range when the machine is set at 2.0 GeV. The performances of the undulator, as measured by the average flux in the photon energy range 0.1 ÷ KeV (for which interval the machine should be optimized according to user's requirements) are, in this case, quite superior. For this reason it was decided that the machine energy should have the possibility to be raised up to 2 GeV.

Higher harmonics have not been considered since it has been shown that (unavoidable) small magnetic field errors would rapidly wash them out[4.1].

The undulator U2 is designed for high flux beam lines in the vacuum ultraviolet. Fig. 4.3 shows its tunability range with the ring energy set at 2.0 GeV. Further detailes on the proposed undulators and their tunability ranges are reported in Ref. 4.2.

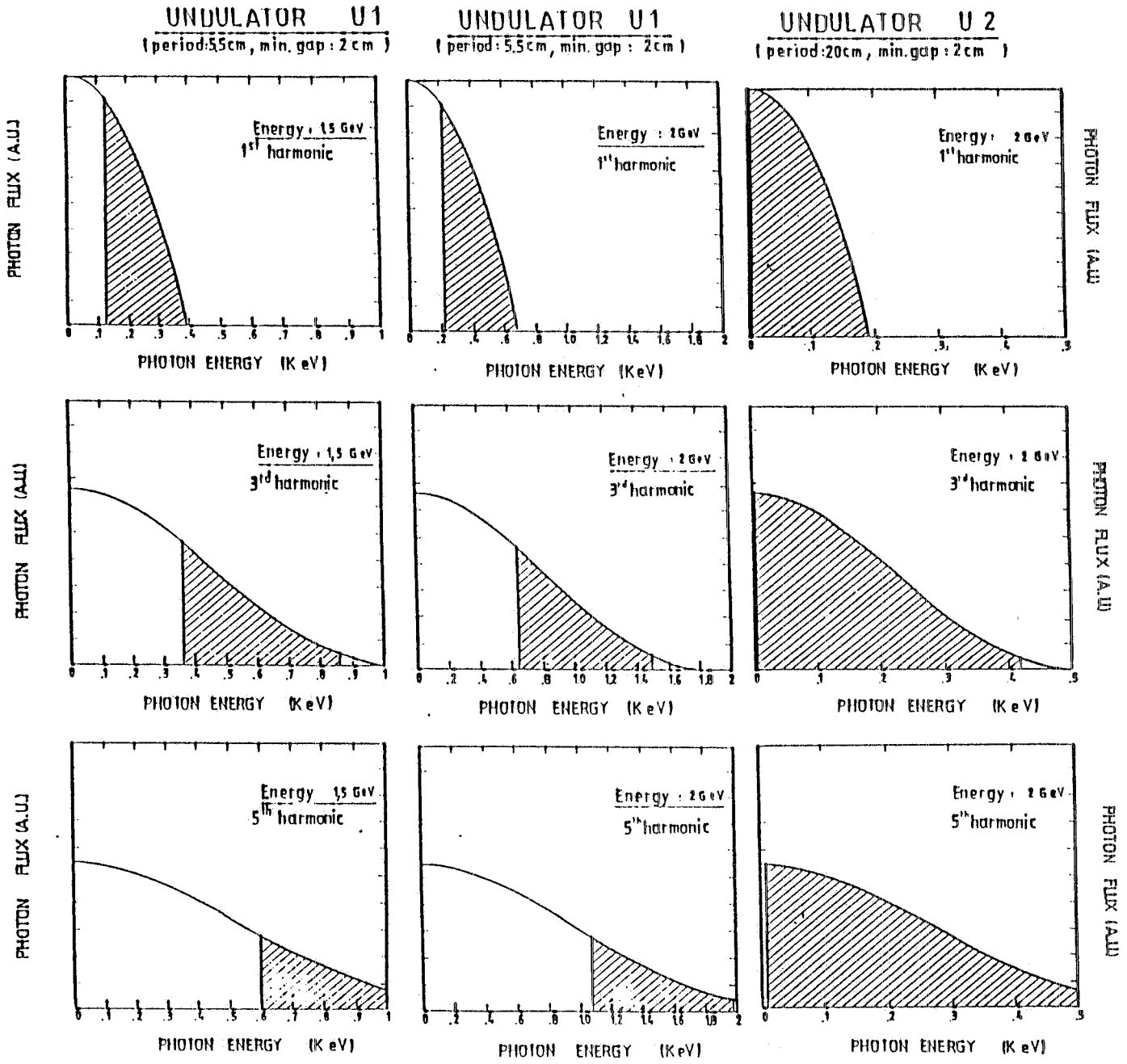

FIG. 4.1 FIG. 4.2 FIG. 4.3

4.3. - Wiggler

The possibility of inserting a 10 pole superconducting wiggler, with a maximum magnetic field on the axis of 5 Tesla, has been considered.

The large number of proposals from the Italian scientific comunity for beam lines at medium-hard X-rays (for EXAFS, crystallography, fluorescence and angiography) call for the inclusion of at least two wigglers of this kind on the Trieste ring. Although the European Machine which is being built in Grenoble will have much higher photon fluxex in this energy range (between about 3 to 40 KeV), these experimental stations are very advisable for accomodating a large number of experiments which do not need the exceptional performances of the European machine.

Figs. 4.4 and 4.5 show the photon flux which will be obtainable[4.3] from the bending magnets, the wiggler(s) and the undulators U1 and U2 at the Trieste Laboratory for a machine energy of 1.5 and 2.0 GeV, respectively.

The superior performance of the 2 GeV machine is obvious also in this case. In particular it allows to reach the K edge of iodine (~ 33 KeV) with a flux sufficient for implementing an angiography beamline, if requested.

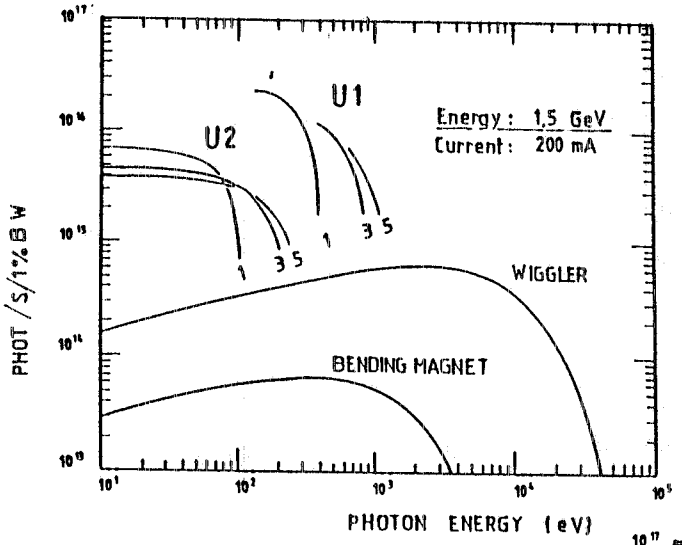

FIG. 4.4

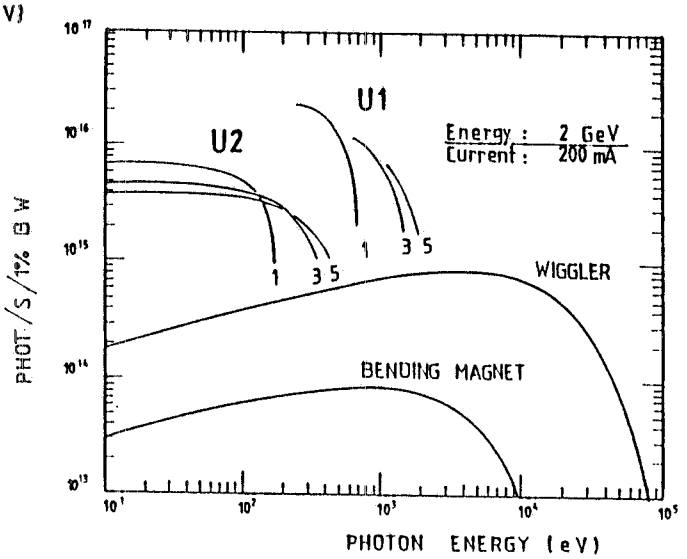

FIG. 4.5

4.4. - Monochromators

Two different kinds of monochromators have been studied: a Plane Grating Monochromator for the hard X-ray region. For the vacuum ultra-violet, Normal Incidence Monochromators are commercialized by several firms and their performances are widely known. For this reason no simulation of this kind of monochromator has been carried out.

PGMs are still very critical and expensive instruments. The PGM which has so far shown the best performances is the SX-700 which has been implemented at BESSY (Berlin)(4.4). For this reason we have studied in detail the theoretical behaviour of the SX-700 as mounted on a beamline equipped with the undulator U1. Fig. 4.6 shows the resolution which is going to be obtained at this beam line versus the machine emittance(4.5). The calculation has been made for two different exit slit widths (20 and 10 μm), both for the theoretical behaviour and the expected practical one (due to slope errors on the optical elements). From Fig. 4.6 we can see that the performance of the monochromator does not depend much on the machine emittance (and would not change appreciably on going from the nominal energy of 1.5 GeV to 2.0 GeV). Instead it is profoundly influenced by the quality of the optical elements.

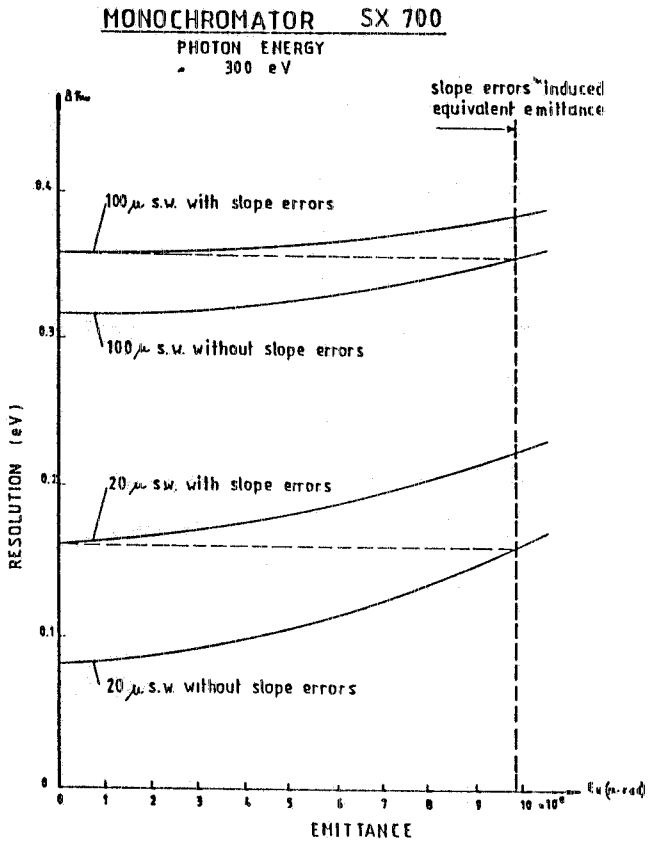

FIG. 4.6

Fig. 4.7 (a and b) shows the photon flux which will be available on the sample as a function of photon energy for several different energy resolutions, at the machine energies of 1.5 and 2.0 GeV, respectively(4.6).

The results are shown within the tunability range of the first harmonic of the undulator. Since the SX-700 has good performances also in the low photon energy range, we have simulated the behaviour of this monochromator as mounted on a beamline served by the U2 undulator.

Fig. 4.8 shows the photon flux versus photon energy (for different energy resolutions) which will be obtainable form such a layout.

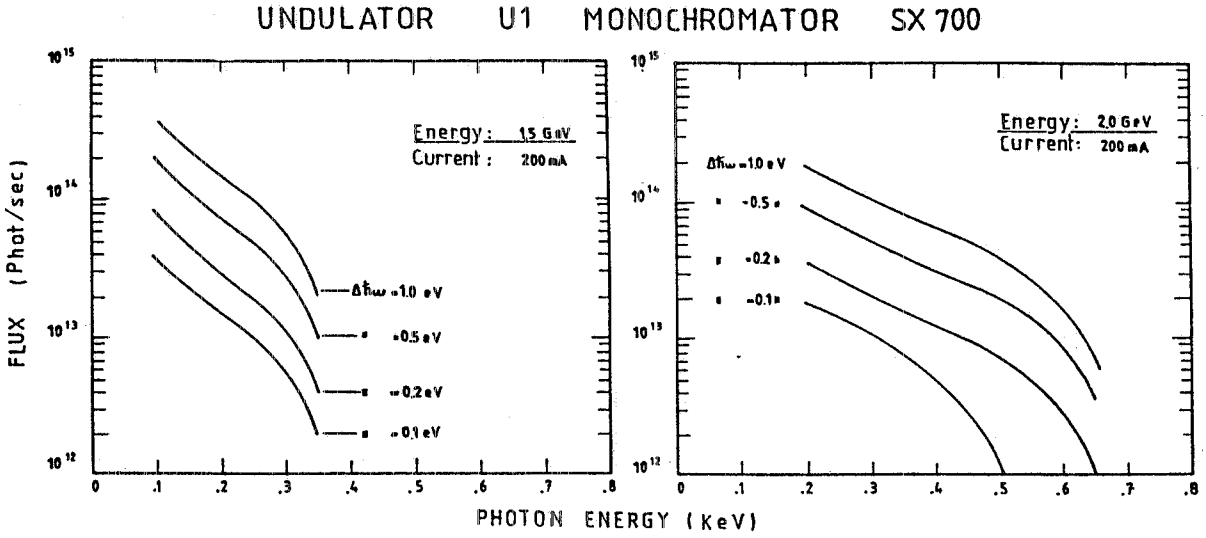

FIG. 4.7

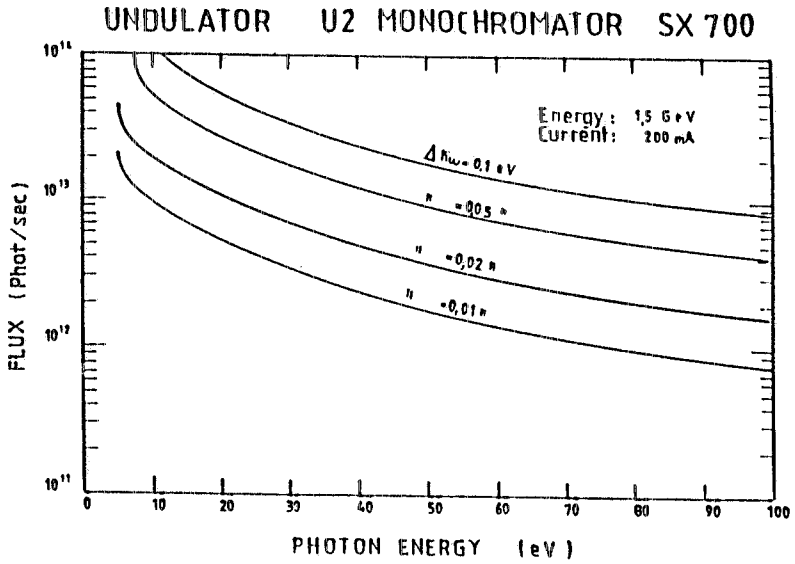

FIG. 4.8

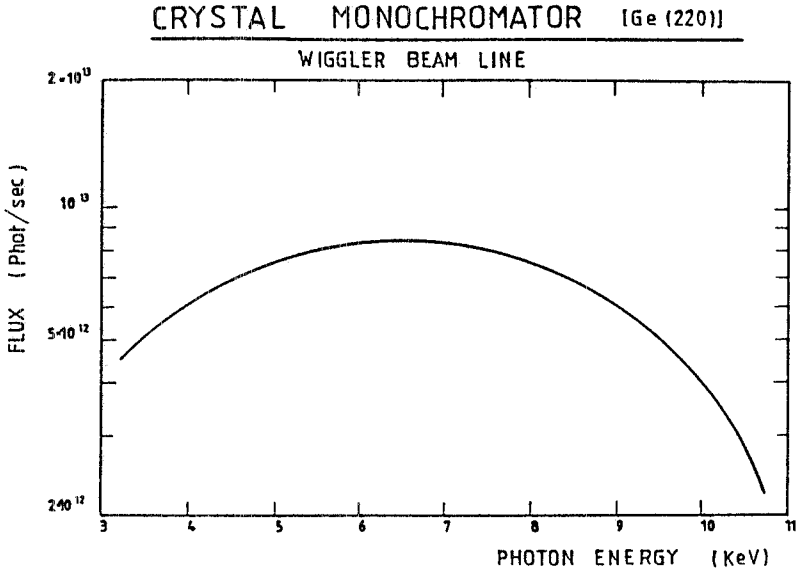

FIG. 4.9

As far as the hard X-ray region is concerned, Fig. 4.9 shows are estimate of the photon flux which will be obtainable in the spectral range up to about 10 KeV. The estimate has been carried out by considering the performances of a Crystal Monochromator (Ge(220)), recently built in Daresbury[4.7], as mounted on a wiggler beamline.

REFERENCES

(4.1) B.M. Kincaid, J. Opt. Soc. Am. **B2**, 1294 (1985).
(4.2) B. Diviacco, R. Rosei e R. Coisson, Internal Report TSRP - IUS 3/86 (1986).
(4.3) B. Diviacco, R. Rosei e R. Coisson, Internal Report TSRP - IUS (in preparation).
(4.4) H. Petersen, Technischer Beriect BESSY TB 66/84 (1984).
(4.5) R. Rosei, F. Della Valle, F. Zanini, F. Cerrina and B. Lai, Internal Report TSRP - IUS 9/86 (1986).
(4.6) B. Diviacco, F. Zanini e R. Rosei, Internal Report TSRP - IUS (in preparation).
(4.7) A.A. Macdowell, D. Norman, J.B. West, J.C. Campuzano and R.G. Jones, Nucl. Instr. & Meth. *A246*, 131 (1986).

5. - D.C. MAGNETS

5.1. - General remarks

The lattice described in Chapt. 2 has 32 identical bending dipole magnets, 176 quadrupoles and 192 sextupoles. Six families of quadrupoles and two families of sextupoles are needed.

All magnets have been designed to reach 2 GeV; however, all parameters including cost have been optimised at the 1.5 GeV field level. Correction elements are also required; the main ones are the horizontal and vertical steering dipoles, needed to correct the closed orbit. These dipole correctors have been incorporated into the quadrupoles. It is possible, if needed, to incorporate correction windings in the sextupoles too.

5.2. - Dipole magnets

With a nominal field of 1 Tesla at 1.5 GeV the dipole is quite conventional. However, to reach 2 GeV, a field of 1.33 Tesla is required, and iron saturation could cause some field distortion. Special attention has therefore been paid to the dimensioning of the magnetic circuit.

The field profile, as predicted by MAGNET, is shown in Fig. 5.1 at both 1.5 and 2 GeV.

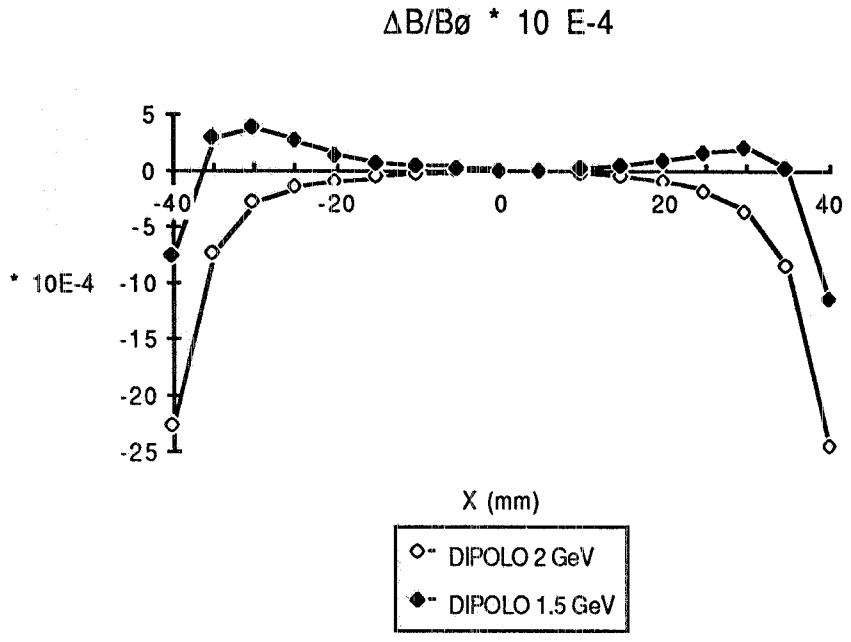

FIG. - 5.1

The following field quality has been obtained:

	@ x=±20 mm	@ x=±30 mm
$(\Delta B/B_o) \times 10^{-4}$ @ 2 GeV	+0 ÷ -1.1	+0 ÷ -3.7
$(\Delta B/B_o) \times 10^{-4}$ @ 1.5 GeV	-0 ÷ +1.4	-0 ÷ +3.6

This field quality is within the specified tolerance with no allowance for the trajectory sagitta since it is foreseen to manufacture a curved parallel ended magnet. A possible technical arrangement is schematically shown in Fig. 5.2.

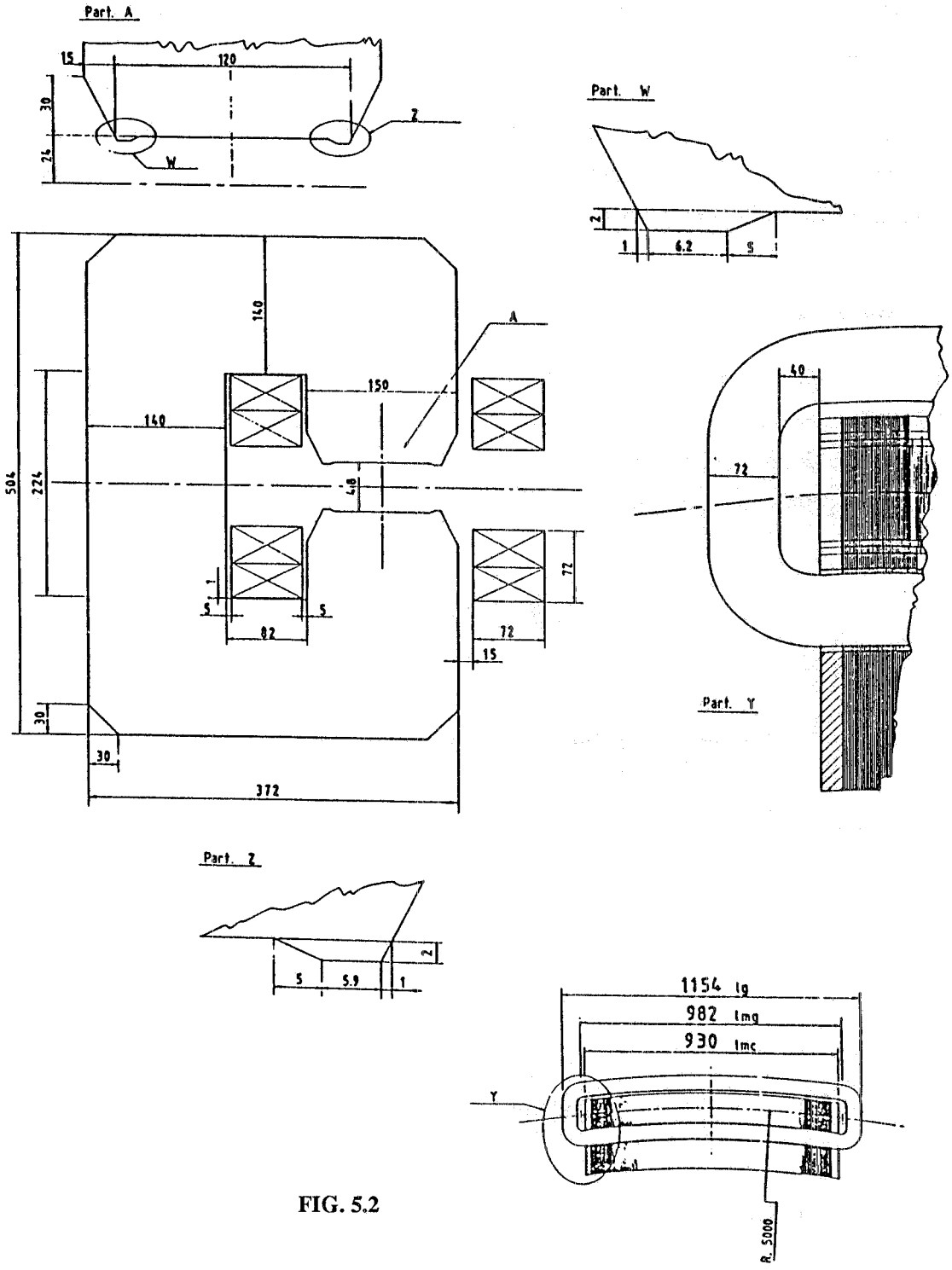

FIG. 5.2

In designing the coil the optimum current density is usually found by minimizing the sum of capital plus operating costs. It must be noted that the optimum for cost is rather flat.

The present design slightly favours the containment of the capital cost (and also of the magnet radial dimension) at the expense of long term operating costs. The current density has accordingly been pushed towards values higher than optimum.The selected current density at 1.5 GeV is correspondingly 6.85 A/mm^2. This determines the coil and the window cross-section as shown in Fig. 5. 2.

With the chosen steel dimensions, a linearity of better than 98% is expected at 1.5 GeV. The value at 2 GeV drops to 92%.

The dipole basic parameters are listed in Table 5.1.

TABLE 5.1. - Basic dipole parameters

		2 GeV	1.5 GeV
ENERGY (NOMINAL)	(GeV)	1.5	
ENERGY (MAXIMUM)	(GeV)	2	
BENDING RADIUS	(m)	5	
MAGNETIC LENGTH	(m)	0.982	
NOMINAL FIELD (1.5 GeV)	(T)	1.0	
MAXIMUM FIELD (2 GeV)	(T)	1.33	
POLE/GAP RATIO		3.125	
RETURN LEG/POLE RATIO		0.933	
GAP	(mm)	48	
POLE WIDTH	(mm)	150	
AMPTURNS PER COIL		28800	19450
LINEARITY		≈ 92 %	> 98 %
CURRENT	(A)	450	304
CURRENT DENSITY	(A/mm^2)	10.14	6.85
TURNS PER POLE		64	
CONDUCTOR		□8*8 Ø 5 Cu	
COIL RESISTANCE (@ 60°C)	(Ω)	0.16	
COIL INDUCTANCE	(H)	0.08	
POWER	(KW)	32.4	14.9
VOLTAGE 2 GeV	(V)	72	49
IRON WEIGHT	(Kg)	1312	
COPPER WEIGHT	(Kg)	150	
TOTAL WEIGHT	(Kg)	1462	

For a further approximation, the azimuthal behavior of the dipole field must be taken into account, including the higher order terms in the field integral.

MAGNET predicts the following field components at 1 centimeter from the equilibrium orbit in the horizontal plane:

	$(\Delta B/B_o) \times 10^{-4}$ Quadrupole	$(\Delta B/Bo) \times 10^{-4}$ Sextupole
@ 2 GeV	- 0.025	-0.3
@ 1.5 GeV	+ 0.064	+0.17

At this stage the design has not been pushed any further but there are areas that will require more effort. For instance the end field distribution influences the variation of the integrated field lengths with radius, and a tridimensional code should be used. The present level of approximation is however well sufficient for a cost estimate.

5.3. - Quadrupole Magnets

A fully symmetric quadrupole with an aperture radius of 30 mm (cross-section shown in Fig. 5.3) meets both the magnetic and mechanical specifications for 160 over 176 of the quadrupoles included in the machine lattice. The remaining 16 interfere with the synchrotron radiation output piping emerging from the preceding dipole magnets and will be of special design. The exact cross-section is still under investigation; a possible technical arrangement has been proposed in Reference 5.1.

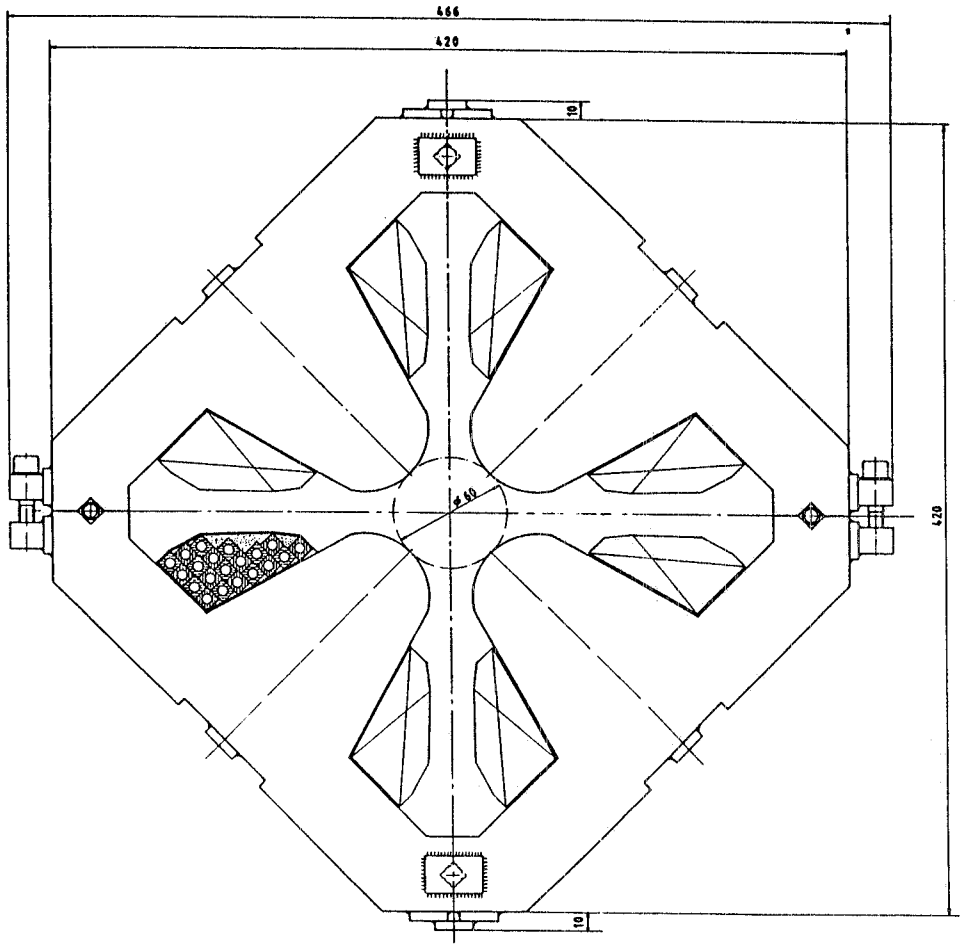

FIG. 5.3

The standard lens has ben studied for a maximum gradient of 18.4 T/m to take the estimated field increment due to the correction windings (two independent per pole) into account.

The worst case gradient quality predicted by MAGNET at 18.4 T/m is :

$\Delta G/G\phi < 1.7 * 10^{-3}$ peak to peak @ x= ± 18 mm

The quadrupole family with the minimum excitation (G = 8.33 T/m) has the best gradient uniformity (see Fig. 5.4). The gap geometry (polar profile and tips) can be further improved to increase the useful field region. With the chosen steel dimensions, a linearity of 98% is expected at 2 GeV.

Having adopted a single cross-section design and a single type of coil for the six quadrupole families, the currents scales with the required gradients. Lengths, gradients and the values of the coil current at 2 GeV are listed in Table 5.2.

TABLE 5.2. - Quadrupoles.

Type	Length (m)	K (m^{-2})	Gradient (T/m)	Current (A@2 GeV)
QF1	0.40	1.749	11.66	271
QD1	0.40	1.923	12.80	298
QF2	0.40	2.356	15.7	365
QW1	0.40	1.249	8.33	194
QW2	0.55	2.555	17.0	396
QW3	0.40	2.356	15.7	365

Corrector windings give the field shown in Fig. 5.5. The final arrangement and dimensioning of such windings requires further study, and various options are possible without significant changes in the quadrupole cross-section.

Table 5.3 shows the basic parameters list and the results of the harmonic analysis predicted by MAGNET.

TABLE 5.3 - Basic parameters list.

			Main coil		Corrector coil
GRADIENT (MAXIMUM)	(T/m)		18.4		
INSCRIBED RADIUS	(mm)		30		
POLE FIELD	(T)		0.55		
POLE SHAPE			CIRCULAR + TIPS		
AMPERTURNS PER POLE			6700		670
CURRENT	(A)		419		335
CURRENT DENSITY	(A/mm^2)		9.44		7.55
TURNS PER POLE			16		2+2
COPPER CONDUCTOR			❑8*8 ø 5		
LINEARITY			> 0.98		
MAGNETIC LENGTH	(m)	0.4		0.55	
MAGNET RESISTANCE (@ 60°C)	(mΩ)	31.7		40	1.64
POWER	(KW)	5.57		7.243	
VOLTAGE	(V)	13.3		17.3	
IRON WEIGHT	(Kg)	229		314	
COPPER WEIGHT	(Kg)	37.5		51.4	
POWER PER POLE	(W)				187
VOLTAGE PER POLE	(V)				0.55
GRADIENT QUALITY (@ X = 10 mm and Go = 18 T/m)					
Mechanically perfect q-pole:					
$\Delta G_{12\text{-pole}} / G_o$			$-0.14*10^{-3}$		

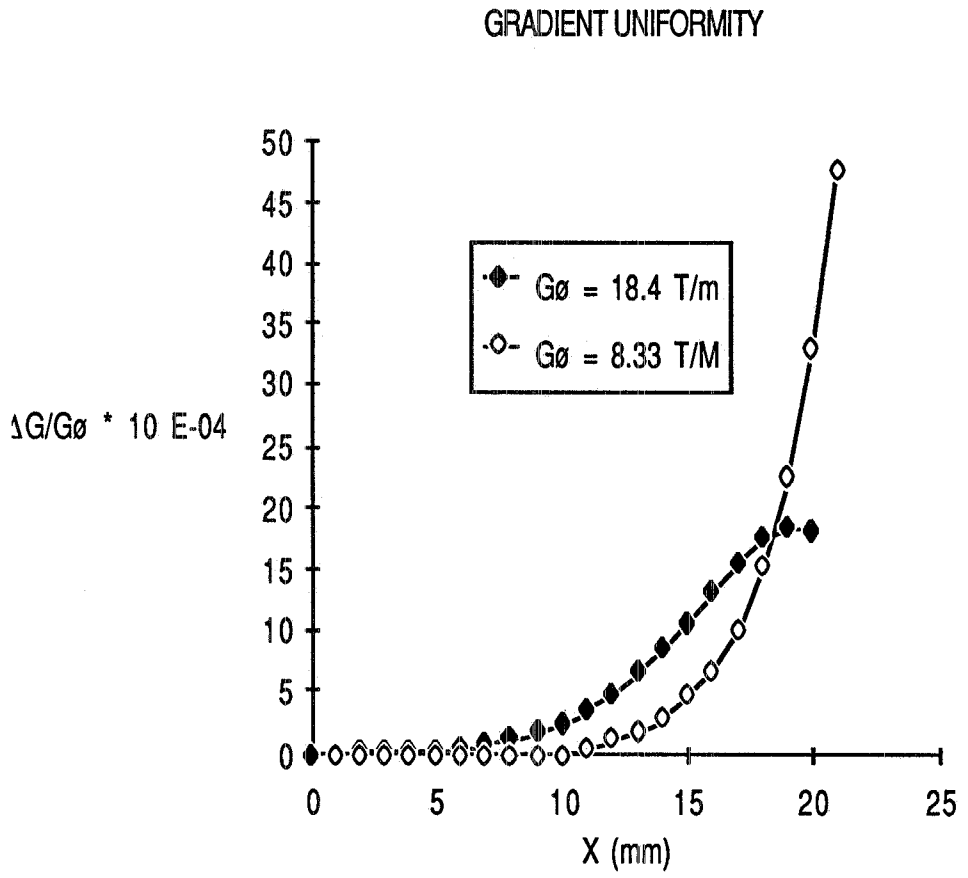
GRADIENT UNIFORMITY
ΔG/Gø * 10 E-04
50
45
40
35
30
25
20
15
10
5
0
Gø = 18.4 T/m
Gø = 8.33 T/M
0
5
10
15
20
25
X (mm)

FIG. - 5.4

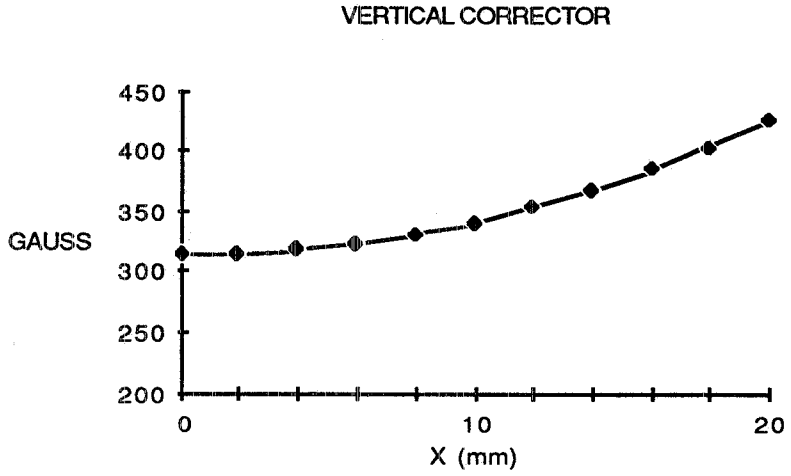
VERTICAL CORRECTOR
GAUSS
450
400
350
300
250
200
0
10
20
X (mm)

FIG. - 5.5

5.4. - Sextupole magnet

As many as 32 out of the 192 sextupoles interfere with the synchrotron radiation channels from the preceding bending magnet. 16 of them can simply have a bore radius enlarged to 45 mm; their return legs are then far enough from the center to allow the beam vacuum vessel to pass through.

The remaining 16 need a special mechanical arrangement, with an open side. The design of special sextupoles is in progress and a final decision on the most cost effective way solution has not been reached. Costs have been based on an average standard sextupole design. A possible solution for the open sextupole is proposed in Ref. [5.1].

TABLE 5.4. - Sextupoles.

TYPE	Bore radius (mm)	Length (m)	K (m^{-3})	Gradient (@ 2 GeV) (T/m^2)	Current (A)
SF	30	0.20	15.66	261	208
SD	30	0.20	18.44	307	244
SF	45	0.20	15.66	261	302
SD	45	0.20	18.44	307	355

For most sextupoles a cross-section that minimizes the dimensions and therefore the construction cost can be adopted, leading to a bore radius of 30 mm. Figures 5.6 and 5.7 show the transverse cross-sections of the two sextupoles developped so far.

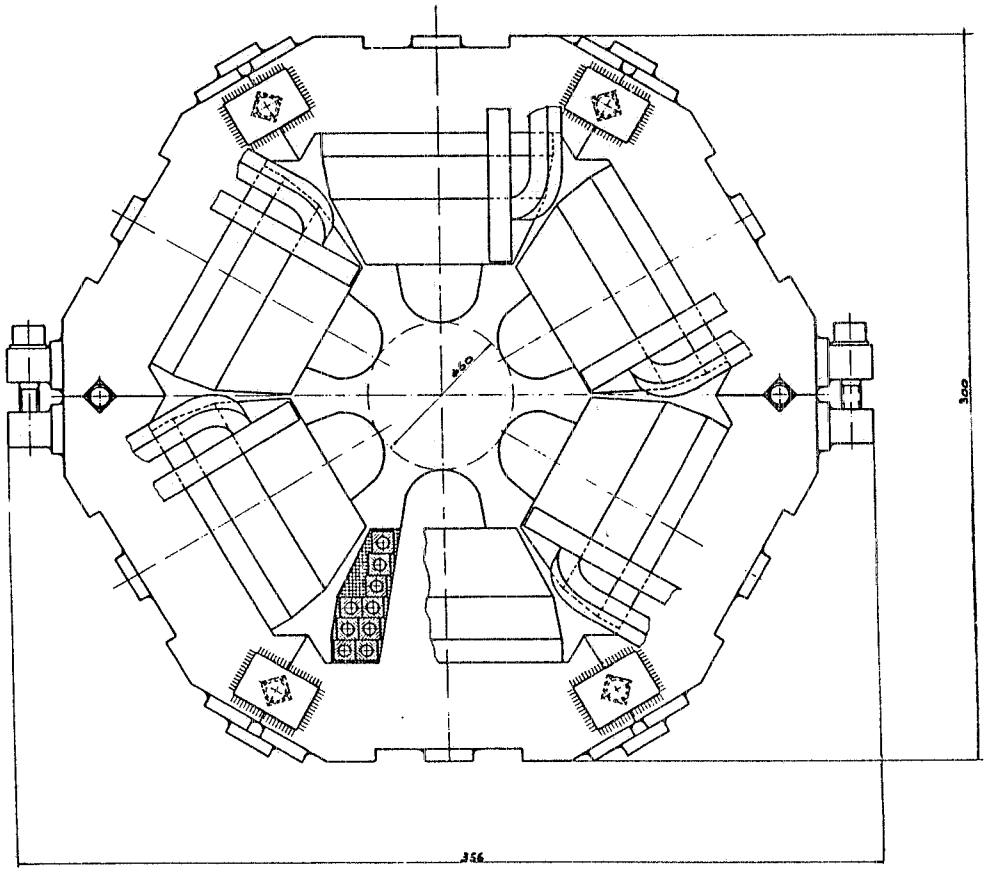

FIG. 5.6

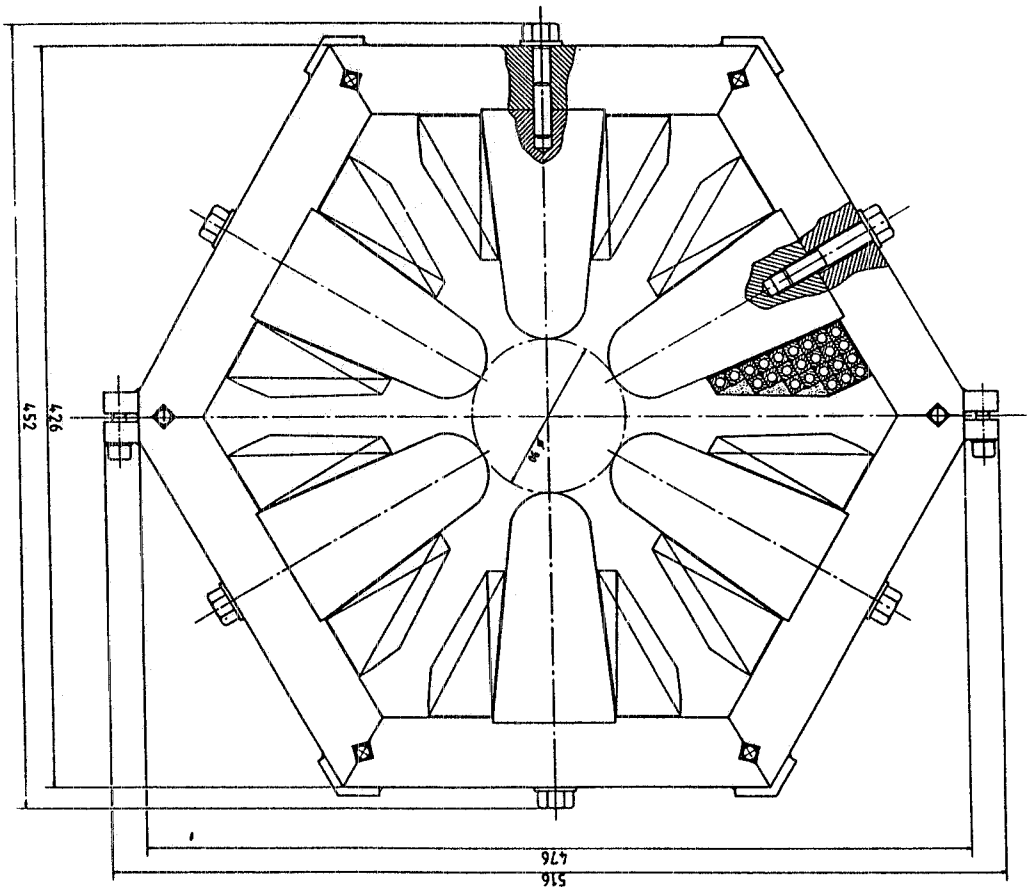

FIG. 5.7

The basic parameters of the two different families are listed in Table 5.4.

The quality of the sextupole field has been calculated using MAGNET and is predicted to be: $\Delta G_S/G_{SO} < 1.3$ % peak to peak @ x = ±16 mm, $\Delta G_S/G_{SO} < 1.3$ % peak to peak @ x = ±26 mm for the standard sextupole, and the enlarged bore one respectively. This quality is obtained with a simple circular pole profile. Fig. 5.8 shows the gradient profiles for the two sextupoles.

Further pole profile optimization is expected to extend the useful field region.Cost and feasibility estimates can however be derived from the present design stage.

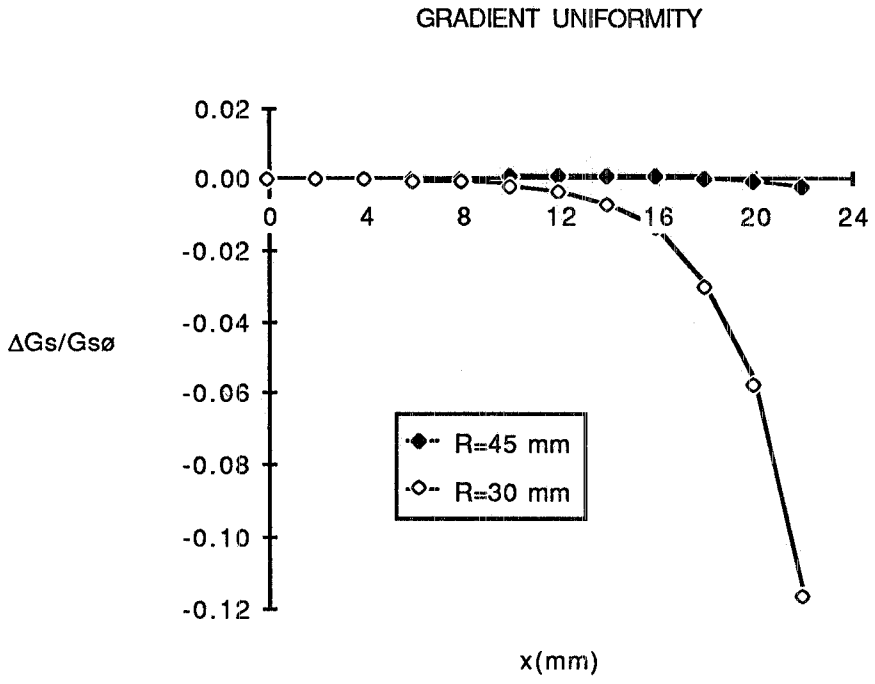

FIG. 5.8

5.5. - Main ring power supplies

The lattice[5.2] requires 32 dipoles, 176 quadrupoles and 192 sextupoles. The power supply characteristics are presented for the case when families of quadrupoles and sextupoles are connected in series and powered each by a separate power supply.

All power supplies will be of the thyristor type. Their stability will be about 10^{-4} or better. To obtain the prescribed performance a parallel current loop using a very precise transductor is needed. Solutions for trimming the setting of each magnet individually are being studied.

5.5.1. - The dipole power supply

The magnet characteristics are listed in Table 5.1. When two Graetz bridges connected in series are used to halve the voltage, one obtains a ≈ 3.5% /600 Hz, voltage ripple. The dipole power supply characteristics are listed below. No additional filtering is required.

Output voltage	(V)	2304
Output current	(A)	450
Power	(KW)	1040
Current ripple, rms	(mA)	2.5
I ripple/I d.c. ratio		$5.3 * 10^{-6}$

5.5.2. - Quadrupole power supplies

For 2 GeV operation, and with a 10% safety margin to allow for voltage drops on the cables, the 6 quadrupole families require power supplies having the output characteristics listed below:

Type	Voltage (V)	Current (A)	Power (kVA)	Voltage ripple (%)	Current ripple (mA)	Iripple/Idc * 10^{-3}
QF1	152	300	49	2.8	20	7.2
QD1	335	330	117	2.9	23	7.7
QF2	408	400	174	2.7	26	7.2
QW1	218	215	50	2.9	15	7.7
QW2	572	435	265	2.8	29	7.3
QW3	408	400	174	2.7	26	7.2

Two Graetz bridges in parallel can be used. Also in this case the ratio (I_{ripple}/I_{dc}) is small enough that no additional filters are needed.

5.5.3. - Sextupole power supplies

The sextupoles, all of the same length but with different apertures (30 and 45 mm), are grouped into four families. The power supply characteristics, considering 2 GeV operation and a 10% safety margin and using only one six phase bridge with a 300 Hz ripple, are:

Type	Voltage (V)	Current (A)	Power (kVA)	Voltage ripple (%)	Current ripple (mA)	Iripple/Idc * 10^{-3}
SF(30)	242	229	56	7.1	212	1.0
SD(30)	284	269	77	7.0	248	1.0
SF(45)	513	332	171	7.0	307	1.0
SD(45)	603	390	235	7.0	359	1.0

The 0.1% ripple, at the maximum current value, can be lowered, if necessary, using two bridges in parallel or a smoothing filter.

REFERENCES

(5.1) 1-2 GeV Synchrotron radiation source , LBL PUB-5172, June 1986.
(5.2) M.E. Biagini, C. Biscari, LNF Int. Memo AF-15.

6. - RF SYSTEM

The RF system replaces the energy lost by the particles circulating in the machine and ensures the needed beam lifetime.

At 2 GeV, synchrotron radiation losses add up to 285 keV per turn. A further radiation loss of about 85 KeV has to be added to account for losses in the insertion devices (wigglers and undulators). A total of about 370 keV per turn is therefore radiated.

As a consequence, the peak RF voltage required to ensure a quantum lifetime of at least 15 hours is 1.5 MV, at the chosen frequency of 500 MHz.

6.1. - Choice of the frequency

The choice of the frequency depends very much on considerations such as the availability of hardware, the compactness of the cavities and other devices, the bunch-length that is required.

Having considered all technical options, and given the general specifications laid out in Chapter 1, a 500' MHz system, similar to those used or under design in several other laboratories, appeared to be the best choice.

6.2. - RF cavities

The cavity resonator is presented in Fig. 6.1. It consists of a single copper cell under vacuum with small reentrant cones for the maximum transit time factor (i.e., shunt impedance), resonating in the fundamental mode (0 mode).

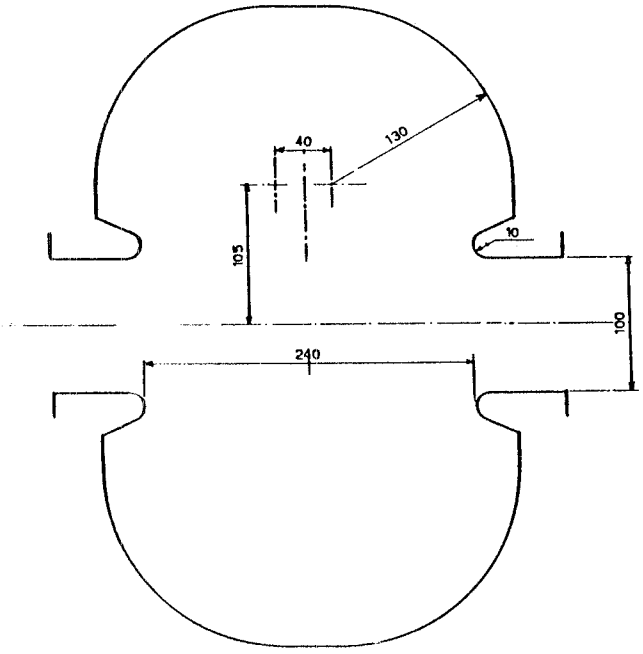

FIG. 6.1. - Cavity resonator.

Four such cells, each providing up to 375 kV at the gap, are used to provide the requested peak voltage of 1.5 MV.

The proposed system consists of four separate chains, each feeding one cavity. Each klystron amplifier is protected by a ferrite circulator.

The modularity of the layout makes for flexibility and in particular it makes further extensions, that may be required by future requirements such as higher particle energy or higher stored currents, rather easy. A further feature of the system is the complete separation between the different amplification chains to prevent cross-talk. The arrangement is also believed to improve the operational reliability of the whole system.

The parameters of the cavity resonator are listed in Table 6.1.

TABLE 6.1 - RF parameters.

Energy of the machine	(GeV)	2
Circumference	(m)	300.20
Revolution frequency	(KHz)	999.33
Transit time factor	(s)	0.675
Effective shunt-impedance	(MOhm)	8
Quality factor		45,000
Gap voltage	(kV)	375
RF frequency	(MHz)	499.66
Harmonic number		500
Max. beam current	(A)	0.4
Energy loss (arcs)	(keV/turn)	285
Energy loss (W/U)	(keV/turn)	85
Number of single cell cavities		4
Cavity length	(cm)	30
Drift tube diameter	(cm)	10
Transit time factor, T	(s)	0.675
Effective shunt-impedance, ZT	(MOhm)	8
Quality factor, Qo		45,000
Gap voltage, Vc	(kV)	375
Dissipated power, Pc	(kW)	18
Total shunt-impedance	(MOhm)	32
Max. peak voltage	(MV)	1.5
Synchrotron frequency	(kHz)	6.20
Power dissipated per cavity	(kW)	18
Total parasitic mode losses	(kW)	12
Total power to cavities	(kW)	232
Number of klystron		4
Power output per klystron	(kW)	60

Servo-controlled mechanical tuners are required in order to compensate for mechanical tolerances, thermal expansion and beam loading. The resonant frequency of the unloaded

cavity is 499.300 MHz. An inductive cylindrical plunger of 4 mm dia., having a run of 5-6 cm., provide the frequency excursion needed to reach the right frequency (499.66 MHz) under all load and temperature variations foreseen during operation.

Damping of higher-order modes will also be necessary to figth the multi-bunch instabilities; suitable dampers have already been developed at KEK, BNL and Daresbury for similar cavities.

6.3 Third harmonic system

By reducing the slope of the RF wave seen by the particle, the bunch can be lengthened and, if a nonlinearity is also introduced in the local RF voltage, enough Landau damping to fight various single bunch longitudinal instabilities can be introduced.

Bunch length can be controlled by adding a supplementary RF system at a higher harmonic of the main frequency. The third harmonic is in our case the most convenient choice. The characteristics of the system are listed in Table 6.2.

TABLE 6.2 - Third harmonic system parameters.

Frequency	(MHz)	1,499.98
Number of cavities		1
Cavity length	(m)	1.0
Shunt-impedance	(MOhm)	20
Total peak voltage	(kV)	485
Total dissipated power	(kW)	12

6.4. - Feedback systems

Longitudinal instabilities are mainly caused by unwanted high order modes in the accelerating cavities. As shown in § 3.3, the beam current thresholds for instabilities are rather low when no mode suppression is provided. Even after suppression of the most dangerous modes, it is advisable to introduce active feedback systems to counteract possible residual coherent instabilities.

The lowest order coherent instability is usually suppressed by modulating the phase of the main RF cavities by a signal proportional to the amplitude of the coherent radial beam oscillation. To suppress relative coupled bunch oscillations a multichannel system that picks up the radial oscillation signal and, after selecting specific sidebands and amplification values, acts back on the beam by means strip-line kickers, is envisaged.

6.5. - System layout

The proposed layout for the main RF system is shown in Fig. 6.2.

As explained earlier (6.2), the system consists of four separate channels each including a 60 kW klystron amplifier feeding a single cell cavity resonator, via a ferrite-circulator.

60 kW-CW klystron amplifiers, working at 500 MHz, are widely used for broadcasting purposes and can be easily purchased. Ferrite circulators for such a relatively low power level are not currently in production but are being developed.

Alternatively, a scheme similar to the one adopted at SRS where a single high power klystron feeds all cavities through magic-Tee splitters, could be used. A high power circulator (or isolator) must also be installed to protect the klystron, since the magic-Tees do not completely separate it from the cavities.

Low level phase shifters provide the necessary phase adjustment for individual RF gap voltages. The reference signal, coming from a master generator, is split into several outputs as requested.

An automatic tuning control system for each cavity and automatic level control of the gap voltages are foreseen. The main system parameters (vacuum, relative phase of the cavities, RF level, cooling, etc.) will be controlled and managed via computer.

A list of the RF parameters is presented in Table 6.1.

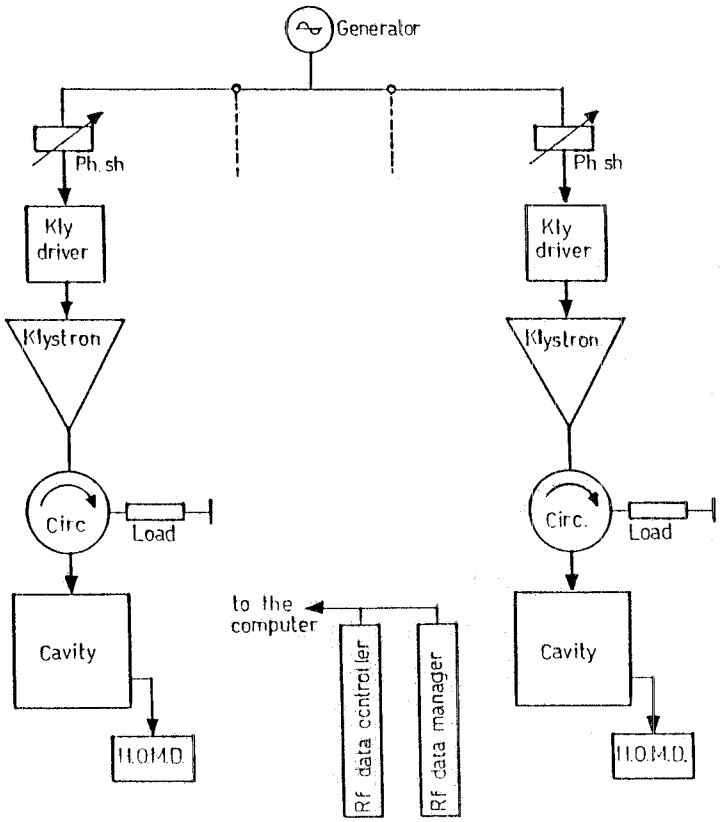

FIG. 6.2 - Layout of the system.

7. VACUUM AND COOLING SYSTEM

7.1 - Introduction

The design of the vacuum system for an electron storage ring is dominated by the large amount of synchrotron radiation generated by the circulating beam.

High energy ($\geq$ 10 eV) photons radiated emitted by the beam, hit the wall of the vacuum chamber and create photoelectrons that in turn extract gas atoms and molecules from the walls (typically H_2, CO, etc.).

The physical parameter used to describe the process is the photodesorption yield, η, representing the average number of desorbed molecules per photon. Typical values of η range from as high as 10^{-1} molecules/photon at startup, down to 10^{-7} mol/ phot after a steady state is reached following an appropriate period of conditioning by the circulating beam.

Conditioning and a good vacuum system design , possibly including in-situ bakeout , are needed to achieve the good vacuum needed for the desired long beam life time.

Synchrotron radiation sources in particular suffer - from the point of view of vacuum - from having vacuum chambers with rather small physical aperture giving small conductances, from the stringent requirement of having a pressure distribution as much as possible uniform, and from requiring complicated shapes of the vacuum vessel to accomodate the many light output ports. In addition the chamber should be electromagnetically "smooth" to reduce coherent and incoherent instability excitation to a minimum.

The aperture specifications for the present machine are given in § 2, and the desired pressure, at 2GeV and with a circulating current of 0.4 A, is specified in Chapter 3 to be $\approx$2 nTorr.

Many different provisions to control the effects of the gas load produced by the radiation on the pressure at the beam location have been devised for modern SR dedicated storage rings: special light absorbers and proper shaping of the vacuum chamber so that the radiation emerging from bending magnets is collected at selected places, preferably next to a pump; distributed ion pumps in the field of bending magnets and/or quadrupoles; titanium or non evaporable getters either distributed along the chamber or, better, located right next to the absorbers; uniform in situ bake-out at a proper temperature (typically 150 °C for Aluminium, 300 °C for Stainless Steel) ; high temperature firing of all components before installation (steel only); ion discharges, etc.

Beam conditioning is however the ultimate mean to achieve good beam life-time. It is the only practical way to reduce the photodesorption yield and its effect is proportional to beam energy and current . The lowest achievable value of the yield η and the conditioning time (or the

circulated charge) required to reach it are the most important parameters in designing the vacuum chamber and the vacuum system.

7.2. - Vacuum system

7.2.1. - General parameters

In order to evaluate the size of the problem , the performance of a vacuum system having no special pumping elements but equipped with standard titanium ion pumps only is presented. For such a system, maintenance problems are reduced to to a minimum.

The input parameters are:

Maximum operating energy , E	(GeV)	2.
Magnetic bending radius , ρ	(m)	5
Vacuum chamber dimensions	(mm)	50 x 38
or diameter	(mm)	50
Circumference	(m)	300
Circulating current, i	(mA)	400
SR Critical energy, ε_e	(KeV)	3.5
Pressure with beam, p	(Pa)	$2.6*10^{-7}$
	(torr)	$2*10^{-9}$
Total radiated power, P	(KW)	112.6

Equation 7.1 (see, for example, Ref. 7.2) gives the total rate of photons per unit current having an energy ε greater than 10 eV . Below this value the photoelectric yield is low enough that it can be neglected.

$$d^2 N_{ph}/(dt\, di) = 6.95 \cdot 10^{13} (\rho/E^2) \int_{10}^{\infty} \left[\int_{\varepsilon/\varepsilon_c}^{\infty} K_{5/3}(x)\, dx \right] d\varepsilon \quad \text{(ph/s/mA)} \qquad (7.1)$$

where $K_{5/3}$ is the modified Bessel function of order 5/3.

For our case eq.(7.1) yields :

$$N_{ph} = 7*10^{20} \text{ (photons/s) @ 2 GeV and 400 mA} \qquad (7.2)$$

Using the desorption coefficient η and eq. 7.2 we comput the rate of molecules extracted from the walls:

$$N_m = \eta N_{ph} \qquad (7.3)$$

From the general law of gases and eq. 7.3 we obtain:

$$Q = (\eta/N) R T N_{ph} = 4*10^{-21} \eta N_{ph} \text{ (Pa m}^3\text{/s)} \; (= 3*10^{-20} \eta N_{ph} \text{ (torr l/s))} \qquad (7.4)$$

The best measured values of η after 150 A*h of beam conditioning are lower than 10^{-6} mol/photon. For safety we use the value $\eta = 1*10^{-6}$ (mol/ph) to estimate the vacuum system requirements.

From 7.2 and 7.4 we obtain :

$$Q = 2.8*10^{-6} \text{ Pa m}^3/\text{s} \quad (= 2*10^{-5} \text{ torr l/s}) \tag{7.5}$$

The overall required nominal pumping speed, S , is :

$$S = 2\,Q/p = 20 \text{ m}^3/\text{s} \quad (= 2\ 10^4 \text{ l/s}) \tag{7.6}$$

where a factor of two has been added to account for pumping speed losses in a real life system.

By installing a 200 liters/s pump every three meters all along the 300 meters long vacuum chamber, the pressure variation around its nominal operating value is small even when the chamber conductance is taken into account.

Combining 7.4, 7.5 and 7.6 one obtains the pressure as a function of the desorption coefficient η :

$$p = 4*10^{-21}\,\eta\ N_{ph}/s \quad \text{(Pa)} \tag{7.8}$$

It is easy to see that the assumed value of η allows the required base pressure of $2.6*10^{-7}$ Pa to be easily achieved , giving beam life times in excess of ten hours .

Finally it is important to estimate the integrated current (or dose D) necessary, at full energy, to reach the base pressure. An empirical formula relating the desorption coefficient to the accumulated dose D is:

$$\eta = \frac{.14}{D^{1.06} + 8.9} + 5\cdot10^{-7} \quad \text{molecules/photon} \tag{7.9}$$

where D is in Coulomb and the numerical coefficients are derived from work done in Frascati on the storage ring Adone.

Rearranging eq. 7.4. and using 7.6. and 7.9. one has :

$$p = 4.10^{-21} \left(\frac{.14}{D^{1.06} + 8.9} + 5\cdot10^{-7} \right) N_{ph}/s \quad \text{(Pa)} \tag{7.10}$$

Fig. 7.1 shows how the pressure decreases with the dose D. The operating pressure is reached after a dose of more than 10^5 Coulomb or about 50 - 100 Amp*hour; this value is in good agreement with what found at other storage rings. The pressure distribution along 1/16 of ring as a function of total accumulated dose of circulating beam is shown in Fig. 7.2.

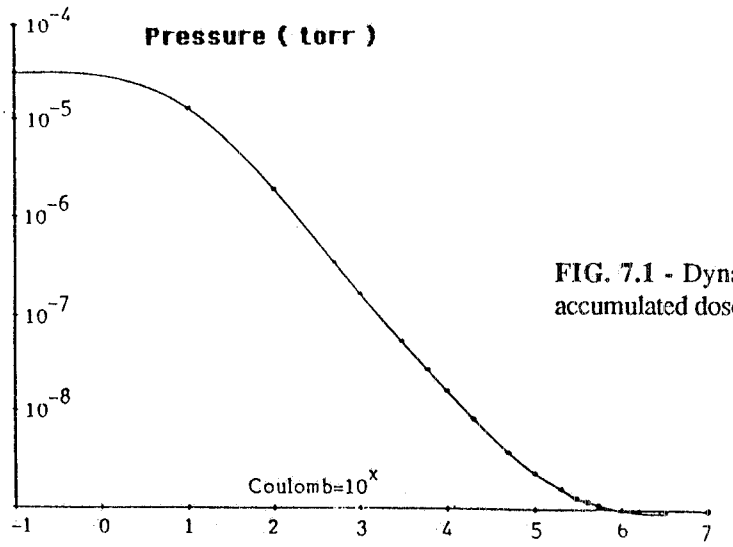

FIG. 7.1 - Dynamic pressure as a function of total accumulated dose.

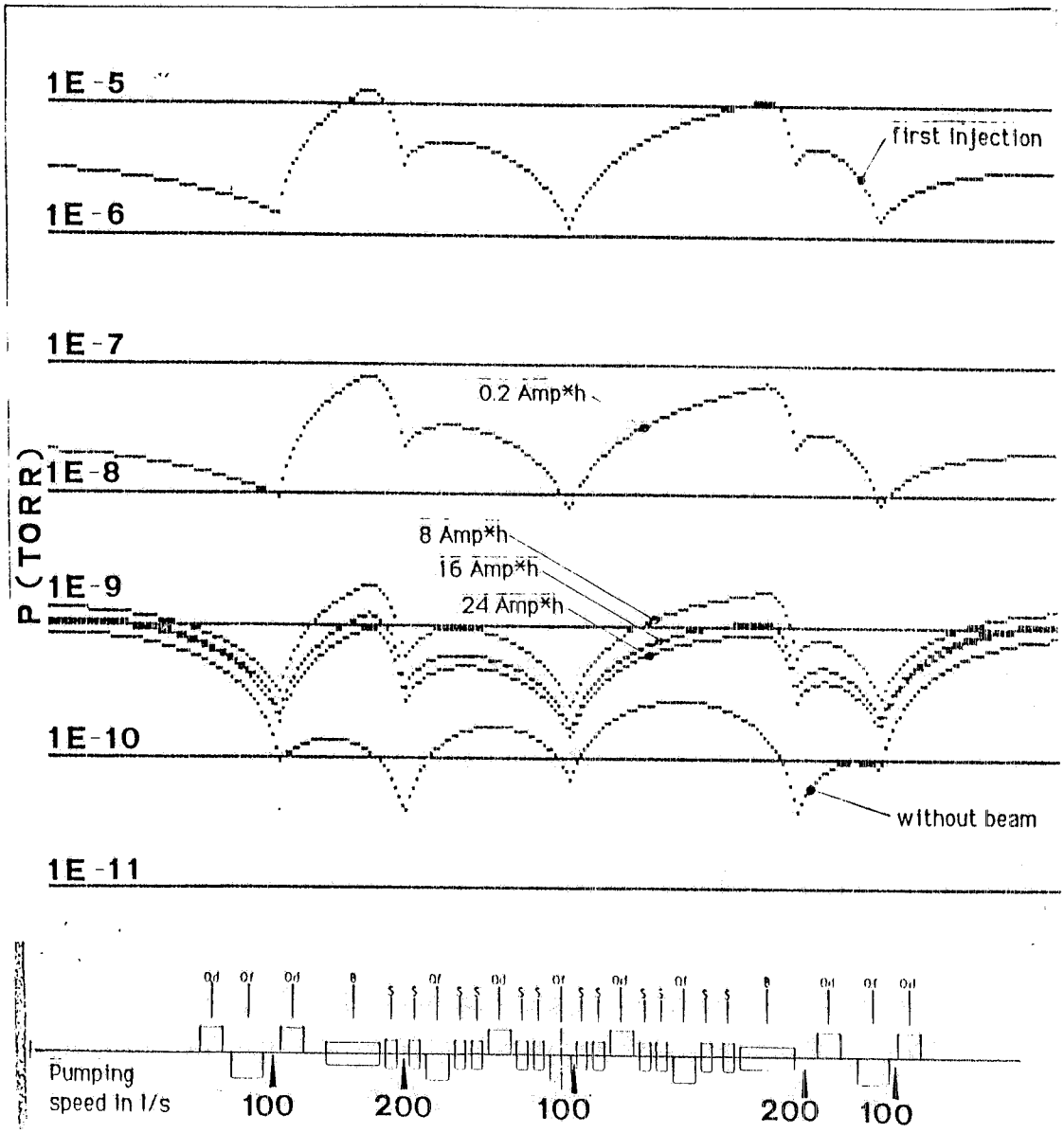

FIG. 7.2. - The pressure distribution along 1/16 of ring as a function of total accumulated dose of circulating beam. Pumping speed is considered not dependent on pressure.

7.2.2 - Materials

Selection has been restricted to Aluminium and Stainless Steel. The choice depends strongly on the shape and the dimensions of the vacuum chamber. For complicated, milled shapes Al is the best choice (see, for example, Ref. 7.1). On the contrary, for simple, TIG welded shapes it is easier to use Stainless Steel. Aluminium is of course easier to bake, due to its high thermal conductance and low bake-out temperature (150 °C against 300 °C). Finally Al seems to have a lower photodesorption yield.

A final choice has not been made yet. For costing purposes, an average cost solution has been evaluated.

7.2.3 - Light Absorbers

For the present design and specification special light absorbers do not seem stricly necessary provided the vacuum chamber is well cooled. Nevertheless they aid significantly in reducing desorption and therefore the conditioning time. A number of them will therefore be installed as near as possible to the vacuum pumps.

The circulating beam loses more than 100 KW of power to synchrotron radiation. This corresponds to approximately 36 Watt/cm along the orbit. The absorbers therefore need to be water cooled since a thermally insulated target hit by synchrotron light would reach too high a temperature. On the other hand, if use of Non Evaporable Getters or Titanium evaporable targets is foreseen, it would appear possible to heat them to their operating temperature by synchrotron radiation only. The actual feasibility of the idea is being checked and should eventually be tested.

7.2.4 - Compatibility between vacuum chamber and magnetic structure

The synchrotron radiation extraction channels interact with a few magnetic elements, namely some of the quadrupoles and the sextupoles. As a conseguence the vacuum chamber design has to be integrated with that of the magnets.

Fig. 7.3 shows 1/16 of the ring. The axis of ports designed for light coming from insertion devices coincides with that of the corresponding long straight section . In between every pair of insertion device ports, an extraction port for radiation coming from a bending magnet is also provided.

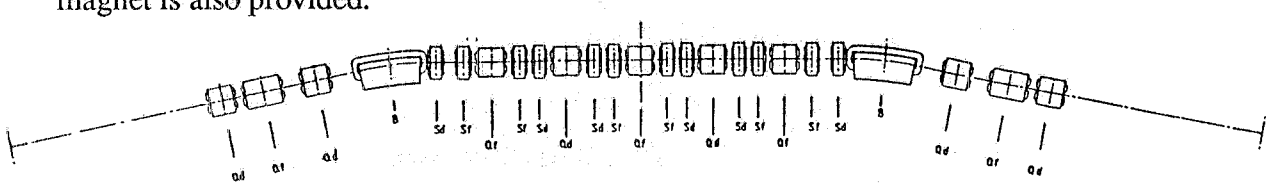

FIG. 7.3 - 1/16 of the machine.

Fig. 7.4 shows an example of vacuum chamber design, in the region of an insertion device light port. Special sextupoles will be used at the place where an interference with the light extraction channels is shown. The detailed design is in progress. Most of the radiation from the bending magnet falls on the absorber, only a small fraction hitting the following vacuum chamber. A pump is placed right next to the absorber.

In each achromat, light is collected from the bending magnet farthest from the preceding long straight. A proposed solution is shown in Fig. 7.5. In this case one quadrupole interferes with the pipe and will have to be specially designed. In all at most 32 sextupoles and 16 quadrupoles will have to be non standard.

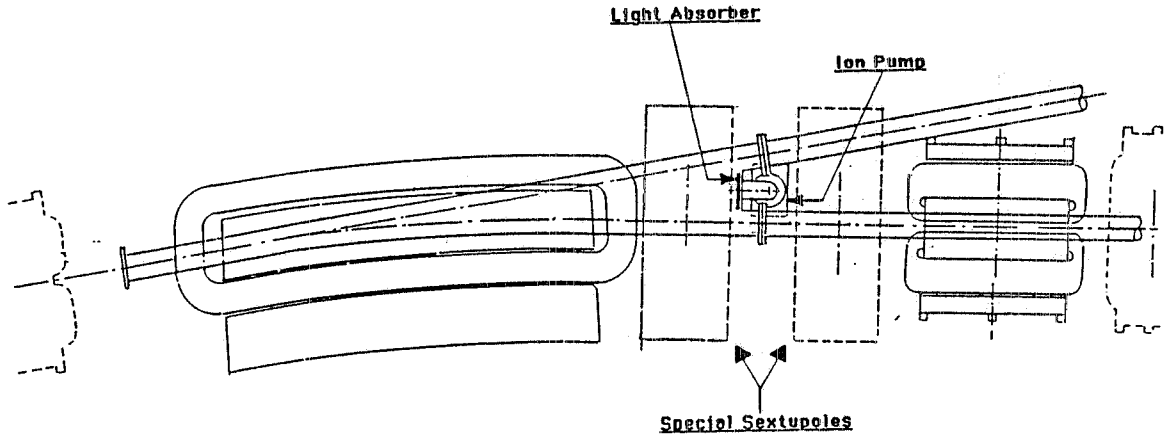

FIG. 7.4 - An example of insertion device radiation extraction port.

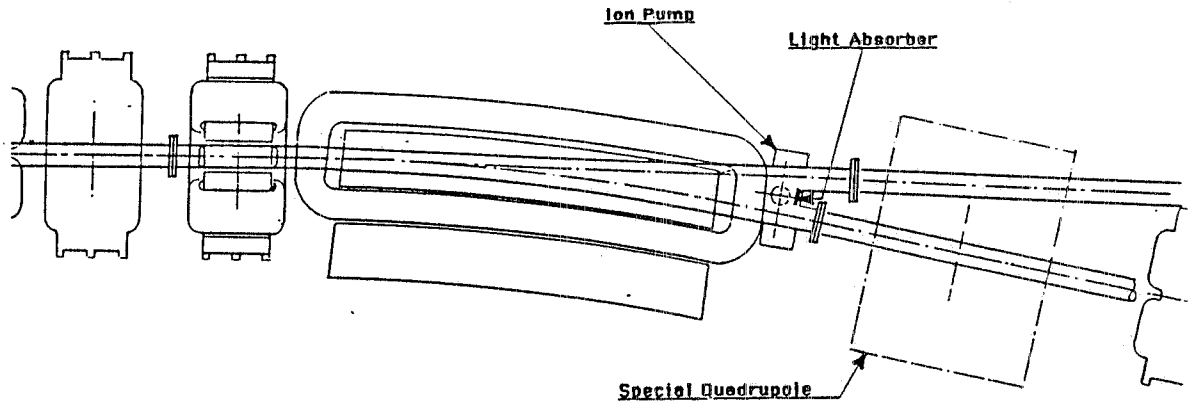

FIG. 7.5 - An example bending magnet radiation extraction port.

7.2.5 - Vacuum monitoring

The simplest way to monitor the total pressure along the vacuum chamber is to read the diode ion pump currents. Total and partial pressure gauges are also necessary: the latter to control residual gas composition and to detect leaks; a gauge every 1/16 of the ring is sufficient.

7.2.6 - Roughing system

Roughing pumps must be oil-free. Oil-free turbomolecular pumps or cryogenic pumps will be used. For starting, Sorption pumps or mechanical pumps equipped with efficient traps will be used. One roughing pump per octant is sufficient, giving a total of 8.

7.2.7. - Bake-out System

We believe that in situ bake-out is necessary to reduce the base pressure, to shorten the conditioning time and to minimize the photodesorption yield (Ref. 7.4). The chamber will have to be designed and equipped to allow for it. Cost estimates for bakeout provisions have been included.

REFERENCES

(7.1) 1 - 2 GeV S.R.S. - Conceptual Design Report - LBL PUB. 5172 Rev., July 1986.
(7.2) V. Chimenti, G. Turchetti: Impianto da vuoto di Afrodite. Internal memo AF 14 (1986).
(7.3) B.A. Trickett: Performance of the SRS Vacuum System, Nov. 1985, Daresbury.

8. - EVALUATION OF THE SHIELDING REQUIREMENTS

A preliminary evaluation of the shielding required for the accelerator complex has been made, based on the data set forth in Table 8.1. The loss parameters liste in the table correspond to the worst localized loss expected at any given spot along the machine.

TABLE 8.1 - Data used for calculating the shielding.

	Beam parameters			Loss parameters	
	Energy (MeV)	Current (nA)	Power (W)	Energy (MeV)	Power (W)
LINAC, Low energy	100	1000	100	100	10
Converter	100	1000	100	100	100
LINAC, High Energy	250	45	12	250	1.2
Booster	2000	2	4	2000	1.3
Main ring injection region	2000	0.5	1	2000	1
Main ring	2000	400 (mA)	670 (J)	2000	670 (J)

Since detailed information regarding the distribution of the losses is not available, assumptions that are probably on the conservative side were made and are listed in the second section of the above Table 8.1. Local shielding may have to be eventually added should there be points where systematic beam losses are localized.

Reference was made to the provisional layout plan of the building (DwgAE.G.O20) for the geometry.

The calculation was made taking into consideration the three following types of area:

a) the area A is accessible under stored beam conditions but not during injection;
b) the area B is accessible also during injection;
c) the area C is never accessible while the machine is operating.

It was also assumed that no building higher than the ring shielding wall is nearer than 40 m to the main ring tunnel.

For the calculation, the old concepts of dose equivalent and the conversion factors introduced in the ICRP- 21 Report were used. This assumption is prudent with respect to the use of the effective dose equivalent at present used by the ICRP to express primary limits.

The new international recommendations regarding radioprotection (ICRP 26) and the actual correct tendency to reduce the doses received by workers and members of the general public to "as low as reasonably achievable" (ALARA principle) were also adopted in defining the

objectives used as the basis for the calculation. The disinclination on the part of workers to operate in the presence of radiation, when simply thickening the shielding would be enough to eliminate the problem, was also taken into account. Possible future lowering of the admissible dose limits , very likely to be introduced in the course of the next decade, was also considered.

TABLE 8.2 - Preliminary evaluation of the shielding (all thicknesses are in cm of ordinary concrete with $\rho = 2.35$ G /cm^3).

	Area A			Area B*			Area C		
	side		roof	side		roof	side		roof
LINAC Low Energy	170		120	210		120	170		120
Converter	210		170	250		170	210		170
LINAC High Energy	130		80	170		80	130		80
	Ext.	Int.	roof	Ext.	Int.	roof	Ext.	Int.	roof
Booster	170	100	100	200	100	100	170	100	100
RING	100***	100	30-50	100***	100	30-50	100***	30	30-50
RING Injection region	170**	100	80	170**	170	80	100**	50	30-50

* The area inside the booster is not included.

** At beam height 15 cm of lead and 115 cm of additional concrete must be on the terminal wall of the transport channel.

*** In line with the straight section exit ports, it is advisable to install some lead to further reduce the gas-bremsstrahlung background. At a residual gas pressure of 10^{-9} torr, 5 to 10 cm will be sufficient.

Moreover, it was assumed that the dose levels in the areas immediately adjacent to the shielding, i.e. ≥ at 5 m from the point where the hypothetical loss is assumed to be localized (it should be impossible to get any closer), must not exceed a few μSv h^{-1} (a few tenths of mrem h^{-1}) or a fraction between 1/5 and 1/10 of the actual limits derived for class A workers (professionally exposed). This is quite a prudent designed aim if the fact that injection should actually occupy only a small fraction of the overall operating time is kept in mind.

The maximum freedom in the use of the machine and tsavings to be derived during

operation in the general area of radioprotection monitoring and surveillance were also taking into account in designing the shielding.

Furthermore, the shielding as calculated need not be modified in the case of limited variations (within a factor of 2 or 3) of the beam loss data set forth in Table 8.1.

For details on the calculation and on the assumptions made regarding the production and the attenuation of the secondary radiation, the reader is referred to Ref.8.1 .

The recommended shielding thicknesses are set forth in Table 8.2.

REFERENCES

(8.1) M.Pelliccioni , LNF Techn.Note AF-7.

9. INSTRUMENTATION AND CONTROLS

9.1. - Beam Diagnostics Instrumentation

9.1.1 . - Purpose

- Initial commissioning: on line monitoring of single shot, or single turn operation is necessary. The use of intercepting monitors is accepted.
- Measurement of lattice and beam parameters: necessary to understand and control the operation of the whole complex: indeed, the formulation of a reliable lattice model is mandatory if accelerators have to be matched to each other and the transport lines have to be set in a quick and predictable way, as required for high injection efficiency and fast filling rate.
- Optimization of the transfer efficiency and the injection rate.
- Diagnosis (and cure) of instabilities and of malfunctioning hardware resulting in losses or in misbehaviour of the beam .
- Optimization of the Main Ring performance.The very stringent demands of a dedicated synchrotron radiation source include careful control of life-time, beam size, closed orbit distorsion and of the position and stability of many independent photon beam lines, to very high accuracy.

  A peculiar feature of the position and angle control system is that the input data to the control system have to be often provided from instrumentation at the user beam line end stations.

A summary list of the various types of monitors which will be used at different locations in the injection chain and in the ring proper is given in Table 9.1.

9.1.2. - Transfer line instrumentation, initial commissioning, current monitors

Fluorescent screens will be used routinely to set-up the the transport lines. However, a number of them is also provided in the Booster and in the Main Ring where they provide as 'extreme case' diagnostics in case of marginal injection, specially during commissioning.

Secondary Emission Monitors, also intercepting, are placed where the dispersion is high, in the transport lines or behind analyzer magnets, to measure the beam energy distribution.

Aperture scrapers are used in conjunction with DC current monitors to observe the beam energy distribution at the tails by measuring lifetime as a function of the scraper position.

Partially intercepting energy defining slits are used in the transport lines to intercept any portion of the beam drifting out of the acceptance limit, to prevent distributed beam spills.

TABLE - 9.1

TYPE OF DIAGNOSTICS	Linac	Linac to Booster	Booster	Booster to Ring	Main Ring	USE
SEM GRIDS	1	1		2		Energy spread
LUMINESCENT SCREENS	2	2	4	2	8	Shape; position; emittance
APERTURE SCRAPERS/ ENERGY SLITS	1	1	1	1	2	Energy distribution(tails) Prevent distributed losses
FARADAY CUPS	2	1	1	1		Total charge (absolute); time envelope
AC CURRENT MONITORS	8	2	1	3	1	Total charge
WALL CURRENT MONITORS			1		1	Wide band longitudinal
DC CURRENT TRANSFORMER					1	Average current/Lifetime
BEAM POSITION MONITORS (high resolution)					128	Measurement and correction of COD. Measurement of optical functions
BPM (normal resolution)	8	10	22	6		
SR MONITOR			1		1	Beam size
TUNE MONITOR			1		1	Frac. tune; BTF; damping
EMITTANCE MONITOR					1	Emittance
BEAM LOSS MONITORS	1	2	8	2	32	Beam spill

A Faraday cup is used to dump the Linac beam and to measure its absolute total charge. If given a coaxial structure it can also monitor the time structure of the beam. It is particularly useful for calibration of other current monitors in the transport lines.

Toroidal current monitors are placed in between the accelerating sections of the Linac and downstream from each bending magnet in the transport lines. In the Booster and in the Main Ring they are used to measure filling rates and to monitor lifetime.

Wall current monitors are used in the Booster and in the Ring to observe the longitudinal beam behaviour.

Absolute measurements of the circulating current are performed using DC Current Transformers (DCCT). The latter are also useful to cross-calibrate other devices such as photodetectors.

Beam loss monitors are distributed all around the Facility and are part of the personnel safety system. They are mentioned here because, specially during commissioning they can complement the 'official' diagnostics.

9.1.3. - Beam Position Monitor (BPM)

The beam position monitor system is a primary diagnostic tool . The highest precision and reproducibility are required in the Main Ring; here the monitors, consisting of four "button" electrodes mounted flush with the vacuum pipe, are located next to the quadrupole magnets. Their design is such as to keep the coupling impedance and parasitic losses within acceptably low values in spite of the large number of units required.

A similar solution is used on the Booster. For the Linac and the transfer lines the low intensity of the positron pulses calls for high sensitivity, but a higher value of coupling impedance is allowed so that strip-line electrodes can be used.

Each monitor is separately connected to the measuring electronics so that the beam trajectory can be measured on a single shot. Provisions are also made to inject a calibration pulse to measure the gains and correct for individual fluctuations.

The nominal resolution, for a 25 mm radius round pipe and 10-bit ADC's, is of the order of a few tens of microns. Once a stored beam is established, averaging over several subsequent passages will considerably improve this figure; the value aimed at is 5÷10 μm.

The position accuracy is related to the position error of the electrical center of monitor with respect to the center of the nearest quadrupole. This error can be removed by modulating the quadrupole strength and correcting the orbit until no correlated deflection in the beam trajectory is detected; the beam must then be traversing the quadrupole center and the position read-out gives the relative offset of the BPM.

It is worth noting that, although very demanding,the tight requirements of the BPM system can be met by mechanical and electronic techniques presently at hand. Nevertheless the large number of devices calls for a great deal of development oriented towards reducing the unit cost.

9.1.4 - Synchrotron Radiation Monitor

The visible and UV part of the SR emerging from a bending magnet is brought to an optical bench where it is split into various beams and used to simultaneously measure the beam longitudinal and transverse dimensions and to directly observe the beam shape with a TV camera.

The bunch length in the Main Ring is 100 ps FWHM typically and can be measured with a resolution of ≈10 ps by means of a streak-camera and a computer controlled scan density converter.

The resolution achievable with a transverse dimension monitor consisting of an optical scanner equipped with a UV photomultiplier is sufficient to observe the beam transverse distribution variations occurring in connection with instabilities and used to study incoherent

phenomena, but is not high enough for absolute measurements of the beam dimensions; for these an X-ray pin-hole camera in a beam-line is used.

9.1.5 - Tune Measurement

The fractional part of the betatron tunes ΔQ_x , ΔQ_z is measured by transversely exciting the beam with a pair of strip-line kickers and looking at the (coherent) response of a transverse pick-up and observing the (coherent plus incoherent) beam cross section increase seen by SR monitor. The swept excitation to the kicker is given by the tracking generator output of a spectrum analyzer boosted with a power amplifier; the coherent response is detected with the spectrum analyzer.

The synchrotron tune is measured in a similar way by phase-modulating the RF cavity voltage and observing the longitudinal beam response on the wall-current monitor.

9.2. - Controls

9.2.1. - General Information

The control system provides the operator with means to control and monitor the hardware and the performance of the facility in general. It also provides test capabilities and local control switch-over during installation or maintenance of large systems.

The control system also includes:

- the computer system;
- the timing and synchronization system;
- an analog (200 MHz), TV and voice multiplexer;
- the control room instrumentation.

9.2.2. - Computer System

The importance of having full remote control is generally acknowledged. The larger being the number of equipments the more the use of a powerful computer system is dictated by considerations of automation, speed, ease and reliability of operation[9.1].

Furthermore, a powerful computer system naturally leads to:

- meaningful and concise presentation of global data regarding the status of complex equipments and the status and performances of the components (Linac, Booster, Main Ring, Transport lines) of the facility;
- data storage for subsequent analysis, statistics, error reporting and logging;
- capability to automatically "reset" a component to a given condition in a consistent and safe way;

- capability to simulate the effect of commands based on elaborate mathematical or empirical modelling of the components;
- transparent input-output interaction in terms of machine-physics parameters such as betatron and synchroton tunes, bunch length, lifetime etc.

All the above points require setting up, from the very beginning, a central Data-Base containing:

- name list, type of hardware, geographical positions;
- physical and logic interconnections;
- control system interconnnections;
- hardware limits, alarm thresholds;
- calibration data, magnetic measurements.

The computer system architecture is based on a high performance central computer equipped with mass-memories and graphic workstations for operator interaction.The system is connected to a Local Area Network (LAN). The same LAN accomodates a development computer and workstation.

The central computer is connected via I/O highway to several equipment computers controlling the input/output modules. The communications between central computer and hardware take the form of high-level commands decoded and executed by the equipment computers. The equipment computer is typically a single-board microcomputer controlling a crate of I/O modules.

9.2.3. - Hardware Interface

The major requisites of the input/output modules and the equipment computers are

- compliance with a widely used International Standard;
- market availability;
- mature technology;
- reliability.

CAMAC is the obvious candidate. However, the impulse given by industry and, more specifically, in the field of accelerator control by LEP, forces to consider the utilization of other standards such as VME (equipment computer) plus G-64 (intelligent I/O control).

Sufficient R&D capability in the controls group could make it convenient to develop a private standard better suited to interface with the particular accelerator system.

REFERENCES

(9.1) P. Clout, M. Serio: The ESRF Control and Diagnostic System - ESRP-IRM-49/84 (1984).

10 - THE INJECTION SYSTEM

10.1 - General specifications and remarks

The general specifications for any synchrotron light source injection system are[10.1]:

- full main ring (MR) energy. For the Trieste machine (CARST) this means that the injector should be able to provide a beam energy of up to 2 GeV.
- MR filling time to maximum foreseen current, much shorter than the beam lifetime.

Both requirements point to more costly solutions than the" minimum configuration" ones that would still work. However the larger initial investment is in our opinion more than repaid by the savings afforded during operation through shorter commissioning time, faster start up after a vacuum breakdown, and high overall operating efficiency.

Full energy injection guarantees that the problems to arise, in connection with the need for keeping a large number of beam lines independently aligned to very high precision, will be reduced to a minimum. Also, lifetime under poor vacuum start-up conditions can be much shorter than its design value for the steady state regime. A high energy, high current injector can reduce the time needed to achieve a good vacuum by large factors, thereby improving the MR overall reliability. At start-up injection times should ideally be of the order of a minute; in the steady state they can be compared to the asymptotic lifetime (in our case = 6h) and be correspondingly longer.

The injected beam emittance and energy spread are of paramount importance when considering very low emittance storage rings. This because, on one hand strong focusing and good field quality are required so that it is advantageous for both cost and reliability considerations to keep the MR physical chamber aperture to a minimum (compatible with the other constraints) and, on the other, the MR space and momentum acceptances can be limited by nonlinear dynamics effects to below what afforded by the chamber physical size.

Finally, the potential for (cost effectively) upgrading the injector energy in view of possible unforeseen developments is a definite advantage.

10.2. - Electrons versus positrons

The next important issue is whether one should operate the MR on electrons or positrons.

Several existing SR sources, having beam emittances much larger than those expected from the 'third generation rings' such as CARST, are proven to operate more reliably and efficiently with positrons than with electrons. This because electron beams tend to trap the positive ions they create in the residual gas, the trapped ion cloud can then produce instabilities that result in sudden lifetime changes and/or beam blow-up.

Experimental results on ion trapping are scarce and in qualitative agreement only with theoretical prediction. Thus although the theory predicts ion trapping to become more difficult when the beam emittance is decreased, enough uncertainty exists to justify designing for an injector with e^+ capability (at least as an option).

However, for any injection system in the energy range we are considering the ratio of electron to positron production is large (electron current is usually limited only by the acceptable energy spread and, possibly, by instabilities). This means that it is much easier to satisfy start-up filling time requirements with electrons. e^- injection should therefore be available for use under start-up conditions and be designed to achieve filling times of the order of one minute: positrons filling times will then fall automatically in the range of a few (tens of) minutes, still compatible with the requirement of being much shorter than the steady state lifetime of 360 mins.

From the point of view of cost the e+ versus e- issue is extremely important; an adequate e- only injector is intrinsecally cheaper than a system having positron capability.

As a consequence, cost-conscious designers tend to design injection systems that can be built in stages: a lower cost e^- only first stage to which a second e^+ stage can be added if and when required.

10.3 - Linac plus booster synchrotron

According to the above general specifications and remarks the injection system for CARST should fulfill the following requirements:

- The system must provide a beam to the storage ring at its nominal operating energy of 2 GeV.
- The filling time required to reach the full current of 400 ma in the main ring should be short, below one minute in the case of electrons and less than ten minutes for positrons.

To achieve these goals we propose the injection system illustrated schematically in Fig 10.1. It consists of a high intensity electron gun, a 220 MeV electron linac, an e^-/e^+ converter, a 220 MeV positron linac, and a 10 Hz/ 2 GeV booster synchrotron.

Two operation modes are foreseen: single (or few) bunch and multibunch. In the first mode a single bunch of less than 10 ns duration is injected in a single bucket of the 50 MHz RF of the booster; it is then accelerated, ejected and transferred to the main ring. In the multibunch mode a long pulse (≈200 ns) partially fills the booster circumference, leaving only a gap to accomodate the kicker risetime.

The injector complex is capable of filling the storage ring to its full 400 mA current in about 10 minutes in the case of positrons and in a few secs in the case of electrons[10.4].

In Table 10.1 we show the transmission efficiencies of the various steps of injection for positrons. Below we first describe single bunch operation and then in § 10.4.7 the multibunch mode.

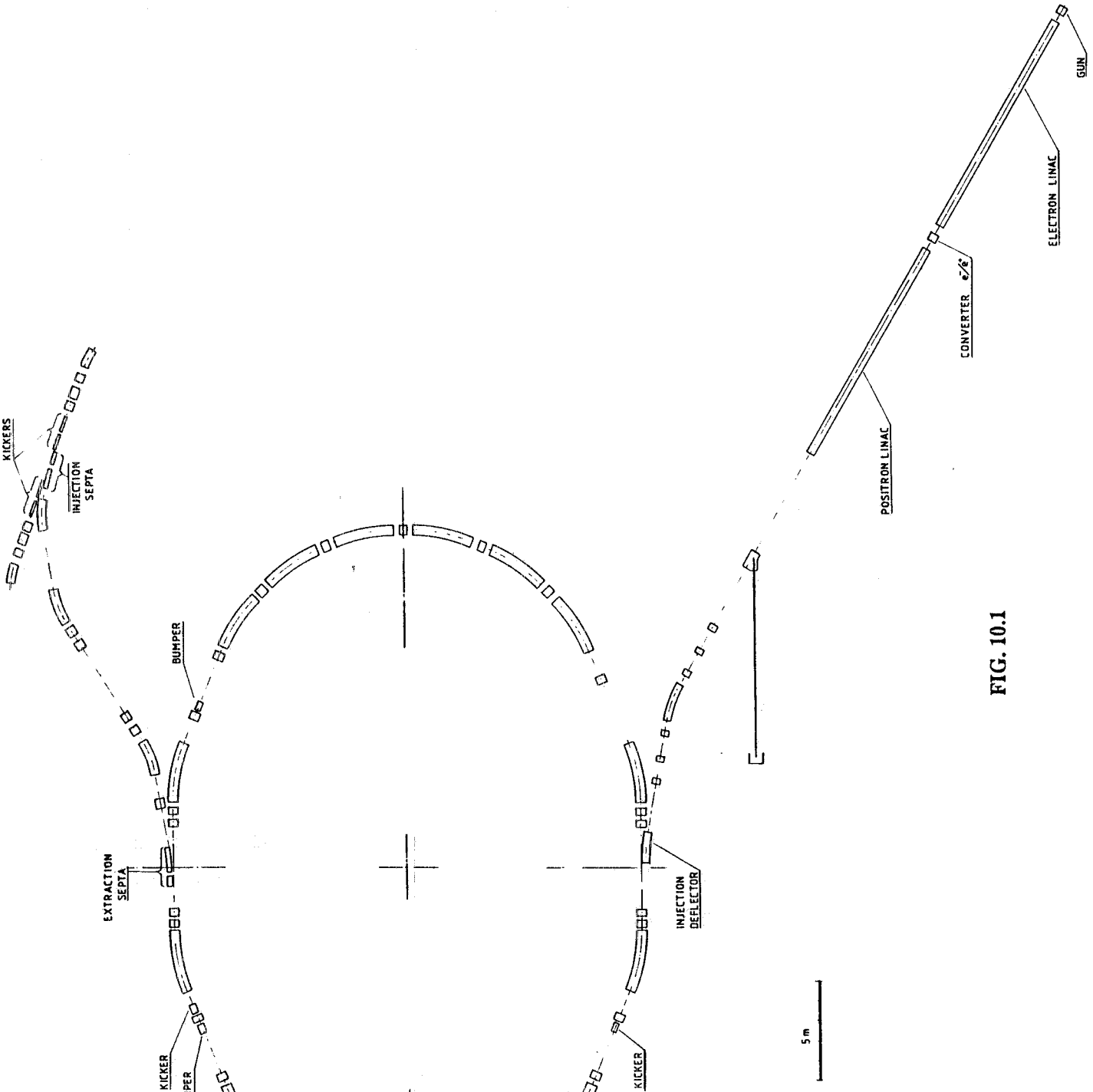
KICKERS
INJECTION SEPTA
BUMPER
EXTRACTION SEPTA
KICKER
BUMPER
KICKER
INJECTION DEFLECTOR
POSITRON LINAC
CONVERTER e⁻/e⁺
ELECTRON LINAC
GUN
5 m

FIG. 10.1

TABLE 10.1 - Transmission Efficiency at the various steps of positron injector.

	CHARGE nC	NUMBER OF ELECTRONS X 10 -10	EFFICIENCY	TRANSMISION
GUN CHARGE /PULSE	200	124		
			0.5	
ACCEPTED BY HIGH CURRENT LINAC	100	62		0.5
			0.9	
HIGH CURRENT LINAC EXIT	90	56		0.45
			0.004	
ACCEPTED BY e+ LINAC	0.36	0.23		1.8x10-3
			0.9	
e+ LINAC EXIT	0.32	0.20		1.6x10-3
			0.5	
ACCEPTED BY BOOSTER	0.16	0.10		0.8x10-3
			0.8	
EXTRACTED FROM BOOSTER	0.13	0.08		0.65x10-3
			0.5	
ACCEPTED BY MAIN RING	0.06	0.04		0.32x10-3

10.4. - Description of the system

10.4.1. - The Gun

It is proposed to use a triode gun like those built for LIL-LEP and for Adone. Its description and performance can be found in Ref. 10.3. Currents in excess of 16 A for pulse durations of $\leq$ 10 ns have been achieved. The main characteristics of the gun are given in Table 10.2.

TABLE 10.2 - The high intensity electron gun.

Type		Pierce, triode
Output energy	(KeV)	80÷100
Peak current	(A)	20
Pulse length	(ns)	10
Pulse rise time	(ns)	3
Charge per pulse	(nC)	200

10.4.2. - The Linacs

There are two linacs in the injection chain: a high current electron linac and low current positron or electron linac. Both have the same structure: they consist of an S -band standing wave buncher or capture section followed by an S-band travelling wave main accelerator. The unloaded energy of each linac is ≤ 220 MeV; it is determined by the following requirements:

- Positrons: they are emitted from the converter with an invariant emittance $\varepsilon \leq 6*10^{-3}\ \pi$ m*rad. In order to achieve $\varepsilon = 10^{-5}\ \pi$ m*rad they have to be accelerated to an energy ≥ 200 MeV.
- Electrons: the e^-/e^+ conversion efficiency is about 2%/ GeV, so that a primary electron energy > 100 MeV is recommended. Taking into account the possibility of compressing the Klystron RF pulse (SLED or LIL type, see below) a solution where the high current linac is similar in structure to the low current one appears to be the most efficient and economical[10.4].

10.4.3. - The buncher

For the buncher, a π/2 biperiodic standing wave accelerating section similar to the one built for the Adone injector is proposed. It is based on the experience gained with the similar buncher of the LIL-LEP injector. The main parameters of the buncher are given in Ref. 10.2 and in Table 10.3.

TABLE - 10.3

		Buncher	HE Sections	
Type :		Combined prebuncher-buncher		
Accelerating structure		π /2 SW, biperiodic	2π/3 TW	
Frequency	(MHz)	2998.5	2998.5	2998.5
Quality factor		15000	15200	
Shunt impedance(ZT^2)	(MΩ/m)	50	68	70
Filling time	(μs)		1.2	0.7
Length	(m)	1.2÷1.5	4.5	2.5
Input power	(MW)	5 ÷ 10	17.5	30
Average energy gain (no load)	(MeV)	15 ÷ 25	63	55.4
Energy dispersion : no load	(MeV)	0.6÷1.3		
@100 nC	(MeV)	3 ÷ 8	18.4	11.7
Attenuation factor	(Np/m)		0.64	0.44
Stored energy	(J)		10	
Phase dispersion	(deg)	20		
Output current	(A)	10	10	10
Pulse length	(ns)	10	10	10
Accelerated charge : e^-	(nC)	100	100	100
e^+	(nC)		0.4	0.5

10.4.4. - Travelling wave accelerating sections

To accelerate electrons after the preliminary bunching we propose to a use travelling wave structure. This because compared to a standing wave one it requires about 23% less power for the same energy.

The chosen constant gradient $2\pi/3$ TW structure has the following advantages: constant power dissipation, higher unloaded beam energy, higher energy conversion efficiency. The shunt impedance for $2\pi/3$ is close to the maximum. Furthermore it has been successfully tested at least in two large accelerators (SLAC and LIL-LEP).

We propose to adopt the same frequency as LIL, namely 2998.5 MHz; LIL parameters have consequently been taken as a basis for our design.

Two linac configurations, with different RF powering systems have been examined:

- A traditional solution where power is fed to the sections directly from a klystron. The optimized section length is then L=4.5 m and the corresponding filling time is $\tau_f = 1.2$ μs. The main parameters of such TW section are given in Ref. 10.2 and in Table 10.3.
- A solution with pulse compression. The optimized section length is then $L = 2 \div 2.5$ m and the filling time $\tau_f = 0.6 \div 0.7$ μs. Since this solution is more economical than the previous one we propose it as our first choice for both linacs and discuss it in some detail below.

10.4.5. - Electron - positron converter

The design of the electron-positron converter that follows the 220 MeV high current LINAC, is based on that of the converter installed on the Frascati Linac[10.14-16]. It consists of a gold target brased unto a water cooled copper radiator.

Most of the positrons leaving the converter have energies between 5 and 15 MeV. The conversion efficiency is about 0.02/GeV. The positron design current is 40 mA. The positrons are focused by a strong pulsed solenoidal field before entering the capture section. Solenoids also provide the focusing along the HE Linac.

10.4.6. - The pulse compression scheme

The successful use of power multiplication by pulse compression at SLAC, DESY and CERN[10.5,10.6,10.7], justifies the application of such a system to this project.

It is known [10.5] that by this scheme a power gain of the order of 3 to 4 can be achieved. It can be shown that by using a TH2094 klystron with a pulse duration τ_p=4.5 μs and a peak power of 35 MW, the power multiplication factor F_p changes from about 2.4 to about 4 when the length of the proposed CG accelerating sections varies from 4.5 m to 2 m, with a

corresponding decrease in the filling time from 1.2 μs to 0.6 μs. From one klystron one accordingly expects to receive 84 to 140 MW of peak power.

Assuming 20 to 30 MW is the maximum safe power input to one section (the limiting element is likely to be the RF ceramic windows) one klystron can feed 4 to 6 accelerating sections independent on their lengths.

Another limiting parameter is the electric field level in the structure. Most of the existing high energy S- band electron linacs have electric field intensities in the range of 12 to 15 MV/m. However recent measurements made at SLAC[10.8] on their 2/3π structure have shown that accelerating field levels higher than 130 MV/m can be achieved without breakdown. We have threfore assumed that 25 MV/m is safe as far as breakdown is concerned.

There are now two possibilities:

A) Apply the pulse compression to the long TW sections proposed in Ref.10.2.

B) Design new, shorter accelerating structures with higher gradients (> 20 MV/m), that are better suited to the high input power levels offered by the pulse compression scheme[10.4].

A) Pulse compression using long sections

One can apply pulse compression to the already proposed 4.5 m long TW sections , having a filling time t_f =1.2 μs and attenuation 2t =1.24. The klystron pulse length is assumed to be 4.5μs. The resulting energy gain per section corresponding to an input power of 20 MW (25 MW) is 66.5 MV (74.3 MV).

Taking the above figure as a basis, several configurations can be devised, as explained in detail in Reference 10.4. In the most favourable case, compared to the system without pulse compression one could save one klystron (and its modulator) and almost double the positron current by almost doubling the electron energy on the converter.

B) Short optimized accelerating sections

In Ref. 10.4 it is shown that shorter accelerating sections having length L=2 to 2.5 m and corresponding filling time Tf= 0.6 to 0.7 μs are better matched for use with pulse compression. Results are given in detail in Reference 10.4 but some of the characteristics of the short section are listed in Table 10.4.

TABLE 10.4

T filling μs	Q cavity	β opt	F_E	F_E^2(power)	Max. power MW	L m
1.2	200000	6	1.55	2.4	84	4.5
1.0	180000	7	1.75	3.06	107	4.5
0.7	180000	8.5	1.94	3.76	132	2.5
0.6	160000	8.5	2.1	4.41	154	2.0

The power multiplication factor, Fp, is 4 so that one 35 MW klystron can deliver about 140 MW at the peak. Each klystron can therefore feed 4 to 5 accelerating sections, supplying more than 25 MW per section. The resulting energy multiplication factor, Fe, is 2.

An additional advantage of the short section is that it can be designed to have higher shunt impedance. This because the shunt impedance of a constant gradient structures decreases with increasing iris diameter so that shorter structures with smaller variations of it is diameter have higher effective shunt impedance. The results of the calculations are given in Ref. 10.4.

For L=2.5 m and Po= 25 MW the energy gain per section is 50.5 MeV giving 202 MeV per four sections fed by a single klystron. At the highest power input the RF window can sustain, e.g. 30 MW, an energy gain per section of 55.4 MeV (corresponding to 221.6 MeV per klystron) can be achieved with an average accelerating field of 22 MV/m. The total active length of the linac then becomes 10 m.

This last solution, sufficiently simple and giving more than 200 MeV per one klystron , is our preferred choice (See also Fig.10.2).

A comparison of all solutions is given in Table 10.5.

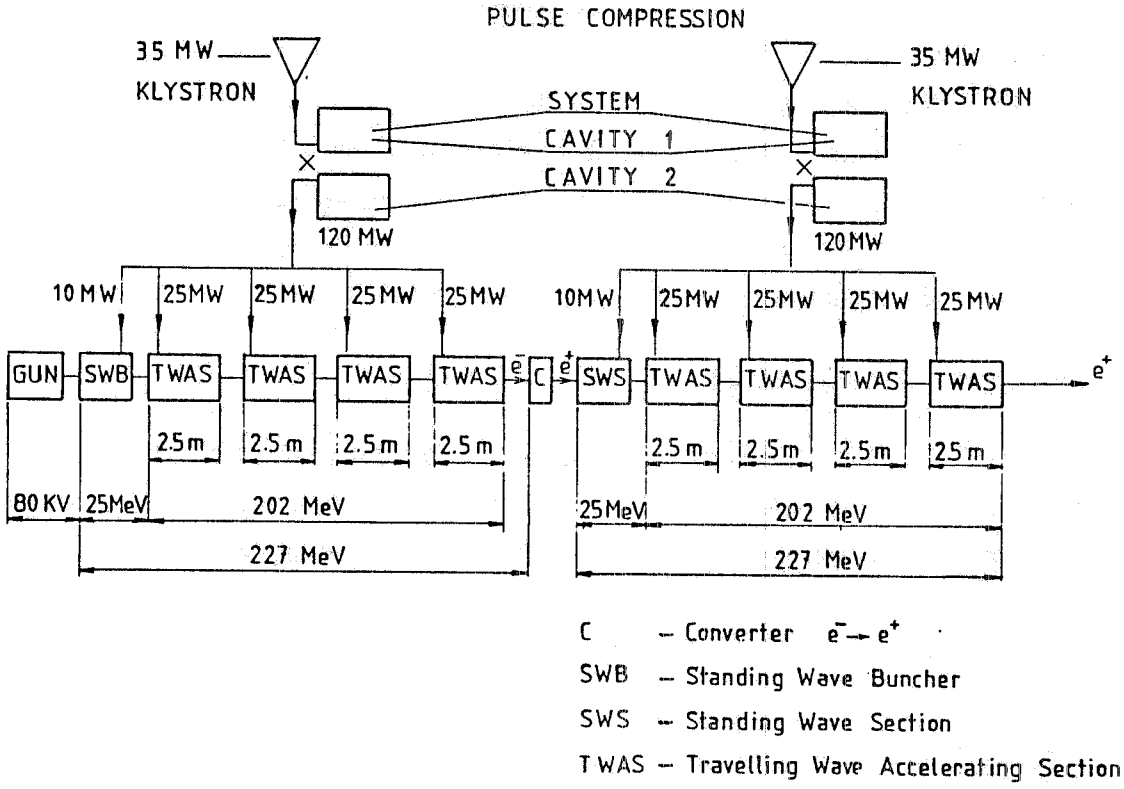

FIG. 10.2

TABLE 10.5 - Main parameters of travelling Wave Linacs without and with Pulse Compression.

	HIGH CURRENT LINAC				LOW CURRENT LINAC				
	LONG SECTION		SHORT SECTION		LONG SECTION			SHORT SECTION	
PULSE COMPRESSION	NO	YES	YES	YES	NO	YES	YES	YES	YES
SECTION LENGTH m	4.5	4.5	2.5	2.5	4.5	4.5	4.5	2.5	2.5
NUMBER OF SECTIONS PER KLYSTRON	2	3	4	4	2	4	3	4	4
POWER INPUT PER SECTION (MW)	15	25	25	30	17.5	20	25	25	30
ENERGY GAIN PER SECTION (MeV)	58	74.3	50.5	55.4	63	66.5	74.3	50.6	55.4
FIELD GRADIENT(MV/m)	12.9	16.5	20.2	22.2	15.7	16.6	16.5	20.2	22.2
NUMBER OF SECTIONS PER LINAC	2	3	4	4	4	4	3	4	4
ENERGY GAIN UNLOADED (MEV)	116	223	202	222	252	266	223	202	222
BEAM LOADING PER SECTION MV	18.4	18.4	11.7	11.7	0.09	0.10	0.09	0.06	0.06
Δ E/E FULL LOAD	0.32	0.25	0.23	0.21	0.02	0.02	0.02	0.02	0.02
LINAC LENGTH (m)	9	13.5	10	10	18	18	13.5	10	10
NUMBER OF KLYSTRONS	1	1	1	1	2	1	1	1	1
BEAM CHARGE PER PULSE (nC)	100	100	100	100	0.52	0.56	0.48	0.44	0.48

10.4.7 - Multibunch operation

For multibunch operation (e^+ or e^-) all the buckets of the main ring have to be filled and it is may be easier (from the point of view of control) to use the longest possible Linac pulse. A 200 ns long pulse can be obtained from the proposed pulse compression system.

In this case the main limitation for e^- is the energy spread acceptance of the booster synchrotron, assumed to be $\Delta W/W \leq 1\%$. This conditions the maximum charge, q_b, transmitted through the last Linac accelerating section before injection into the booster. Injecting the beam in the section before the maximum of the acceletaring voltage waveform, in such a way as to compensate the energy loss due to beam loading by the rise in accelerating voltage, it is possible to inject, in 200 nsecs pulse, an optimum value of charge equal to 46 nC, with a resulting energy spread smaller than 0,5%.

The corresponding electron filling time is then equal to 4.3 secs.

For positrons, a 200 ns, 500 mA e- current pulse from the high current linac is used giving a maximum positron charge of 0.4 nC in a 200 ns long pulse, when the conversion efficiency of 2%/GeV is used. The positron filling time in the multibunch mode is 10 min.

10.5. - Linac to booster transfer line

The linac to booster transfer line transports a 250 MeV beam having the following characteristics[10.17]:

- Radial and vertical emittances 10^{-5} m rad.
- Envelope functions, $\beta_x=\beta_y = 5$ m $\alpha_{xi}=\alpha_{yi}=0$

The transport channel is achromatic and it must match the input beam functions to those of the booster injection point:

$$\beta_x= 17\text{m}, \beta_y= 8\text{ m}, \quad \alpha_{xf} = \alpha_{yfi}=0.$$

The length of the channel is 22.85 m and the beam is injected in the booster by deflecting it through 10°.

The channel, shown schematically in Fig. 10.1, can be subdivided in three parts:

a) A straight section consisting of a 10 m long drift space and of quadrupoles QF_1, QD_1 and QF_2. The drift space also contains a pulsed magnet that can be used to deflect the beam into a measuring station.

b) A 20° deflection magnet, M.

c) An injection section consisting of quadrupoles QD_2, QF_3, QD_3 and the inflector magnet MD.

The six quadrupoles in the transport channela are used to match the six beam envelope output parameters to the booster acceptance, namely to: $\beta_{xf} = 17$ m, $\beta_{yf} = 8$ m, $\alpha_{yf} = \alpha_{xf} = 0$, D=0, D'=0.

The characteristics of the magnetic elements are given in Table 10.6.

Diagrams of the beam envelope and of the dispersion function are shown in Fig.10.3. To trim the beam position and angle at injection, two pairs of steering coils are foreseen. Beam diagnostics consisting of strip lines and fluorescent screens is also foreseen.

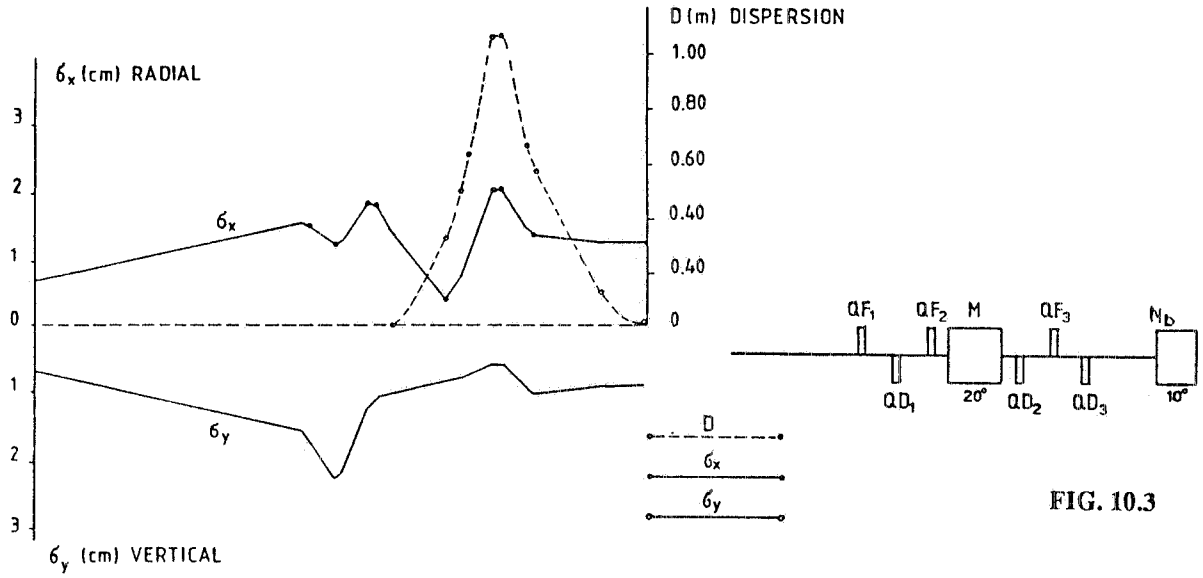

FIG. 10.3

TABLE 10.6

QUADRUPOLE				
	Magnet Length (cm)	Half Aperture (cm)	Gradient (KGauss/cm)	Number Quadrupoles
QF_1	32	5	0.0682	1
QD_1	32	5	0.1711	1
QF_2	32	5	0.1833	1
QD_2	32	5	0.0399	1
QF_3	32	5	0.2048	1
QD_3	32	5	0.1072	1
MAGNETS				
	Magnet Length (m)	Bend Angle (deg.)	Bend Radius (m)	Field Strength B (KGauss)
M	2	20°	5.729	1.455
M_D	1.5	10°	8.594	0.970

10.6 The booster synchrotron

10.6.1 Booster design criteria

The booster ring for the AFRODITE injector chain has been studied to achieve a low emittance in the order of 10^{-7} m rad. It accepts the injected beam directly from the positron linac without an intermediate positron accumulator.

The basic version of the booster structure consists of two FODO arcs, joined by matched insertions with zero dispersion sections. Two versions have been studied, one [10.9] optimized for a low emittance of 1 10^{-7} m rad at 1.5 GeV and the other [10.10] designed to operate 2 GeV but capable of reaching 3 GeV. The latter version, besides fulfillling the the requirement of full energy injection at 2 GeV, was studied to explore the implications of providing a very powerful injector for possible future unforeseen developments of the facility. The 3 GeV ring is not much longer than the 1.5 GeV one because the number of FODO cells has been reduced at the expense of an increase in the emittance to 3.3 10^{-7} mrad at 1.5 GeV.

The 3 GeV version, the emittance of which is still well acceptable for injection into the main ring at 2 GeV, is described in the following.

Beam losses in the first stage of acceleration, before the injected beam is fully damped, have been estimated to provide realistic efficiency figures (10.11). The main ring filling rate, in both the single bunch and the multibunch mode, is essentially only determined by the positron current that can be obtained from the linac.

10.6.2. - The lattice

The booster ring structure consists of two FODO arcs connected by two long insertions matched to the arcs. Each insertion contains a long dispersion free straight section and two shorter straights. The long straights accomodate the injection and extraction septa.

The lattice consists of 16 bending magnets and of 26 quadrupoles (see Table 10.7). In the matching sections between the FODO arc and the dispersion free section there is room enough to accomodate the RF cavities and the kicker and bumper magnets, at the right phase with respect to the septa.

TABLE 10.7

Energy	1500	MeV
Emittance	$9.5 \cdot 10^{-8}$	$m \cdot rad$
Length	79.060	m
Q_x	5.117	
Q_z	2.844	
Q'_x	−7.0	
Q'_z	−5.0	
α_C	$4.1 \cdot 10^{-2}$	
σ_P	$5.8 \cdot 10^{-4}$	
$\Delta E/turn$	90	keV
$\nu_{revolution}$	3.7920	MHz
$\tau_{betatron}$	8.8	ms
$\tau_{synchrotron}$	4.4	ms
Superperiodicity	2	
FODO cell/superperiod	5	
straight section length	5.00	m
magnet number	24	
curvature radius	5	m
B_{max} @ 1.5 GeV	1.0	$Tesla$
quadrupoles, q. families	38, 5	
$dB/dx\|_{max}$	10.2	$Tesla/m$

The optical functions $ß_X$, $ß_Z$ and D_X are shown in Fig. 10.4 for one quarter of the machine. A summary of the main booster parameters is given in Table 10.7.

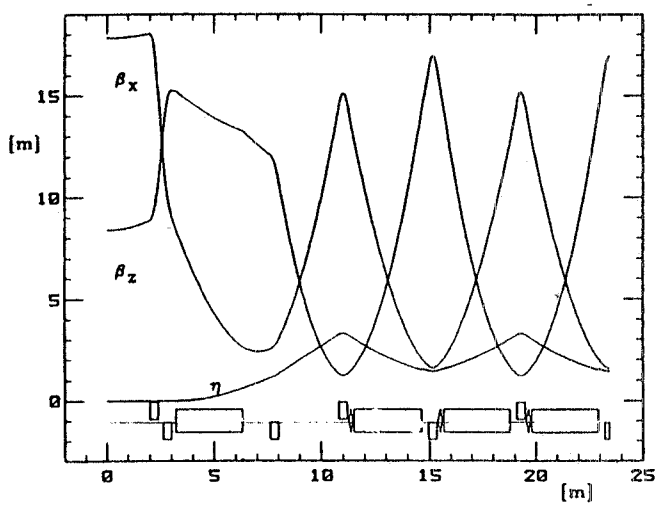

FIG. 10.4 - Optical function in 1/4 machine.

TABLE - 10.8

ELEM NOME	LUNG	L.TOT.	K	β_x	α_x	$\mu_x/2\pi$	η_x	η'_x	β_z	α_z	$\mu_z/2\pi$
MARK M0	0.000	0.000	0.0000	17.8287	0.0000	0.0000	0.0036	0.0000	8.3829	0.0000	0.0000
DRIFT LLONG	2.000	2.000	0.0000	18.0531	−0.1122	0.0178	0.0036	0.0000	8.8601	−0.2386	0.0373
QUADRQF	0.400	2.400	1.1610	14.9895	7.2907	0.0215	0.0032	−0.0016	10.8461	−5.0302	0.0440
DRIFT LDF	0.200	2.600	0.0000	12.2178	6.5682	0.0239	0.0029	−0.0016	12.9552	−5.5152	0.0467
QUADRQD	0.400	3.000	−1.0232	9.0928	1.6661	0.0301	0.0025	−0.0005	15.2608	0.0691	0.0511
DRIFT LBR	0.200	3.200	0.0000	8.4429	1.5830	0.0337	0.0024	−0.0005	15.2358	0.0559	0.0532
RBENDB1	3.142	6.342	0.0000	2.6419	0.3116	0.1460	0.6099	0.3973	13.2748	0.5195	0.0886
DRIFT LBL	1.290	7.632	0.0000	2.5291	−0.2241	0.2291	1.1224	0.3973	12.0937	0.3961	0.1048
QUADRQD0	0.400	8.032	−0.5867	3.0333	−1.0756	0.2526	1.3369	0.6837	10.7109	2.9519	0.1103
DRIFT LD	2.781	10.813	0.0000	14.5150	−3.0530	0.3214	3.2382	0.6837	1.3063	0.4298	0.2438
MARK M1	0.000	10.813	0.0000	14.5150	−3.0530	0.3214	3.2382	0.6837	1.3063	0.4298	0.2438
QUADRHQF	0.400	11.213	1.0409	14.5165	3.0494	0.3257	3.2382	−0.6837	1.3063	−0.4297	0.2947
DRIFT L05	0.050	11.263	0.0000	14.2134	3.0139	0.3262	3.2040	−0.6837	1.3515	−0.4750	0.3007
SEXTU SF	0.200	11.463	0.9500	13.0362	2.8721	0.3286	3.0673	−0.6837	1.5778	−0.6564	0.3226
DRIFT L05	0.050	11.513	0.0000	12.7507	2.8366	0.3292	3.0331	−0.6837	1.6457	−0.7017	0.3275
RBENDB1	3.142	14.655	0.0000	2.0315	0.6643	0.4319	1.5489	−0.2858	14.4165	−3.0453	0.4391
DRIFT L3	0.300	14.955	0.0000	1.6968	0.4515	0.4577	1.4631	−0.2858	16.3079	−3.2591	0.4422
QUADRHQD	0.400	15.355	−0.9896	1.6991	−0.4574	0.4966	1.4631	0.2858	16.3080	3.2588	0.4460
DRIFT L05	0.050	15.405	0.0000	1.7466	−0.4930	0.5012	1.4774	0.2858	15.9839	3.2232	0.4465
SEXTU SD	0.200	15.605	−2.0000	1.9722	−0.6353	0.5184	1.5345	0.2858	14.7232	3.0807	0.4486
DRIFT L05	0.050	15.655	0.0000	2.0376	−0.6709	0.5224	1.5488	0.2858	14.4169	3.0450	0.4491
RBENDB1	3.142	18.797	0.0000	12.8182	−2.8500	0.6246	3.0329	0.6836	1.6463	0.7020	0.5607
DRIFT L3	0.300	19.097	0.0000	14.5923	−3.0635	0.6281	3.2380	0.6836	1.3067	0.4299	0.5935

K in m^{-2} for quadrupoles, m^{-3} for sextupoles

Table 10.8 lists the values of the optical functions. Values are given at the end of each element, starting from the mid point of the insertion and ending at the end of the first FODO cell in the arc. The magnet strenghts are also given.

Chromaticity has been corrected in both planes using two families of sextupoles, with one focusing (SF) and one defocusing (SD) sextupole per FODO cell. No additional families are required to correct the amplitude dependence of the tunes.

Although non-linear and energy dependent effects are rather small, carefull consideration has to be given to field distortions induced by eddy current in the vacuum pipe during the acceleration cycle. The main effect of the eddy currents is to generate sextupolar field superimposed on bending magnets dipole field.

The strength of the sextupole depends very much on the shape and the material of the vacuum pipe. The estimate given here is based on assuming a vacuum pipe similar to that of the DESY II Synchrotron booster and on a main field ramping rate of 30 T/s; the resulting induced chromaticity is +65. This can be corrected by the field in the standard chromaticity correcting sextupoles; the resulting requirements in terms of sextupolar gradients have been taken into account in designing the sextupoles. The tracking between the dipolar and the sextupolar fields is not critical. The strength required to compensate the induced field and to keep both chromaticities close to zero during ramping is shown in Fig. 10.5. The sextupole parameters are summarized in Table 10.9. The behaviour of Q_X and Q_Z and of the optical function relative variations versus momentum are shown in Fig. 10.6 to 10.8.

The dynamic aperture is by far larger than the physical aperture, both for on-energy particles and for particles with energy deviations of up to 1.8 %. The dependence on amplitude of Q_x is shown in Fig. 10.9.

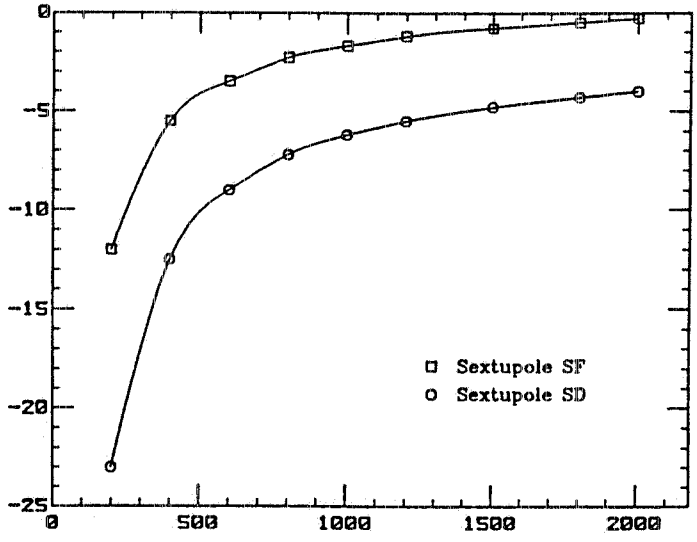

FIG. 10.5 - Sextupole strength (m^{-3}) vs energy (MeV).

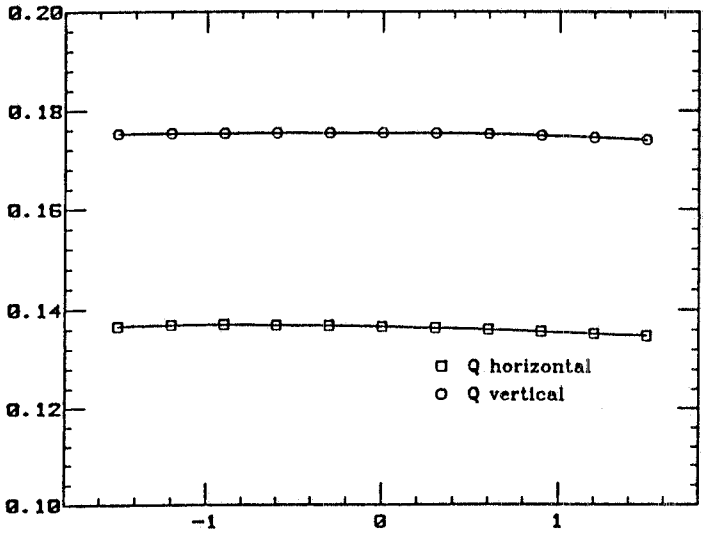

FIG. 10.6 - Variation of tunes vs ΔP/P (%).

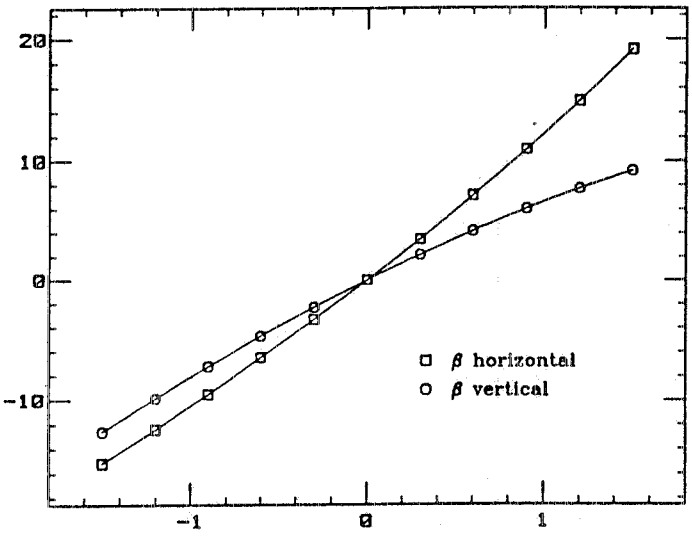

FIG. 10.7 - Δβ/β (%) dependence on ΔP/P (%) in insertion straigths.

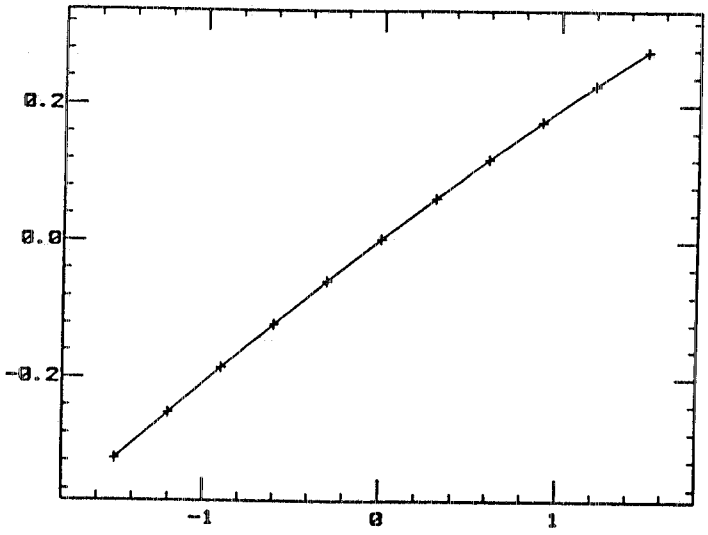

FIG. 10.8 - η variation (m) vs ΔP/P (%).

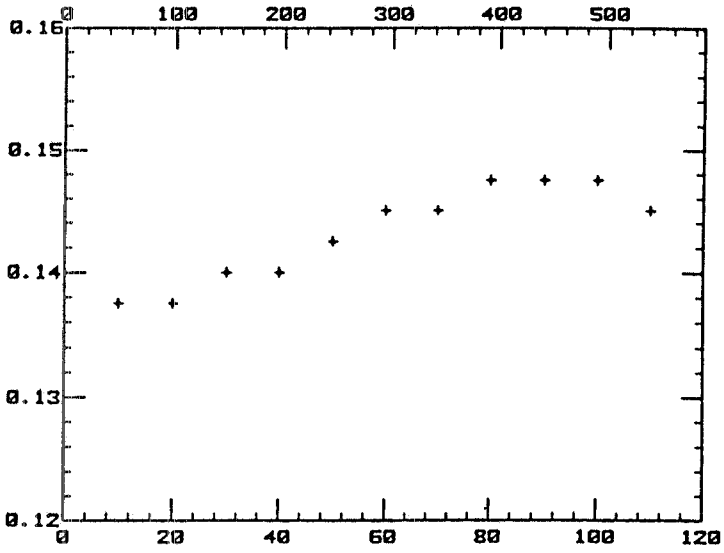

FIG. 10.9 - Radial Q-shift vs horizontal betatron oscillation amplitude upper scale = mm, lower scale = # σ_x.

TABLE 10.9

sext.	*no.*	$K2$ @ $\dot{B}=0$ $E=2000\,MeV$	B''	$K2$ @ $\dot{B}=30\,T/s$ $E=200\,MeV$	B''	$K2$ @ $\dot{B}=30\,T/s$ $E=2000\,MeV$	B''
SF	3	0.950	6.3	−12.0	−8.0	−.3	−2.0
SD	3	−2.000	−13.33	−23.0	−15.3	−4.0	−26.7

$K2$ units are m^{-3}; B'' units are T/m^2

10.6.3 - Hardware

The cost estimate for the lattice magnetic elements has been based on designs similar to those for the main ring elements. A further, more specific, optimization is in progress.

The dipole AC parameters are similar to those for the DESY II bending magnets, when due allowance is made for their being 10 % longer and designed to operate at 12.5 Hz and 1.23 T peak field.

The machine operation mode has to be defined in more detail before a final choice can be made between possible options for the magnet power supply. The well proven resonant White circuit, on which the cost estimate is based, is perfectly adequate for 2 GeV operation, but less so at 1.5 GeVwhere not quite enough damping time is provided. Nonresonant or hybrid options would of course be much more flexible but have to be more carefully evaluated.

10.6.4. - Injection into and extraction from the Booster

A single turn, single shot injection into the horizontal plane is envisaged. In Fig. 10.10 details of the long straight sections are given, showing the position and the phase of the injection and extraction devices. The nominal injection energy is set at 250 MeV.

The linac beam leaves the injection septum (inflector) parallel to the orbit, in a high horizontal beta straight section, and is deflected unto the reference orbit by a kicker, KJ, located $\pi/2$ downstream.

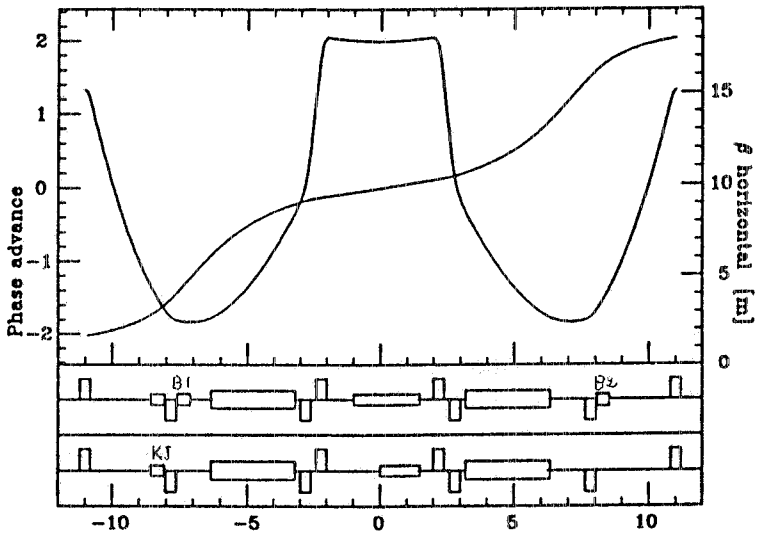

FIG. 10.10 - Optical function and layout in the straight sections for extraction (upper) and injection (lower).

Owing to the absence of residual oscillation around the reference orbit, the booster acceptance is only determined by the linac emittance and energy spread. With a linac emittance of $1*10^{-5}$ m*rad and a 0.3 % energy spread, a maximum beam size at injection energy of 21.7 mm is obtained in the focusing quadrupoles of the arcs.

The designed elliptical vacuum pipe, that fits in the 30 mm quadrupole bore radius, can accomodate 1.5 standard deviations, which we consider sufficient to ensure a good injection efficiency.

The rather low energy spread we assume for the injected beam implies that the Linac is equipped with an energy compressor. Any blow up of the beam energy spread due to synchrotron oscillations has to be avoided by injecting at the center of the RF bucket. With the design RF frequency of 50 MHz this means that a positron pulse lenght of less than 10 ns is required.

At injection energy the inflector specifications are not severe. It is effectively an air core single turn coil. It has a coaxial configuration so as to contain the magnetic flux by eddy currents[10.12]. Its characteristics are listed in Table 10.10.

The injection kicker design is more critical because one is keeping the option of injecting a train of bunches in a single turn. In this case current pulse must have a flat-top of at least 200 ns long and must fall in less than 50 ns . This can be achieved by making the kicker electrodes part of a transmission line loaded with ferrite and capacitive plates [10.13].

The kicker main parameters are listed in Table 10.10

TABLE 10.10

		Inflector	Kicker	Bumper
Length	(m)	1.5	0.5	0.5
Magnetic field	(mT)	100	15	33
Vertical aperture	(mm)	80	30	30
Horizontal aperture	(mm)	20	60	60
Peak current	(KA)	13	0.35	
Line impedance	(Ω)		30	
Peak voltage	(KV)		11	

Single turn extraction will be accomplished by means of a pair of slow bumper magnets (called B1 and B2 in Fig. 10.10 that move the beam near the extraction septum, plus a fast kicker to provide the final deflection into the septum magnet aperture. Extraction devices are dimensioned for 2 GeV operation.

A 20 mm bump is obtained with the bumper characteristics as listed in Table 10.10. The deflection produced by the extraction kicker must be equal to the beam width plus the septum thickness, adding up to 21 mm. The extraction septa asimmetrically placed in the extraction section, produce > 25 cm displacement of the extracted beam at the location of the next downstream quadrupole, thereby providing enough room for the extraction channel. The kicker and the septum are similar to those for injection into the main ring described in paragraph 10.8.

10.6.5. - Repetition rate and filling time

Barring technical considerations, the upper limit to repetition rate is imposed , in our case, by the betatron damping time which is 7.1 ms at 2.0 GeV. A "flat top" longer than twice the damping time is required to assure that the asymptotic emittance is approached. With a resonant power supply and taking the acceleration cycle rise and fall times into account, a 10 Hz repetition rate is found to be adequate.

For a booster current of 44 mA and a 10 Hz repetition rate, and allowing for an overall Linac to Main ring efficiency of 25%, a filling rate of 1.1 mA/s into the main ring is obtained.

The required nominal fill of 400 mA can therefore be achieved in less than ten minutes.

10.7. - Booster to storage ring transfer line

The booster to storage ring transfer line transports a 2 GeV beam with the following characteristics:

- radial emittance, ε_x	5.9×10^{-7}	π rad.m
- vertical emittance, ε_y	7.37×10^{-8}	π rad.m
- β_x	17	m
- β_y	8	m
- $\alpha_{xi} = \alpha_{yi}$	0.	

The line should be achromatic and match the characteristics of the beam extracted from the booster to those of the main ring at the injection point, namely β_x=1.66 m, β_y=3.46 m, $\alpha_{xf} = \alpha_{yf}$=0.

The length of the channel is 23.37 m.

The channel is schematically shown in Fig.10.1, and it can be subdivided in three parts:

a) Extraction channel from the booster

It contains septa M_1 and M_2 and quadrupole QF_1. The total deflection of both septa is 10°. Quadrupole QF_1 is used to curb the dispersion caused by M_1 and M_2.

b) Deflection channel

It consists of two oppositely deflecting magnets M_3 and M_4, two focusing quadrupoles QF_2 and QF_3 and two defocusing quadrupoles QD_2 and QD_3. The central part of the channel is a 4 m long drift space going through the shielding wall between the booster and the main ring.

c) Injection channel

The injection channel consists of focusing quadrupole QF_4, magnet M_5 and septa M_6 and M_7 providing the final deflection through 10°.

There are six quadrupoles in the transport channel to match the six beam envelope output parameters to the main ring acceptance, namely to: β_{xf} =1.66 m, β_{yf} =3.46 m, $\alpha_{xf} = \alpha_{yf} = 0$, D=0, D'=0.

Diagrams of the beam envelope and dispersion function are shown in Fig.10.11.

The characteristics of the magnetic elements are given in Tables 10.11.

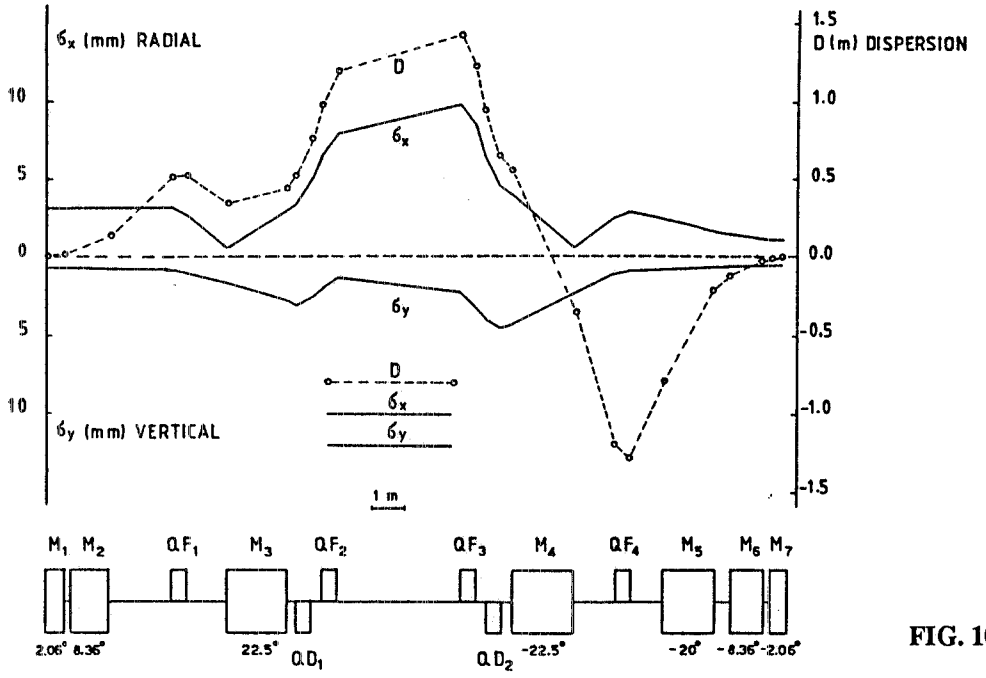

FIG. 10.11

10.8. - Main ring injection magnets

We describe only the main ring elements, the booster extraction magnets being very similar. The elements are a thick and a thin septum and four kickers. The septa are inside the vacuum envelope of the machine while the kickers are in air and have a ceramic vacuum chamber.

- The thin septum is a one turn coil with a C-shaped ferrite yoke; it is powered by a half -sine wave. It is only 1 mm thick which may give some cooling problems that will have to be studied.

Its main characteristics are listed in Table 10.10

- The thick septum has a laminated steel yoke and the following characteristics listed in Table 10.8.2
- The kickers will consist of a single turn coil wound on a window-frame ferrite yoke. The current waveform will be a half-sine. The kickers have a ceramic vacuum chamber to allow field penetration. The required magnetic field value of 0.1 T is rather high for a ferrite yoke device, but still achievable.

Its main characteristics are given in Tables 10.11.

TABLES - 10.11

QUADRUPOLES

	MAGNET LENGTH (cm)	HALF APERTURE (cm)	GRADIENT (KGauss/cm)	NUMBERS QUADRUPOLES
QF_1	48	5	0.7648	1
QD_1	48	5	1.2193	1
QF_2	48	5	0.8573	1
QF_3	48	5	1.0560	1
QD_2	48	5	1.2322	1
QF_4	48	5	1.2961	1

MAGNETS

	MAGNET LENGTH (m)	BEND ANGLE (deg.)	BEND RADIUS (m)	FIELD STRENGTH B (KGauss)	NUMBER MAGNETS
M_1, M_7	0.60	2.06°	16.666	4.002	2
M_2	1.2	8.36°	8.219	8.116	1
M_3, M_4	1.9	22.5°	4.838	13.788	2
M_5	1.7	20°	4.870	13.698	1
M_6	1	8.36°	6.843	9.739	1

REFERENCES

(10.1) S. Tazzari: Philosophy and cost of the injection system for CARST.- LNF Int.Memo AF-9.

(10.2) S. Kulinski, B.Spataro, F. Tazzioli, M. Vescovi: Linac for Afrodite. - LNF Int.Memo AF-1.

(10.3) R. Belbeoch et al.: Rapport d'études sur le projet des linacs injecteurs du LEP(LIL). LAL/PT/82-01/T, Janvier 1982.

(10.4) S. Kulinski, B. Spataro, F. Tazzioli: Linac for Afrodite, solutions with pulse compression. Adone Int.Memo AF-13.

(10.5) S.D. Farkas et al: SLED, a method of doubling SLAC's energy,Proc. 9th Int. Conf.on high energy accelerators, SLAC, Stanford, Cal. May 2-7 1974.

(10.6) A. Febel: Linacs upgraded, DESY journal 85/2, p. 6.

(10.7) D. Warner: First electron beam from the LEP injector linacs, SLAC Conference on Linear Accelerators 1986.

(10.8) G. Loew and J. Wang: Measurements uf the ultimate accelerating gradients in the SLAC disc loaded structure. IEEE Trans. NS-32; also SLAC pub. 3597.

(10.9) P. Patteri, F.Tazzioli, The Afrodite booster, Adone Int.Memo AF-2

(10.10) P. Patteri, Booster da 3 GeV per Afrodite, Adone Int.Memo AF-16 (1987).

(10.11) P. Patteri, Efficienza di iniezione nel booster per Afrodite, Adone Int. Memo AF-31 (1987).

(10.12) The injection system of Adone.- LNF 72-24.

(10.13) Design of a matched fast kicker system. SLAC-PUB 3453.

(10.14) R. Boni, S. Guiducci and M. Vescovi: A new system for positron focusing at the Frascati LINAC.

(10.15) G. Stange: A pulsed magnetic lens for positron focusing report DESY S1-73/4(1973).

(10.16) R. Andreani and A. Cattoni: Positron converter for the Frascati linear accelerator. Nuclear instruments and methods 129 (1975), 365.

(10.17) M. Bassetti, B. Spataro: Canale di trasporto Linac Booster, ADONE Int. Memo AF-27 (1987).

11. - ELECTRICAL DISTRIBUTION, COOLING, VENTILATION

11.1. - Electrical distribution

A preliminary technical description and cost evaluation for the accelerator complex electrical distribution system has been carried out. Several assumptions were made that will have to be verified when an optimized design, taking into account the final requirements and all details concerning the site, will be produced.

TABLE 11.1 - Power Inventory

Bending magnet	1040	kw
6 quadrupole families	640	kw
4 sextupole families	450	kw
R.F. System	600	kw
Booster	400	kw
Linac	500	kw
Wigglers and Undulators	1000	kw
Cooling system	750	kw
Vacuum chamber bakeout	250	kw
General utilities and experiments	500	kw
Lighting	450	kw
Total	6580	kw

Assuming a 75% efficiency and a power factor of 0.9 (the minimum required by law), the resulting installed power requirement comes to 9.75 MVA, or in round numbers to 10 MVA.

It is assumed that the electrical power is delivered at medium voltage level (20,000 V) through unipolar underground cables (120 mm^2, insulation grade 40).

For simplicity we assume the distribution system to be a simple radial network.

One M.V. line is dedicated to each of the following unit or groups of units:

- Dipole
- Quadrupoles and sextupoles
- R.F.
- Booster
- Linac
- Wigglers and Undulators
- Cooling power station

a total of 7 lines is needed to which 9 additional ones, to connect 3 MV/LV transformer stations, are added to account for general utilities and lighting. Each transformer station consists of three 630 KVA - 20000/380/220 transformer units.

The average cable length is assumed to be 250 m long, with a total of 4000 m of MV cable. The cable cross section is 70 mm^2 to account for thermal stresses in the case of short-circuit, even though the minimum cross section needed to handle the assumed power loads is smaller.

On medium voltage lines the voltage drop along the lines is not thought to be a problem.

To protect each line separately with an individual circuit breaker, 16 breakers are needed. Adding a master input breaker and other as spares we total 20 medium voltage breakers. Considering that each unit served by dedicated line will need its own input circuit breaker, 9 further breakers have to be added in the distribution stations, bringing the total up to 29 switches.

About the LV switchboards, we assume, for each 630 KVA unit, three 0.5x0.5x2.1 m^3 "modules", holding all the necessary equipment.

To estimate the number and cost of all other components needed to complete the network, such as: cable ducts and trenches, distribution bars, distribution piping and cable trays, cables, etc., we have made an educated guess based on our experience and compared it to an extrapolation from the work done for the Report of the ESRP (IDT-18).

11.2. - Water Cooling System

Cooling requirements have been estimated for operation at 2 GeV and including:

A - Storage Ring.
B - Booster and Transfer Channels.
C - Linac.
D - Services.

The general characteristics are listed in Table 11.2

TABLE 11.2 - Cooling system characteristics

1	- Average operating temperature	(°C)	50
2	- Temperature difference	(°C)	20
3	- Pressure level	(atm.)	20
4	- Efficiency factor		0.8
5	- Maximum dissipated power	(KW)	4800
6	- Installed power	(KW)	1800

The system (described in more detail in Ref. 7.3) consists of primary circuits fed by water available on site, cooling the distilled water circulating in secondary circuits by means of forced ventilation cooling towers. Distribution manifold rings for different pressure levels, regulation valves and monitoring equipment for every user are foreseen. Modular parallel plate heat exchangers and pumping groups will be used.

11.3. - Ventilation

The heating and ventilation system, has not been considered in detail at this stage. A rough estimate based on medium cost solutions has been made for costing purposes.

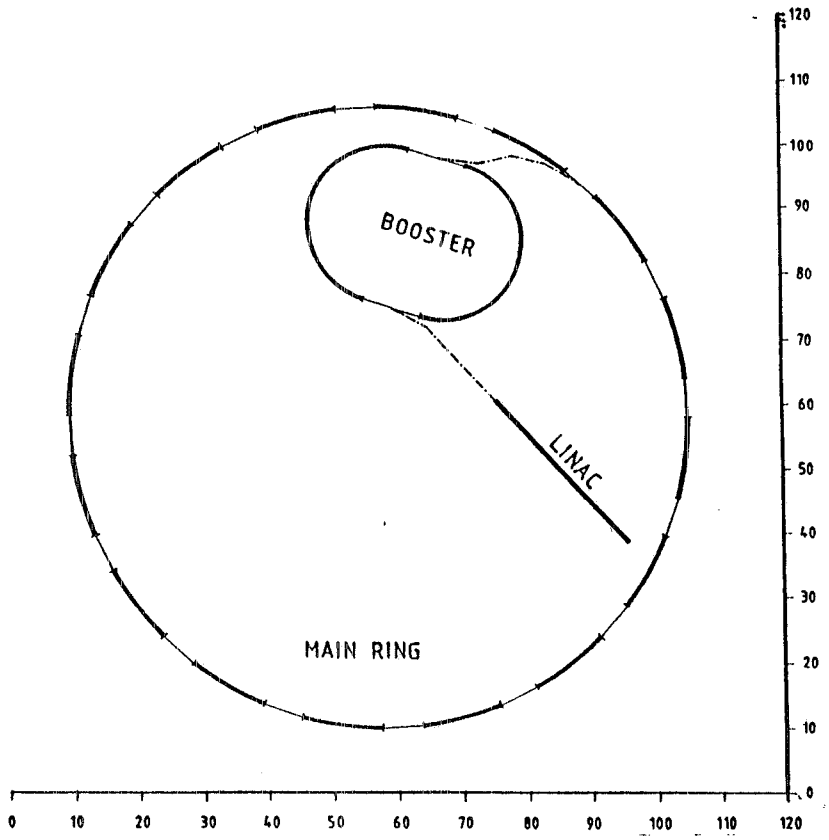

FIG. 11.1 - General Layout. Experimental area not shown.

References

(11.1) The report of the ESRP, presented by B.Buras and S.Tazzari, CERN (1985)
(11.2) A.Aragona, S.Faini: Afrodite Cooling System, Adone Int. Memo AF-19 (1986).

PARAMETER LIST

All parameters of Storage Ring and Booster refer to nominal energy unless otherwise noted

1. Storage Ring Performance Parameters

Nominal energy	2.00	GeV
Maximum circulating current, multibunch	400	mA
Number of stored electron, multibunch	$2.5 \cdot 10^{12}$	
Maximum circulating current, single bunch	10	mA
Number of stored electron, single bunch	$6.2 \cdot 10^{10}$	
Natural emittance	$8.32 \cdot 10^{-9}$	$m \cdot rad$
Natural energy spread, rms	$5.8 \cdot 10^{-4}$	
Bunch length,rms,natural	40	mm
Beam lifetime,half-life		
Gas scattering,20 mm vert. gap, 1 nTorr N_2	108	h
Toushek, maximum current		
Multibunch	16	h
Single bunch	8	h
Filling time		
Multibunch, to 400mA	6	min
Single Bunch, per 10 mA/bunch	9	s

2. Storage Ring Lattice and Orbit Parameters

Circumference	300.200	m
Orbital period	1.001	μs
Harmonic number	500	
Radio frequency	499.66	MHz
Number of superperiods	16	
Insertion straight length	6	m
Mean radius	47.778	m
Mean pipe radius	25	mm
Bending field	1.333	T
Bending radius	5.000	m
Injection energy	2.00	GeV
Injection field	1.333	T
Betatron tunes		
Horizontal	19.83	
Vertical	11.64	
Synchrotron frequency, @ $1.5\,MV_{RF}$	6.20	kHz

Natural chromaticities		
Horizontal	−32.4	
Vertical	−22.9	
Maximum β function		
Horizontal	9.7	m
Vertical	13.6	m
Maximum dispersion	.343	m
β function at insertion points		
Horizontal	3.333	m
Vertical	3.461	m
Momentum compaction	$6.83 \cdot 10^{-4}$	
Damping partition		
Horizontal	1.000	
Vertical	1.000	
Longitudinal	2.000	
Radiation loss, per turn	285	keV
Radiation loss, in insertion device, per turn	≤ 40	keV
Number of dipoles per superperiod	2	
Number of quadrupoles per superperiod	11	
Magnetic lengths in 1/2 superperiod		
(Q=quad, D=drift, B=bend)		
D1 $(\frac{1}{2})$	3.000	m
QW1	.400	m
D2	.150	m
QW2	.550	m
D3	.300	m
QW3	.400	m
D4	.400	m
B	.988	m
D5	.800	m
QF2	.400	m
D6	.400	m
QD1	.400	m
D7	.400	m
QF2 $(\frac{1}{2})$	.200	m
Beam size at light source points,rms		
in undulator straight		
σ_x	160	μm
σ'_x	48	μrad
σ_z, 0.1 coupling	51	μm
σ'_z, 0.1 coupling	15	μrad
in magnet		
σ_x	124	μm
σ'_x	191	μrad
σ_z, 0.1 coupling	64	μm
σ'_z, 0.1 coupling	30	μrad

3. Storage ring tolerances

Misalignments, gaussian distribution rms		
Displacement		
Horizontal	0.1	mm
Vertical	0.1	mm
Roll angle error	0.01°	
Random dipole field error, $\Delta B/B$	$5 \cdot 10^{-4}$	
Random quadrupole strength error, $\Delta k/k$	$5 \cdot 10^{-4}$	
Average closed orbit error amplification factors		
Horizontal, $< x_{c.o.} > /\Delta x$	41	
Vertical, $< z_{c.o.} > /\Delta z$	28	

4. Storage Ring Hardware

Magnets and power supplies		
Dipoles		
Number	32	
Magnetic length	98.2	m
Bending radius	5.000	m
Dipole field	1.333	T
Beam stay clear		
Horizontal	60	mm
Vertical	24	mm
Quadrupoles		
Number	32	
No. of families	6	
Max. gradient	17.0	T/m
Beam stay clear, radius	30	mm
No. of types	2	
Type A		
Number	144	
Magnetic length	.400	m
Type B		
Number	32	
Magnetic length	.550	m
Sextupoles		
Number	192	
No. of families	2	
No. in family SF	96	
No. in family SD	96	
Magnetic length	.200	m
Max. gradient	307.	T/m^2
No. of types	2	
Type A		
Number	128	
Beam stay clear, radius	30	mm

Type B		
Number	64	
Beam stay clear, radius	45	mm
Correctors, dipole windings in quadrupoles		
Strength, fraction of maximum q-pole field	10	%
Number		
Horizontal	80	
Vertical	48	
RF system		
Number of cavities	4	
Frequency	499.66	MHz
Harmonic number	500	
Peak effective voltage	1.5	MV
Transit time factor	.675	
Quality factor, loaded Q	10500	
Effective shunt impedance, ZT^2L	32	$M\Omega$
Fundamental mode cavity dissipation	18	kW
Synchrotron radiation power, dipoles	114	kW
Synchrotron radiation power, unds. + wigglers	34	kW
Parasitic mode losses	12	kW
Waveguide and other losses, 10%	8	kW
Total trasmitter power available	240	kW
Injection hardware		
Injection septa		
Thin septum		
Length	.600	m
Bending angle	36.	$mrad$
Field	.400	T
Pulse width	100	μs
Thick septum		
Length	1.900	m
Bending angle	146.	$mrad$
Field	.973	T
Pulse width	100	μs
Kicker magnets		
Number	4	
Length	.800	m
Bending angle	12.5	$mrad$
Field	.104	T
Pulse width	2	μs
Beam diagnostics		
Beam-position monitors		
Number	128	
Accuracy	0.03	mm
Sensitivity	0.01	mm
No. of travelling-wave electrodes	4	

No. of AC current monitors	1	
No. of wall current monitors	1	
No. of DC current transformer	1	

5. Booster Performance Parameters

Nominal energy	2.00	GeV
Peak energy	3.00	GeV
Cycle rate	10	Hz
Maximum circulating current, single bunch	1.41	mA
Number of stored electrons, single bunch	$2.75 \cdot 10^9$	
Extracted current, single bunch, $\eta = 25\%$	.35	mA
Natural emittance	$5.87 \cdot 10^{-7}$	$m \cdot rad$
Energy spread, rms	$6.1 \cdot 10^{-2}$	%
Bunch length, rms,natural	188	mm
Injection energy	250	MeV
Injected beam emittance	$1 \cdot 10^{-5}$	$m \cdot rad$
Injected beam energy spread	$3 \cdot 10^{-3}$	

6. Booster Lattice and Orbit Parameters

Circumference	93.756	m
Orbital period	312.7	ns
Harmonic number	16	
Radio frequency	51.161	MHz
Lattice structure: FODO with matched dispersion suppressors		
Number of superperiod	2	
FODO cells per superperiod	3	
Mean radius	14.922	m
Bending Field	0.8333	T
Bending radius	8.000	m
Betatron tunes		
Horizontal	3.137	
Vertical	3.175	
Synchrotron tune, (1/1000)		
At injection	.428	
At extraction	5.518	
Momentum compaction	.115	
Damping partition		
Horizontal	1.000	
Vertical	1.000	
Longitudinal	2.000	
Betatron damping time		
Horizontal	7.07	ms
Vertical	7.07	ms
Synchrotron damping time	3.54	ms
Natural Chromaticity		
Horizontal	−3.29	

Vertical	−3.93	
Optical functions, maxima		
In FODO		
β horizontal	14.516	m
β vertical	16.308	m
Dispersion	3.238	m
In straight sections		
β horizontal	18.053	m
β vertical	15.261	m
Magnetic lengths, (Q = quad, L = drift space, B = bend)		
In $\frac{1}{2}$ dispersion suppressor insertion		
LLONG ($\frac{1}{2}$)	2.000	m
QFI	.400	m
LDF	.200	m
QDI	.400	m
LBR	.200	m
B	3.142	m
LBL	1.290	m
QD0	.400	m
LD	2.781	m
QF ($\frac{1}{2}$)	.200	m
In complete FODO cell		
QF ($\frac{1}{2}$)	.200	m
L	.050	m
SF	.200	m
L	.050	m
B	3.142	m
L	.300	m
QD	.400	m
L	.050	m
SD	.200	m
L	.050	m
B	3.142	m
L	.300	m
QF ($\frac{1}{2}$)	.200	m

7. Booster Details

Magnet and power supplies		
Dipoles		
Number	16	
Magnetic length	3.142	m
Bending radius	8.000	m
Dipole field	0.8333	T
Beam stay clear		
Horizontal	60	mm
Vertical	24	mm

Quadrupoles		
Number	26	
No. of families	5	
Max. gradient	7.9	T/m
Beam stay clear,radius	30.0	mm
Magnetic length	.400	m
Sextupoles		
Number	6	
No. of families	2	
No. in family SF	3	
No. in family SD	3	
Magnetic length	.200	m
Max. gradient	26.7	T/m^2
Beam stay clear, radius	30.0	mm
RF system		
Number of cavities	1	
Frequency	51.163	MHz
Harmonic number	16	
Peak effective voltage	.273	MV
Transit time factor	1	
Quality factor, loaded Q	5000	
Effective shunt impedance, ZT^2L	2	$M\Omega$
Fundamental mode cavity dissipation	20	kW
Synchrotron radiation peak power	.252	kW
Total trasmitter power available	50	kW
Injection hardware		
Injection septum		
Length	1.500	m
Thickness	5	mm
Bending angle	175.	$mrad$
Field	$9.72 \cdot 10^{-2}$	T
Pulse width	100	μs
Kicker magnet		
Length	.500	m
Bending angle	8.9	$mrad$
Field	$1.48 \cdot 10^{-2}$	T
Fall time	< 300	ns
Extraction hardware		
Extraction septa		
Thin septum		
Length	.600	m
Bending angle	36	$mrad$
Field	.4002	T
Pulse width	100	μs
Thick septum		
Length	1.200	m

Bending angle	146	
Field	.8116	T
Pulse width	100	μs
Bump magnets		
Number	2	
Length	.500	m
Bending angle	2.49	$mrad$
Field	$3.33 \cdot 10^{-2}$	T
Kicker magnet		
Length	.500	m
Field	$4.25 \cdot 10^{-2}$	T
Rise time	< 300	ns
Beam diagnostic		
Beam-position monitors		
Number	22	
Accuracy	0.1	mm
Sensitivity	0.01	mm
No. of AC current monitors	1	
No. of wall current monitors	1	

8. Linac

Linac element chain
- High intensity electron gun, Pierce triode type
- Combined prebuncher-buncher system, $\frac{1}{2}\pi$ SW biperiodic accelerating section
- e^- linac, $\frac{2}{3}\pi$ TW accelerating sections
- $e^- \rightarrow e^+$ converter
- e^+ linac, $\frac{2}{3}\pi$ TW accelerating sections

Linac length, total	30	m
Electron gun		
Gun voltage	100	kV
Gun current	20	A
Cycle rate	10	Hz
Length of the pulse	10	ns
Rise time of the pulse	3	ns
Buncher		
Length	$1.1 \div 1.5$	m
Output current	10	A
Pulse length	10	ns
Accelerated charge	100	nC
Energy gain, average	$15 \div 25$	MeV
Relative energy dispersion		
without beam loading	0.05	
with beam loading, 100 nC pulse charge	0.21	
Phase dispersion	$< 20°$	
Input power	$5 \div 10$	MW

Effective shunt impedance, ZT^2	> 50	$M\Omega/m$
Quality factor	15000	
Frequency	2998.5	MHz
e^- linac		
Length	10	m
Number of sections	4	
Energy	220	MeV
Peak current	10	A
Charge per pulse	100	nC
Peak power required	140	MW
Power sources		
No. of Klystrons	1	
Power per klystron	35	MW
Converter		
e^- energy on target	220	MeV
e^+/e^- conversion efficiency, @ $100\,MeV$	$2 \cdot 10^{-3}$	
e^+ accepted energies	$4 \div 8$	MeV
e^+ transverse momentum		MeV/c
e^+ capture section length	1.5	m
e^+ linac		
Length	10	m
Number of sections	4	
Energy	220	MeV
Peak current	44	mA
Charge per pulse	0.44	nC
Emittance, rms	$1 \cdot 10^{-5}$	$m \cdot rad$
Energy spread, rms	$1 \cdot 10^{-2}$	
Peak power required	140	MW
Power sources		
No. of Klystrons	1	
Power per klystron	35	MW
Single e^+ or e^- linac accelerating section		
Length	2.5	m
Frequency	2998.5	MHz
Shunt impedance	70	$M\Omega/m$
Quality factor	15200	
Filling time	0.7	μs
Power input	25	MW
Attenuation factor per unit lenght	0.44	$Neper/m$
Stored energy	11.6	J

9. Linac-to Booster (LTB) Transfer Line

Channel length	22.855	m
Magnets		
Dipole number	2	

Type A		
Magnetic length	2.000	m
Field	.1280	T
Bend	20°	
Type B		
Magnetic length	1.500	m
Field	.0854	T
Bend	10°	
Quadrupoles		
Number	6	
Magnetic length	.320	m
Max. gradient	1.80	T/m

10. Booster-to-Storage-Ring (BTS) Transfer Line

Magnets		
Dipoles		
Number, type A	2	
Magnetic length	1.900	m
Field	1.3788	T
Bend	22.5°	
Number, type B	1	
Magnetic length	1.700	m
Field	1.3698	T
Bend	20°	
Quadrupoles		
Number	6	
No. of families	6	
Magnetic length	.480	m
Pole tip inscribed radius	100	mm
Max. gradient	.1296	T/m